KTH Industrial Engineering
and Management

Flow boiling heat transfer, pressure drop and dryout characteristics of low GWP refrigerants in a vertical mini-channel

Doctoral Thesis
By

Zahid Anwar

Division of Applied Thermodynamics and Refrigeration
Energy Technology Department
Royal Institute of Technology Stockholm, Sweden

Doctoral Thesis in Energy Technology
Stockholm, Sweden 2014

Trita REFR Report 14/03
ISSN 1102-0245
ISRN KTH/REFR/14/03-SE
ISBN 978-91-7595-389-2

© Zahid Anwar 2014

Abstract

Two-phase heat transfer in mini/micro-channels is capable of meeting the high cooling demands of modern high heat flux applications. The phase change process ensures better temperature uniformity and control for local hot spots. Furthermore, these compact channels could be helpful in reducing the required charge and material inventories.

Environmental concerns—mainly ozone depletion and global warming—have instigated a search for new alternatives in refrigeration industry. While new compounds are being developed to address stringent legislative demands, natural alternatives are also coming into prominence. A limited number of investigators have reported on thermal performance of such alternatives. The current study is therefore focused on saturated flow boiling heat transfer, pressure drop and dryout characteristics for three low global warming potential (GWP) refrigerants (R152a, R600a and R1234yf) in a vertical mini-channel.

In this study experiments were carried out by uniformly heating a test section (stainless steel tube with 1.60 mm inside diameter and 245 mm heated length) at 27 and 32^{o}C saturation temperature with 50-500 kg/m^{2}s mass velocities. The effects of various parameters of interest (like heat flux, mass flux, system pressure, vapor quality, operating media) on flow boiling heat transfer, frictional pressure drop and dryout characteristics were recorded. R134a, which has been widely used in several applications, is utilized as a reference case for comparison of thermal performance in this study.

Experimental results for saturated boiling heat transfer showed strong influence of heat flux and system pressure with insignificant contributions from mass flux and vapor quality. Two phase frictional pressure drop increased with mass flux, vapor quality and with reduced operating pressure. The dryout heat flux remained unaffected with variation in saturation temperature, critical vapor quality in most cases was about 85%. The experimental results (boiling heat transfer, two-phase pressure drop and dryout heat flux) were compared with well-known macro and micro-scale correlations from the literature.

Keywords: Mini/micro-channels, R1234yf, R152a, R600a, R134a, Boiling heat transfer, Pressure drop, Dryout, Correlation

Acknowledgement

First and foremost, deepest gratitude to my supervisor, Prof. Björn Palm, for providing me with the opportunity to work under his kind supervision. I am grateful for his continuous guidance and support in all academic and related matters.

I am also thankful to my co-supervisor, Associate Prof. Rahmatollah Khodabandeh, for his guidance, support and motivation throughout the entire project.

I am thankful to all my colleagues (ETT-Family) with whom I shared my time of joy and stress. Special thanks goes to Samer Sawalha, Hatef Madani, Aleh Kliatsko, Monika Ignatowicz, Oxana Samoteeva, Erik Björk, Bhezad Monfared, Ehsan Bitaraf Haghighi, Jianyoung Chen, Qingming Liu, Pavel Makhnatch, Omar Shafqat, Mazyar Karampour , Morteza Ghanbarpour and Jose Acuna for your valuable company and support.

Special thanks to our lab manager, Peter Hill, and technical support staff, Benny Sjöberg and Kalr-Åke Lundin, for their help whenever needed.

I am thankful to my Pakistani friends M. Hamid Munir, Mian M. Masoud, Nawaz Ahmed Virk, Afzal Frooqi and Shahid Hussain Siyal for their nice friendship, support and motivation all the time. I really enjoyed your friendship.

Financial support was received from University of Engineering and Technology, Lahore, Pakistan and from Royal Institute of Technology, KTH, Sweden and is highly acknowledged.

Special thanks to my family members in Pakistan for their encouragement, support and understanding throughout the completion of this thesis.

Finally my gratitude to my fiancée Maria Ashraf for her love, care, patience and support.

Zahid Anwar

Stockholm, November 2014

Publications

Journal Articles

Published

1. Z. Anwar, B. Palm, R. Khodabandeh, 2014, Flow boiling heat transfer and dryout characteristics of R152a in a vertical mini-channel, Experimental Thermal and Fluid Science, Vol. 53, 207-217.

Accepted

1. Z. Anwar, B. Palm, R. Khodabandeh, Flow boiling heat transfer and dryout characteristics of R600a in a vertical mini-channel, Accepted for Vol. 36 of Journal of Heat Transfer Engineering.

Under Review Process

1. Z. Anwar, B. Palm, R. Khodabandeh, Flow boiling heat transfer, pressure drop and dryout characteristics of R1234yf in a vertical mini-channel. Submitted to the Journal of Experimental Thermal and Fluid Science.
2. Z. Anwar, B. Palm, R. Khodabandeh, Dryout characteristics of natural and synthetic refrigerants in vertical mini-channels. Submitted to the Journal of Experimental Thermal and Fluid Science.

Peer Reviewed Conferences

1. Z. Anwar, B. Palm, R. Khodabandeh, 2013, Dryout characteristics of R600a in a vertical mini-channel, Eurotherm Seminar No. 96, September 17-18, Brussels, Belgium.
2. Z. Anwar, B. Palm, R. Khodabandeh, 2013, Flow boiling of R600a in a uniformly heated vertical mini-channel, 13TH UK Heat Transfer Conference, September 2-3, London, UK.
3. Z. Anwar, B. Palm, R. Khodabandeh, 2013, Dryout characteristics of R600a in a uniformly heated vertical mini-channel, 13TH UK Heat Transfer Conference, September 2-3, London, UK.
4. Z. Anwar, B. Palm, R. Khodabandeh, Flow Boiling of R1234yf in a uniform smooth vertical mini-channel, 4TH IIR Conference on Thermophysical properties and Transfer processes of Refrigerants, Delft, Netherland.

Other Publications

1. Z. Anwar, 2013, Evaporative heat transfer with R134a in a vertical mini-channel, Pakistan Journal of Engineering and Applied Sciences, Vol. 13, 101-109.
2. Z. Anwar, 2013, Dryout characteristics of R134a in a vertical mini-channel, International Journal of Thermal Technologies, Vol. 3, 36-42.
3. E. B. Haghighi, Z. Anwar, I. Lumbreras, S. A. Mirmohammadi, M. R. Behi, R. Khodabandeh, B. Palm, 2012, Screening single phase laminar convective heat transfer with nanofluids in a micro-tube, 6TH European Thermal Science Conference (Eurotherm 2012).
4. E. B. Haghighi, M. Saleemi, N. Nikham, Z. Anwar, I. Lumbreras, M. Behi, S. A. Mirmohammadi, H. Poth, R. Khodabandeh, M. S. Toprak, M. Muhammad, B. Palm, 2013, Cooling performance of Nanofluids in a small diameter tube, Experimental Thermal and Fluid Science, Vol. 49, 114-122.

Table of Contents

Chapter 1. Introduction and Background

The escalating heat fluxes from compact modern electronic components have outpaced conventional single phase (air and liquid) cooling techniques. The main complications with single phase forced convective cooling for high heat flux applications are enhanced pumping power (increased flow rates), bulky components and high temperature lifts (non-uniform temperature distribution along the chip). With a reliance on the heat of vaporization, the two-phase heat transfer has the capability of withstanding high demands with better temperature uniformity along the chip, and with fairly reduced flow rates.

With compact channels, the increased surface area per unit volume of fluid further enhances the heat transfer capability (due to low thermal resistance between device and coolant). The utilization of these channels in practical devices has additional associated benefits, such as reduced charge, reduced materials and lower weight of devices. However, with compact channels, the channel layout must be designed with care in order to avoid an increased pressure drop compared with large channels. These compact-channels have been used in diverse application areas, including in miniature heat exchangers, refrigeration systems, power electronics, catalytic reactors, fuel injectors for some internal combustion engines, and in the evaporators of fuel cells [1] [2].

While an enormous amount of research can be found in the literature on phase change heat transfer, the general understanding of transport processes in small channels remains limited. This is clear from the drastically different results that have been reported by different researchers. Furthermore, the complex nature of the physics involved is made clear by the lack of mechanistic prediction methods or approaches. Thus, there is still the need for further experimental work using reliable apparatuses under wide operating conditions, in order to enhance the understanding of the transport process in small channels. Furthermore, the analysis of heat transfer, pressure drop and dryout characteristics of environmentally benign mediums is the call of the hour, so that the strict ongoing legislation can be met.

Refrigerant-related environmental concerns—namely ozone depletion and global warming issue—have instigated an intensive search for environment friendly alternatives. Legislative bodies across the globe are attempting to mitigate refrigerant related hazards by implementing strict treaties such as the Kyoto Protocol, the EU F-gas regulation, etc. This study is therefore carried out using low GWP refrigerants, which will likely prove helpful in accomplishing ambitious environmental goals.

The refrigerant R134a has been widely used in stationary and mobile applications; however, its high GWP value restricts further utilization. The recently developed HFO-1234yf has quite a low GWP (GWP=4 on a 100-year time horizon) with transport properties almost identical to R134a. Another good replacement candidate for R134a is R152a, due to a favorable environmental footprint (zero ozone depletion potential (ODP) and a low GWP of about 120) along with good transport properties. In addition, there are natural refrigerants (R717, R744 and hydrocarbons), which are free from chorine and fluorine, and have quite low GWP values with zero ODP.

Overall, huge reserves, good material compatibility, and good transport properties favor the utilization of hydrocarbon refrigerants. However, flammability issues require additional measures with the utilization of R152a and hydrocarbons (refrigerant concentration within the occupied volume should be less than 20% of their low flammability limit [3]). R1234yf, requires comparatively large ignition energy and is less flammable than R152a and R600a. The significantly high heat of vaporization with hydrocarbons and R152a has the

benefit of reducing the mass flow rate for a given heating/cooling demand. This study is therefore carried out using the low GWP refrigerants R1234yf, R152a and R600a (GWP<150), with R134a is used as a basis for performance comparison.

1.1 Macro to Micro-scale transition criteria

Despite an enormous amount of experimental and theoretical research over the last two decades, the scientific community has not reached a consensus on how to distinguish micro-channels from macro-channels. However, there seems a general agreement that the utilization of micro/compact-channels results in improved thermal performance. In such a configuration, the heat transfer coefficient (HTC) normally increases with an increase in heat flux so that local hot-spots are automatically addressed [4]. Researchers do have consensus that there exist a threshold limit below which conventional knowledge (from macro-channels) may not be well extrapolated and this thus requires special consideration or treatment. Several definitions found in the literature for this threshold limit are summarized below.

The two most cited definitions, which are based on the characteristics of channel size, were introduced by Mehedale et al. [5] and Kandlikar and Grande [6]. Mehendale et al. [5] used the term meso-scale which is in between the micro and macro-scales whereas Kandlikar used the term mini-channel for the same. The transition details are summarized in Table 1-1 below.

Table 1-1 Macro to micro-channel transition limits

Channel	**Mehendale et al.** [5]	**Kandlikar and Grande** [6]
Micro-Channel	d 1-100 μm	d 10-200 μm
Meso-Channel	d 100-1000 μm	-
Mini-Channel	-	d 200 μm-3 mm
Macro-Channel	d 1-6 mm	-
Conventional Channel	d > 6 mm	d > 3 mm

As criteria based on characteristic channel dimensions do not account for differences in thermo-hydraulic parameters—operating conditions, flow patterns, bubble growth etc.—their utilization might be questionable. The channel confinement in mini/micro-channels inhibits bubble growth in the radial direction. To account for this restriction, confinement Number (Co) was proposed by Kew and Cornwell [7]. They reported significant confinement effects for channels with Co > 0.5, where Co was defined by,

$$\mathrm{Co} = \frac{\sqrt{\dfrac{\sigma}{(\rho_l - \rho_g)g}}}{d} \tag{1.1}$$

As per the recommendations of Triplet et al. [8], confinement effects become significant for channels with Co > 1. Ong and Thome [9] suggested transition from macro to micro-scale in the range of Co 0.3-1 (based on the uniformity of the thin liquid film on the heating surface) and named this transition meso-scale, whereas micro-scale effects were reported for Co > 1.

Another dimensionless parameter for distinguishing micro-channels from macro-channels termed convective-confinement number was introduced by Harirchian and Garimella [10]. The authors considered flow velocity as an important parameter to be included in the macro to micro-scale transition limit. This criterion was based on their experimental findings with FC-77 and is summarized as follows:

$$\mathrm{Bd}^{0.5}\mathrm{Re} < 160 \text{ (For micro} - \text{channels)} \tag{1.2}$$

Based on the relative importance of surface tension, body, viscous and inertial forces, Li and Wu [11] proposed the following dimensionless parameter as another criterion:

$$\mathrm{Bd} \cdot \mathrm{Re}^{0.5} < 200 \text{ (For micro} - \text{channels)} \tag{1.3}$$

Another definition based on Eötvös Numer (Eo) was given by Ullman and Brauner [12]. This criterion is also based on bubble confinement and relates buoyancy and surface tension forces:

$$\mathrm{Eo} < 1.6 \text{ (For micro} - \text{channels)} \tag{1.4}$$

There are also some other definitions that are based on the wettability of the heating surface and utilize contact angle for the liquid droplet as another criterion.

Gravity, inertia, viscous shear and surface tension are four forces controlling the transport phenomena. It is well accepted that surface tension becomes the predominant force, with almost negligible gravitational effects in the case of small/micro-channels. Furthermore, visualization studies have evidenced the absence of stratified flow and the dominance of elongated bubble flow and annular regimes as well as uniform thin liquid film on the heating surface in the case of mini/micro-channels. These peculiar observations demand special consideration when dealing with mini/micro-channels.

For this study, experiments were carried out using four refrigerants. The channel diameter was < 3 mm, while in most cases Co was either close to or above 0.5 but remained < 1. As per Li and Wu's [11] definition, majority of tested cases (above 85%) fall within the mini/micro-channels limit, whereas using Ong and Thome's [9] definition, all cases lie in meso-scale range. Based on these characteristics, the mini-channel definition is adopted for the cases reported in this study and will be used for all remaining discussion.

1.2 Introduction to Boiling

Boiling is the process of transforming liquid into vapor through the addition of heat. There can be both sub-cooled or saturated boiling cases, depending on the bulk fluid temperature level. In the case of sub-cooled boiling, the bulk fluid temperature remains below that of the saturation condition, whereas the same follows saturation conditions for saturated boiling. The boiling process can occur in a stagnant pool of liquid as well as in a fluid flowing stream. "Pool Boiling" is the name given to the stagnant pool case while the other is known as "Flow Boiling". The boiling process is vital for many industrial applications, such as in power stations (where vapor is expanded in a steam turbine), refrigeration and heat pumps, cooling of electronics, cooling of lasers, nuclear reactors and other high heat flux applications.

The graphical representation for clarifying details related to various regimes during the boiling process is known as the boiling curve. This graph plots heat flux versus degree of wall superheat (t_{wall}-t_{sat}) and is schematically shown in Figure 1.1 for the case of pool boiling. Actual plots may vary according to the properties of the fluid involved and the operating conditions.

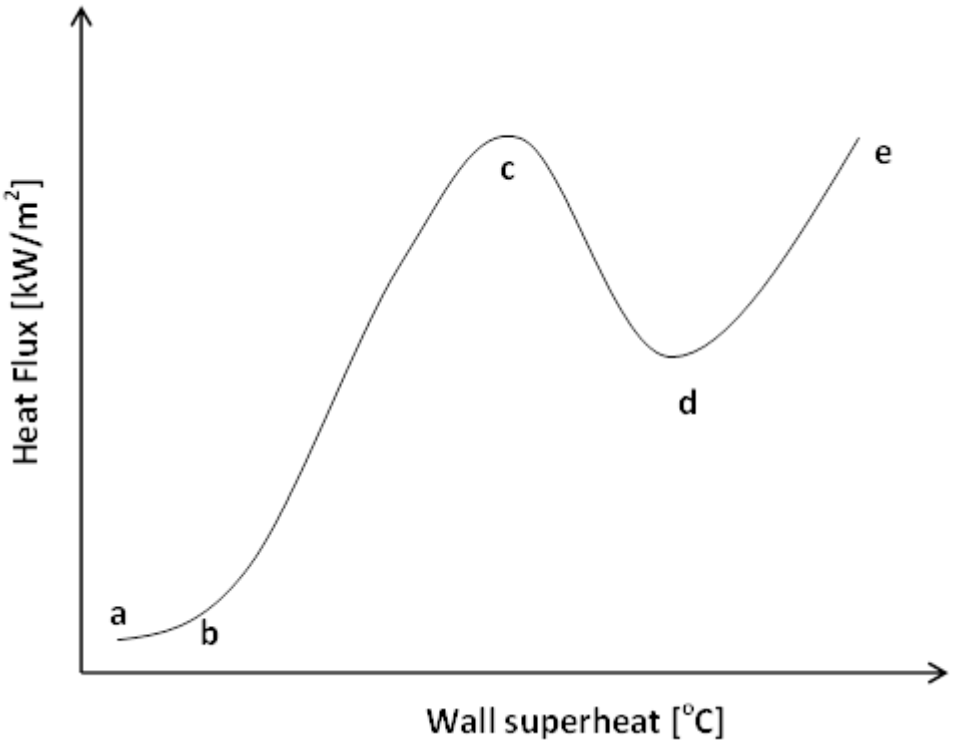

Figure 1.1 Schematic boiling curve for pool boiling process

The boiling curve has four important regions (a-b, b-c, c-d, d-e), as shown in Figure 1.1. The natural convection region spans from a-b. Heat transfer in this region occurs by convection currents as surface and fluid temperature slightly exceeds the saturation condition; bubble nucleation conditions, however, are not fully approached in this region.

The nucleate boiling region spans from b-c, with bubble nucleation starting from gas vapors lying in the cracks on the surface, initially in the form of isolated bubbles. These small bubbles then coalesce into vapor slugs or columns with the increase in supplied heat flux. The collapse of these bubbles improves the circulation of surrounding fluids, hence improves heat transfer. The formation of the vapor slug or column makes it hard for the incoming fluid to wet the heating surface. For heat flux controlled applications, surface temperature rises sharply in c-e, bypassing the in-between steps. Point "c" is the maximum heat flux point and is termed in the literature as critical heat flux (CHF), dryout or departure from nucleate boiling point. As surface temperature shoots up, physical burnout may eventually be approached in heat flux controlled applications—this event is also known as burnout heat flux.

The transition boiling region is from c-d. It is an unstable and undesirable form of boiling. In this region, the heater surface rapidly switches from wet to dry conditions, and liquid in the incoming stream or pool is significantly hindered from wetting the heated surface.

The film boiling region is on the right side of boiling curve, from d-e. In this case, the heater surface is covered by a continuous film of vapor. Point "d" is the minimum film boiling point—also referred to in literature as the Ledienfrost point.

A similar kind of boiling curve can be reproduced when flow boiling occurs inside a heated tube. However, fluid movement adds to complexity of the problem. Figure 1.2 provides a schematics of the flow boiling process along with information about flow patterns and wall and fluid temperature profiles along a uniformly

heated vertical tube. The sub-cooled liquid enters the tube and absorbs heat as it flows in the upward direction.

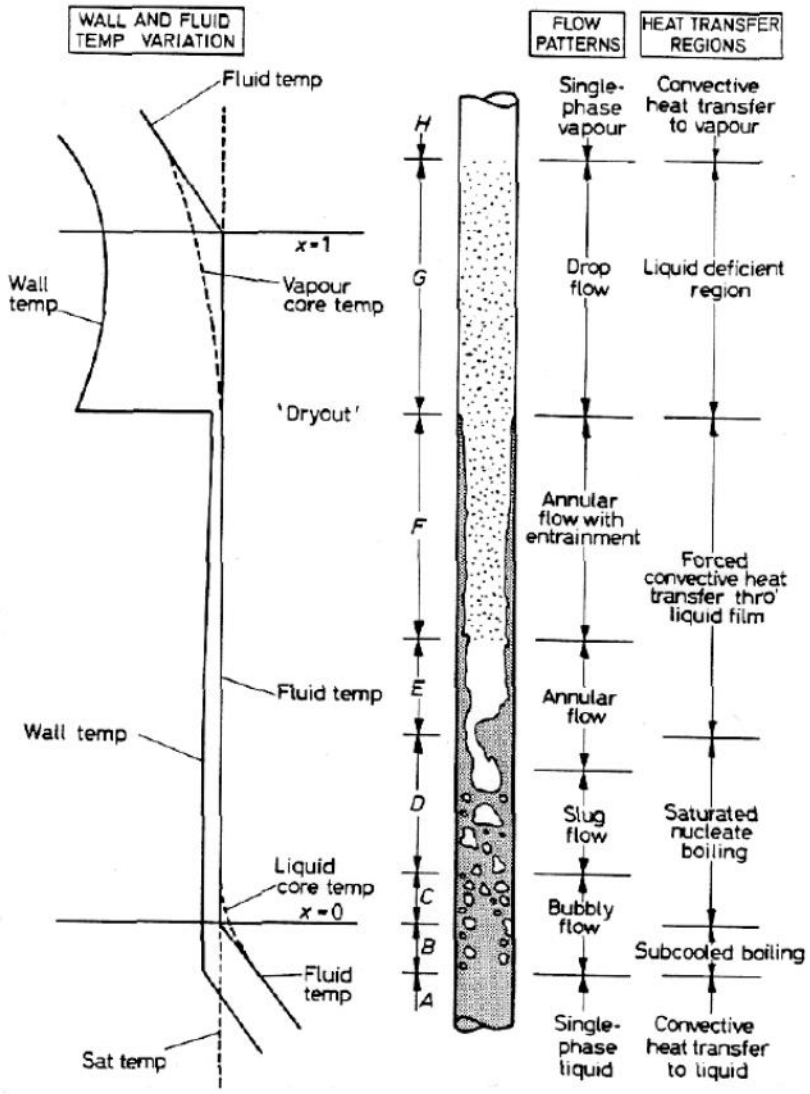

Figure 1.2 Flow boiling inside a uniformly heated vertical tube[1] [13]

Initially close to the inlet, the single-phase convective heat transfer mode is active. Once the required degree of wall superheat is achieved, bubbles will start to nucleate at the active nucleation sites. In the sub-cooled region where the bulk fluid temperature remains below the saturation temperature, these bubbles will condense as they move away from wall/heated surface. Initially, only few nucleation sites are active and a significant portion of the tube is covered by liquid patches. Single-phase convection has a significant effect in this region on overall heat transfer performance. As more sites become active, the contribution from the nucleate boiling mechanism takes over single-phase convection. As the bulk temperature increases with the flow, saturation conditions are established. Moving further down, the bubbles merge together to form the vapor core, an annular flow region where liquid travels in the form of a thin film on the heated surface, with

[1] Figure schematically shows the case for conventional channels, actual flow regimes as well as transitions may differ for mini/micro-scale channels.

vapor in the central core and evaporation occurring at the liquid vapor interface, without any nucleation. The complete evaporation of this liquid film causes dryout of the heating surface, which is characterized by sharp increase in wall temperature in heat flux controlled applications.

Experimentally, it is not easy to obtain a complete boiling curve as shown in Figure 1.1, and furthermore, the trend varies in heat flux controlled devices, as explained in the above paragraphs. For practical reasons, the operation of the majority of devices should occur in the nucleate boiling region of the curve, as this is the safest and most effective region, where high heat fluxes can be tolerated over small temperature lifts.

1.3 Objectives of this study

The main aim of this study is to contribute to the understanding of the saturated flow boiling heat transfer, pressure drop and dryout characteristics of environmentally benign refrigerants in a vertical mini-channel. Data on single-phase heat transfer and pressure drop were also collected; however, these were only used for system validation. The key objectives with this study are as follows:

- To explore effects of operating parameters (such as heat flux, mass flux, system pressure, vapor quality) on saturated boiling heat transfer, pressure drop and dryout.
- To assess the predictions of macro and micro-scale correlations for predicting heat transfer, pressure drop and dryout characteristics.
- To perform a comparative study of flow boiling heat transfer and dryout characteristics found in the current experimental results (R134a, R152a, R1234yf, R600a) with those collected earlier by Maqbool et al. [14] [15] (boiling heat transfer withR717, boiling and dryout with R290) and Callizo [16] (saturated boiling and dryout characteristics with R134a, R22 and R245fa).

While the study is not focused on any specific application, the results presented here could be useful for designing compact heat exchangers for the refrigeration and heat pump industries, as well for cooling of electronics.

1.4 Structure of the Thesis

This thesis presents an extensive description of the research work, which is supported with appended papers. The first chapter provides an introduction, including the background and basics of the boiling process, along with a summary of objectives with this work. Chapter 2 contains a literature survey of recent research on flow boiling heat transfer, pressure drop and dryout aspects under similar operating schemes. The details of experimental setup and instrumentation used are then given in Chapter 3. The procedures for data analysis, including calculation procedures and estimates of uncertainty are also provided in Chapter 3, along with a brief discussion on single-phase heat transfer and pressure drop results, and system validation. Chapter 4 provides the results for saturated flow boiling heat transfer for the four refrigerants used in this study (R1234yf, R152a, R600a and R134a), along with a comparison with previous database from our research group ([16] [14] [15]). Results of parametric effects (such as heat flux, mass flux, operating pressure and vapor quality) and comparison of experimental data with correlations are also given in this chapter. Chapter 5 presents the experimental results of the two-phase frictional pressure drop, along with comparison with correlations from the literature. This is followed by a discussion in Chapter 6 regarding the dryout characteristics of the four refrigerants of this study along with the previous dryout database from our research group [2] [16]. The combined database contains 72 data points for dryout and involves 7 refrigerants (natural and synthetic). The effect of operating parameters and comparison with correlations for dryout is also provided in this chapter. Chapter 7 presents the conclusions of the study along with future recommendations, followed by nomenclature and bibliographical details.

Chapter 2. Literature Review

The last two decades have witnessed an exponential growth in two-phase flow research activities at the mini/micro-scale level. Many researchers have reported on flow patterns, heat transfer, pressure drop and dryout characteristics in small channels with different operating mediums and under different imposed operating conditions. Experiments have been conducted with single and multi-channel arrangements and under different flow directions (vertical, horizontal, etc.). In most cases, the channels have been made out of highly conductive materials (copper, steel), directly heated by Joules heating. However, differing trends have been reported by different researchers. This chapter summarizes the recent experimental findings on flow boiling heat transfer, pressure drop and dryout characteristics of refrigerants in mini/micro channels.

2.1 Flow Boiling Heat Transfer

This section begins with a brief summary of recently reported results from the literature that have been obtained from setups and operating conditions that are comparable to this study. The reported trends are graphically presented in Figure 2.1 and the results are summarized in Table 2-1. A brief summary of widely used prediction models (on macro and micro-scales) is provided in the appendix.

Experimental results on the flow boiling heat transfer characteristics of R1234yf in a horizontal stainless steel tube of 2 mm inside diameter and 1.76 m length were reported by Saitoh et al. [17]. In the study, the test section was directly heated using DC electricity and results were collected for 15 ^{o}C saturation temperature with 200-400 kg/m^{2}s mass fluxes. At low mass flux and low heat flux (200 kg/m^{2}s and 6 kW/m^2), heat transfer coefficients (HTCs) increased with increases in vapor quality. Overall, HTCs increased with an increase in mass flux and with vapor quality. In all cases, critical vapor quality for dryout was reported to be about 80%. Under similar operating conditions, identical heat transfer results were reported for R134a. The correlation from Saitoh et al. [18] (originally developed from a R134a-based database from small tubes) satisfactorily predicted their new experimental database for R1234yf.

Hamdar et al. [3] reported experimental findings on evaporative heat transfer for R152a in a square (1*1 mm cross section and 381 mm length) horizontal mini-channel. In this case, the test section was machined between two aluminum blocks. The experiments were conducted at 6 bar with 200-600 kg/m^{2}s. The authors reported a strong influence of heat flux on HTCs, with insignificant contribution from vapor quality and mass flux. The authors speculated that nucleate boiling was the dominant mechanism behind their results. They proposed a modified form of Tran's correlation [19] for prediction of their database.

Flow boiling heat transfer characteristics of R1234yf in 0.96 mm horizontal copper tube were reported by Del-Col et al. [20]. In this case, the test section was indirectly heated with hot water in a counter flow arrangement. The experiments were carried out at 31 ^{o}C saturation temperature with 200-600 kg/m^{2}s mass velocities. The authors reported strong influence of heat flux on heat transfer coefficients, with no significant effect from mass flux. HTCs initially decreased with vapor quality in the low quality region (x<0.3) and then remained unaffected by further increase in vapor quality. Thermal performance of R1234yf was also compared with R134a, and nearly identical heat transfer results under similar imposed operating conditions were reported for both refrigerants.

Two-phase heat transfer and pressure drop characteristics for R600a in a circular horizontal mini-channel (2.6 mm in diameter and 185 mm heated length) were reported by Copetti et al. [21]. The experiments were conducted at 22 ^{o}C with G=240-440 kg/m^{2}s. The authors found an increase in HTCs with heat flux in the low quality region (x<0.4), beyond which HTCs decreased. At low mass velocity, HTCs were not affected by vapor quality; however, they increased with vapor quality at high mass flux conditions. Furthermore, HTCs increased with an increase in mass flux. The authors compared the performance of R600a with their old

database for R134a, and found that higher HTCs and pressure drop for R600a under similar operating conditions. Correlation from Kandlikar and Balasubramanian [22] predicted their data for heat transfer with a modified fluid surface parameter value. None of the tested correlations correctly predicted the data for frictional pressure drop; however, slightly better predictions were obtained using Tran's correlation [23].

The flow boiling heat transfer characteristics of ammonia (R717) in small vertical stainless steel tubes were studied by Maqbool et al. [15]. The authors used vertical tubes of 1.224 and 1.70 mm in diameter and 245 mm heated length, and data was collected for 23, 33 and 43 ^{o}C saturation temperature with 100-500 kg/m^{2}s mass fluxes. A significant effect of heat flux was reported for all tested cases using the 1.70 mm tube and at lower vapor quality (x<0.1) for 1.224 mm diameter tube. The HTCs remained unaffected by vapor quality and mass flux in the 1.70 mm tube, while they had significant contribution at the higher vapor quality region in the smaller sized tube. For both tubes and at lower vapor quality (x<0.1), HTCs increased with an increase in saturation pressure. Higher HTCs were reported using the smaller tube; however, the two tubes had different roughness characteristics so it was difficult to separate out the contribution from each of these two factors. Cooper's correlation [24] was reported as best among those tested for predicting the experimental database.

Ali et al. [25] reported the flow boiling heat transfer characteristics of R134a in a single circular vertical mini-channel (1.70 mm in diameter and 220 mm in heated length). The experiments were conducted at 27 and 32 ^{o}C saturation temperature, with various mass fluxes in 50-600 kg/m^{2}s range. The authors reported an increase in HTCs with increases in applied heat flux. HTCs also increased with vapor quality in the low quality region, leveled off at moderate vapor quality and reduced drastically at high vapor quality regions. It was further reported that HTCs were not dependent on mass flux until x=0.4-0.5, and increased slightly with increase in saturation temperature. The authors explained in an earlier visualization study [26] that nucleation is only active in the vicinity of the test section inlet. Their observed trends resembled what would be expected from nucleate pool boiling.

Boiling heat transfer, flow patterns and critical heat flux (CHF) characteristics for R1234ze(E) were reported by Tibiriça et al. [27]. Their experiments were carried out using 1.0 and 2.2 mm diameter (180 and 361 mm heated length) horizontal stainless steel tubes, at 25, 31 and 35 ^{o}C with direct heating of tube and under wide operating conditions (50-1500 kg/m^{2}s). HTCs were reported to increase with mass flux and vapor quality in the 1.0 mm tube, while they decreased with vapor quality in the larger tube. CHF was reported to increase with mass flux, with insignificant effects of sub-cooling and saturation pressure. The correlation from Saitoh et al. [18] satisfactorily predicted the data for heat transfer, whereas the CHF data-points were captured by the Katto-Ohno correlation [28].

Maqbool et al. [14] reported experimental findings on the flow boiling heat transfer and pressure drop of propane in a single vertical mini-channel (1.70 mm in diameter and 245 mm heated length). The experiments were carried out by uniformly heating the test section at 23, 33 and 43 ^{o}C saturation temperature with five mass fluxes in the range of 100-500 kg/m^{2}s. The findings showed a strong dependency of heat transfer on applied heat flux, while the effects of mass flux and vapor quality were insignificant. The HTCs were reported to increase with saturation pressure. This effect was explained by reduced surface tension force, which reduces bubble departure diameter and hence enhances the contribution of nucleate boiling. The experimental data for heat transfer was satisfactorily predicted (>85 % data points within ±30 %) by Cooper's pool boiling correlation [24].

Experimental findings on flow boiling heat transfer under uniform heating with three refrigerants (R134a, R245fa and R236fa) in small vertical tubes (1.03, 2.20 and 3.04 mm in diameter) were reported by Ong and Thome [9]. The isolated bubble regime in the larger tube (3.04 mm) revealed higher HTC than other two tubes tested; however, for the annular flow regime HTCs were about 30% greater with the small tube. With the increase in mass flux, isolated bubble and coalescing bubble flow regimes were suppressed, whereas the annular flow regime was expanded over a wide range of quality. HTCs in the 1.03 and 2.20 mm tubes

increased with mass flux and vapor quality, with negligible effects of heat flux in the annular flow regime. HTCs were mainly controlled by heat flux in the 3.04 mm tube.

Figure 2.1 summarizes trends found in open literature, the diagram is not as per scale. Each sub figure depicts effect of variation in heat transfer coefficients by varying only one parameter of interest. In Figure 2.1, sub-group "a-d" shows different trends for variation of heat transfer coefficients with variation of mass flux only while other parameters (like diameter, heat flux, saturation temperature) remained unaltered. Similarly trends with variation of heat flux are shown in sub group "e-h" while trends with variation in saturation temperature are presented in sub-group "i-j", and "k" is for variation in channel cross sectional area.

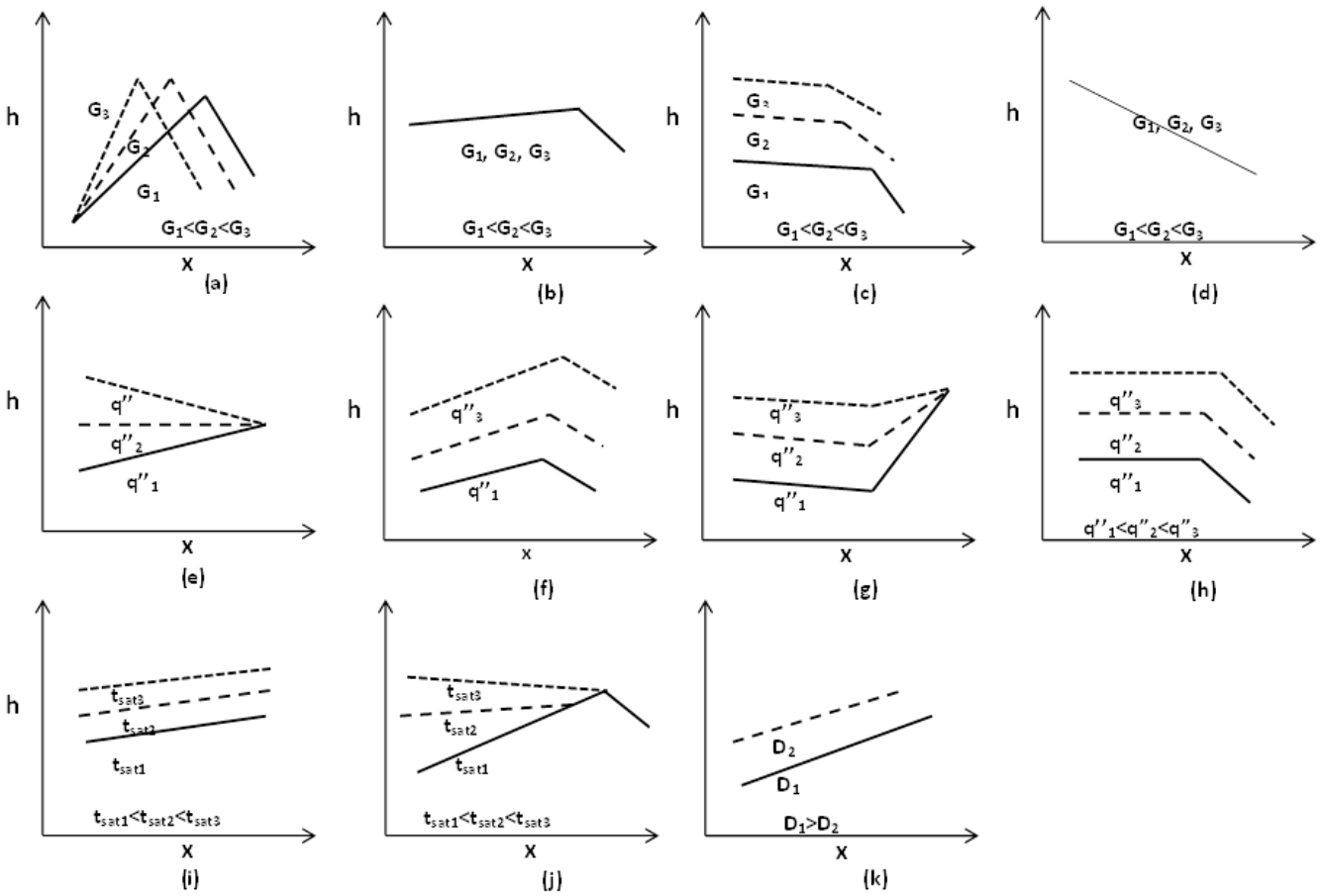

Figure 2.1 Schematics for reported heat transfer trends during flow boiling in mini/ micro-channels

Table 2-1 Summary of recent studies from the literature

Author	**Channel geometry and heating technique**	**Channel dimension, operating medium**	**Surface Characteristics R_a**	**Operating conditions**	**Remarks**
Copetti et al. [29]	o, —, SS tube, Joules heating	2.62 mm diameter and 183 mm heated length, R134a	2.05	G=240-930 t_{sat}=12 and 22 ^{o}C q"=10-100	HTCs increased with heat flux in the low quality region, whereas this effect diminished for high mass fluxes and at high vapor quality regions. Effect of mass flux was also reported at high quality regions. (f)
Saraceno et al. [30]	o, —, SS tube, Joules Heating	1 mm in diameter and 62 mm heated length, FC-72	2.3	G=1000-2000 q"=10-150 p= 3-7 bar	In the sub-cooled region, HTCs were influenced mainly by heat flux. In the case of saturated boiling, HTCs were reported to be independent of vapor quality. The Liu and Winterton correlation [31] predicted the experimental data. (f, b)
Saisorn et al. [32]	o, —, SS tube, Joules heating	1.75 mm in diameter and 600 mm in length, R134a		G=200-1000 q"=1-83 p_{sat}=8, 10 and 13	HTCs increased with heat flux, while no significant effect of mass flux or vapor quality was reported. HTCs decreased with increases in saturation pressure. (b, h, j)
Pamitran et al. [33]	o, —, SS tube, Joules heating	1.5 and 3 mm in diameter and 1500 and 3000 mm heated length, R410a		G=300-600 q"=10-30 *x*-till dryout	HTCs increased with heat flux in the low quality region. Laminar flow domination was reported. (b, f)
Agostini et al. [34]	□□, —, 67 silicon micro-channel, Joules Heating	336 μm diameter and 20 mm heated length, R236fa	160 nm	G=280-1500 q"=3.6-221 W/cm^2 *x*- till dryout t_{sat}=25 ^{o}C	At low heat flux, HTCs increased with vapor quality and were not influenced by heat flux. At moderate heat flux, HTCs increased with heat flux and remained unaffected by increase in vapor quality. HTCs decreased with an increase in heat flux at the high heat flux range and HTCs increased weakly with an increase in mass flux. (c,h)
Huh and Kim [35]	□, —, silicon micro-channel, Joules Heating	100 μm in diameter and 40 mm in length, AR 1, de-iionized water		G=90-267 q"=200-500 *x*=0-0.5	HTCs remained unaffected by variations in mass flux and vapor quality. Flow was characterized by elongated bubble flow that eventually converted into an annular pattern with increases in applied heat flux. (b)

In and Jeong [36]	o, ⎸, SS tube, Joules heating	0.19 mm diameter and 31 mm length, R123 and R134		G=314-470 q"=10-20 x=0.2-0.85 p_{sat}=1.58-11 p_{sat}=6-10 x=0-0.95	For R123, HTCs were affected by heat flux, mass flux and vapor quality. For R134a, HTCs at low and medium quality range were largely controlled by applied heat flux whereas dependence on mass flux was reported at high vapor qualities. (d, i)
Yun et al. [37]	□□, ═, silicon micro-channel, Joules Heating	1.36 and 1.44 mm hydraulic diameter, R410A		G=200-400 q"=10-20 t_{sat}=0, 5, 10 °C	HTCs in multiple micro-channels were higher than those in the single micro-channel configuration. HTCs increased with heat flux when vapor quality was > 0.5. HTCs were not influenced by mass flux when x<0.6. (f for higher vapor fractions)
Saitoh et al. [17]	o, ═, SS Tube, Joules heating	2mm in diameter and 1.76 m in length, R1234yf	-	G=100-400 q"=6-24 t_{sat}=15 x=0-1	HTCs increased with mass flux and vapor quality. Nearly identical values for HTCs were observed with R134a. (a,f)
Mortada et al. [38]	□□, ═, aluminum, Joules Heating	6 mini-channels with 1.1 mm hydraulic diameter and 300 mm heated length, R1234yf		G=20-100 q"=2-15 x=0-1	HTCs increased with vapor quality and mass flux, while a weak dependency on heat flux was reported. R1234yf showed higher HTCs than R134a. CHF increased with increase in mass flux. (a,f)
Hamdar et al. [3]	□, ═, machined in aluminum block, Joules heating	1 mm square channel with 381 mm length, R152a	-	G=200-600 q"=10-60 p=6	HTCs were strongly controlled by heat flux, with an insignificant effect of vapor quality and mass flux. Tran's correlation [19] was modified for prediction of the experimental data. (h)
Del-Col et al. [20]	o, ═, Copper tube, Indirect heating	0.96 mm in diameter and 228.5 mm in length, R1234yf	1.3	G=200-600 t_{sat}=31 °C x=0-1 q"=10-130	HTCs increased with heat flux while remained unaffected by variation of mass flux. HTCs decreased with vapor quality in the low quality region (x<0.3) and remained unchanged with further increases in quality. (h)
Copetti et al. [21]	o, ═, Copper tube, Joules Heating	2.6 mm in diameter and 185 mm heated length, R600a	2.05	G=240-440 q"=44-95 t_{sat}=22 °C	HTCs increased with heat flux in the low vapor quality region (x<0.4), followed by a decrease in HTCs. HTCs increased with mass flux. At low mass flux, HTCs were independent of vapor quality, while at high mass velocities, HTCs increased with increase in vapor quality. R600a had higher HTCs and a higher pressure drop than R134a. (a,f)

Maqbool et al. [15]	o, |, Stainless steel tube, direct heating	1.2 and 1.7 mm in diameter and 245 mm heated length, R717	2.55 and 0.21 (for 1.224 mm tube)	G=100-500 t_{sat}=23, 33 and 43 ^{o}C q"=15-355	HTCs increased with heat flux for all test cases in the 1.70 mm tube and at low vapor qualities in the 1.224 mm tube. HTCs were influenced by mass flux in the high vapor quality region in the case of the 1.224 mm tube. HTCs increased with increases in saturation temperature at low quality for both tubes. (g, i, k)
Tibiriça et al. [27]	o, ─, Stainless steel tube, direct heating	1.0 and 2.2 mm inside diameter and 180 and 361 mm heated length, R1234ze	0.595 and 0.827 (for 2.2 mm tube)	G=50-1500 q"=10-300 t_{sat}=25, 31 and 35 ^{o}C x=0.05-0.99	HTCs increased with mass flux and vapor quality in small tube while decreased with vapor quality in larger tube. CHF increased with increase in mass flux with insignificant effect of sub-cooling and saturation pressure. (a)
Maqbool et al. [14]	o, |, Stainless steel tube, direct heating	1.7 mm inside diameter and 245 mm heated length, R290	0.21	G=100-500 q"=5-280 t_{sat}=23, 33 and 43 ^{o}C	HTCs increased with increase in heat flux and with saturation pressure with insignificant convective contribution. Frictional pressure drop increased with increase in mass flux and for reduced operating pressure. (b, h, i)
Callizo et al. [39]	o, |, Quartz tube, Joules heating	1.33 mm diameter and 235 mm heated length, R134a		G=100-500 $t_{sub\ cool}$=3-8 K p=7.70 and 8.87 bar	Simultaneous heating and visualization. Seven distinctive flow patterns (isolated bubbly flow, confined bubbly flow, slug flow, churn flow, slug-annular flow, annular flow, and mist flow) were reported. The authors reported that an increase in saturation pressure shifted the transition boundaries to higher vapor qualities. While no clear effect of inlet sub-cooling was observed, the authors speculated that a high degree of sub-cooling would move all transition boundaries to lower vapor qualities.
Consolini and Thome [40]	o, ─, SS tube, Joules heating	0.51 and 0.79 mm diameter, R134a, R236fa, R245fa		G=300-4000 q" up to 200 t_{sat}=31 ^{o}C x until dryout	With R134a and R236fa, HTCs increased with increases in heat flux over the entire test span, while HTCs only increased at low vapor quality conditions in the case of R245fa. Beyond this, HTCs increased with increasing vapor quality. (b, h, k)
Agostini and Bontemps [41]	□□, |, aluminum, Joules Heating	11 parallel channels with d_h 2.01 mm, R134a	< 1	G=90-295 q"=6-31.6 t_{sub}= 1-15 P=405-608	Nucleate boiling was reported to be the dominant mechanism for q" > 14 kW/m^2 and dryout incipience was reported at medium vapor qualities x-0.43.
Ali et al. [25]	o, |, Stainless	1.7 mm	0.21	G=50-600	HTC increased with increasing heat flux and system

	steel tube, Joules Heating	diameter and 220 mm heated length, R134a		q"=2-156 t_{sat}=27, 32 °C *x* until dryout	pressure, while no significant effect of mass flux or vapor quality was reported. (b, h, i)
Bertsch et al. [42]	□□, ─, In copper block with cartridge heater	d_h=0.54 and 1.09 mm (33 and 17 channels), R134a and R245fa	0.6 and 0.5	G=20-350 t_{sat}=8-30 °C *x*=-0.2-0.9 q"=0-220 q"=280-4450	HTCs increased with increasing heat flux, while being weakly dependent on mass flux. HTCs increased with decreasing channel size. Correlations from Cooper [24] and Liu and Winterton [31] were reported to have the least error in their predictions. (j, k)
Bortolin et al. [43]	o, ─, Non uniform heating	0.96 mm diameter and 228.5 mm in length copper tube, R245fa	2.34	G=200-400 q"=5-85 t_{sat}= 31 °C *x*=0.05-0.85	HTCs increased with heat flux and were not significantly affected by varying mass flux. HTCs decreased with increasing vapor quality. (h)
Celata et al. [44]	o, ─, Non uniform heating	480 μm id and 102 mm long, FC72, Sub-cooled boiling	-Nil-	G<3500 q"<200 *x*-about 50%	HTCs increased with increasing vapor quality at medium and high heat flux.
Choi et al. [45]	o, ─, SS tubes, Joules heating	1.5 and 3 mm in diameter and 2 m length, R22, R134a and CO_2		G=200-600 q"=10-40 tsat=10 °C *x* until dryout	At low vapor quality, HTCs increased with heat flux, while the effects from mass flux and vapor quality were insignificant. At moderate vapor quality, HTCs increased with increase in mass flux and quality, with an insignificant effect from heat flux. In the high vapor quality region, HTCs decreased with an increase in mass flux. (g, k)

o (Circular/tube), □ (Rectangular), □□ (Parallel channel), ─ (Horizontal), │ (Vertical), G [kg/m²s], q" [kW/m²], p [bar], *x* [-], t [°C], t_{sub} [K]

2.2 Frictional Pressure Drop

The two-phase frictional pressure drop is an important parameter that should be well accounted for when designing any practical system. This will help in selecting the proper size pump and may have some effect on system's thermal performance. Proper selection of the number of parallel channels for a given heating/cooling demand will be helpful in alleviating the enhanced pressure drop due to channel confinement. A detailed summary of recent results using similar operating conditions is provided below, while brief summary can be found in Table 2-2.

Flow boiling heat transfer and pressure drop characteristics of CO_2 in a small horizontal tube (1.42 mm in diameter and 300 mm length) was reported by Wu et al. [46]. The test section was heated by coil wrapped on the outer periphery of the test section and experiments were carried out at -40-0 ^oC saturation temperature with 300-600 kg/m^{2}s mass fluxes. The authors reported an increase in pressure drop with increases in mass flux and vapor quality. Peak pressure drop was observed at about 80% vapor fraction, followed by transition from annular to mist flow (via dryout), resulting in reduced pressure drop. In the low quality region (x< 0.20), a slight effect of heat flux was also reported, in which pressure drop increased with an increase in applied heat flux. Pressure drop decreased with increasing saturation temperature.

Findings on the two-phase frictional pressure drop of R245fa in a 2.32 mm horizontal tube were reported by Tibiriça and Ribatski [47]. The experiments were carried out with direct heating of the test section with DC electricity. Data was collected at 31 and 41 ^oC saturation temperature, and other operating conditions were G=100-700 kg/m^{2}s and till dryout conditions. The authors reported an insignificant effect of heat flux whereas mass flux and vapor quality showed significant influence on the two-phase frictional pressure drop.

Ali et al. [48] reported experimental findings on the two-phase frictional pressure drop of R134a and R245fa in a horizontal 781 μm tube. These experiments were carried out with a glass test section at 25-40 ^oC saturation temperature and with 100-600 kg/m^{2}s mass velocities. The study's single-phase results (for system validation) showed good agreement with classical theory and no early transitions were reported with the micro-channels. The two-phase frictional pressure drop increased with mass flux, vapor quality and with reduced system pressure. Furthermore, the authors observed a higher pressure drop (both for single and two-phase) with R245fa. They reported good predictions using micro-scale correlations of Tran et al. [23] and Mishima and Hibiki [49].

The two-phase frictional pressure drop for ammonia in single vertical mini-channels (1.224 and 1.70 mm in diameter and 245 mm heated length) was reported by Maqbool et al. [50]. Experimental data was collected at 23, 33 and 43 ^oC saturation temperature with mass fluxes in 100-500 kg/m^{2}s range. System validation was done with single-phase experiments, which showed good agreement with conventional classical theory. Experimental results revealed an increase in pressure drop with increasing mass flux and vapor quality and with shrinking the tube size. Comparison of correlations showed that the Müller-Steinhagen and Heck correlation [51] among macro-scale models made good predictions, and Zhang and Web's [52] gave good predictions among micro-scale model. A new correlation (modified Tran correlation [23]) was proposed for estimation of two-phase frictional pressure drop.

Table 2-2 Summary of recent studies on two-phase frictional pressure drop from the literature

Author	Test section and medium	Operating conditions	Brief results
Yun and Kim [53]	0.98-2.0 mm, R744	G=500-3750 q"=5-48 t_{sat}=0, 5 and 10 °C	Pressure drop increased with mass flux, vapor quality and with reduced operating pressure. Two-phase effects in the large tube were greater than with the 0.98 mm tube.
Wu et al. [46]	o, −, 1.42 mm diameter and 0.3 m length, R744	G=300-600 q"=7.5-29.8 t_{sat}=-40-0 °C	Two-phase pressure drop increased with mass flux and vapor quality, and decreased with increasing operating pressure. In the mist flow region (after dryout incipience), low pressure drop than in the annular flow region was reported.
Tibiriça and Ribatski [47]	o, −, 2.32 mm diameter and 464 mm length, R245fa	G=100-700 q"=0-55 t_{sat}=31 and 41 °C	Frictional pressure drop increased with mass velocity, vapor quality and with decreasing operating pressure. A negligible effect of heat flux on frictional pressure drop was observed.
Tibiriça et al. [54]	o, −, 2.32 mm diameter and 464 mm length, R134a	G=100-600 q"=10-55 t_{sat}=31 x until dryout	Frictional pressure drop increased with mass velocity, vapor quality and with decreasing operating pressure. A negligible effect of heat flux on frictional pressure drop was observed.
Tran et al. [23]	o and □ (2.46 and 2.92 mm diameter, 4.06x1.7 mm), R134a, R12 and R113	G=50-832 q"=2.2-129 x_{exit}=0.95 p=138-856 kPa	Frictional pressure drop increased with mass flux and vapor quality, and decreased with increasing operating pressure. The Chisholm correlation [55] was modified based on the experimental database for this study.
Pehlivan et al. [56]	o, −, 3, 1 mm and 800 μm diameter and 200 mm length, water and air		Experimental data was compared with the Homogenous, Friedel and Chisholm models [13] [57] [55] and good predictions were reported with the Homogenous model. The flow regime map showed a difference in the location of transition lines between flow regimes of the study and previous work with micro-channels.
Madrid et al. [58]	□□, (840 μm hydraulic diameter, 40 channels with length 220 mm), HFE7100	G=21-235 q"=1028-8460 w/cm^2 x_{out}=0.72	Pressure drop increased with mass velocity and vapor quality while an insignificant effect of heat flux was reported. Peak pressure drop was observed before the occurrence of dryout, after which lower values were observed. Good predictions were reported with the Homogenous model.
Hwang and Kim [59]	o, −, 0.224, 0.430, 0.792 mm diameter with 60, 180 and 462 mm length respectively, R134a	G=140-950 x_{out} to about 0.88	No early transition to turbulent flow was reported in single-phase tests. Two-phase pressure drop increased with mass flux, vapor quality and decreasing size of tube. A new correlation (modified Lockhart-Martinelli [60]) was proposed for prediction of two-

			phase frictional pressure drop in circular micro-channels.
Huh and Kim [35]	□, −, 100 μm hydraulic diameter and 40 mm length, Deionized water	G=90-267 q"=200-500 x=0-0.4	Two-phase pressure drop increased with mass flux and vapor quality.
Hamdar et al. [3]	□, −, 1x1 mm and 381 mm length, R152a	G=200-600 q"=10-60 p=600 kPa	Parametric effects were not shown; however, a comparison between the experimental results and correlations from the literature was provided. The experimental data was satisfactorily predicted by the Müller-Steinhagen and Heck correlation [51].
Copetti et al. [29]	o, −, 2.6 mm diameter and 183 mm length, R134a	G=240-930 t_{sat}=12 and 22 °C q"=10-100	Frictional pressure drop increased with vapor quality, mass velocity and with reduced operating pressure. A small effect of heat flux was also reported, in which the frictional pressure drop increased with heat flux.
Choi et al. [61]	o, −, 1.5 and 3 mm diameter and 1000 and 2000 mm length, Propane	G=50-400 q"=5-20 t_{sat}=10, 5, 0 °C	Frictional pressure drop increased with mass flux, vapor quality and reduced saturation temperature. The smaller tube showed higher pressure gradients. A new correlation (Lockhart Martinelli [60] type) was proposed for the prediction of frictional pressure drop.
Ali et al. [48]	o, −, 781 μm diameter and 261 mm length, R134a and R245fa	G=100-650 t_{sat}=25-40 °C	Two-phase frictional pressure drop increased with mass flux and vapor quality. R245fa showed a higher pressure drop than R134a. Macro-scale correlation from Müller-Steinhagen and Heck [51] and micro-scale correlation from Mishima and Hibiki [49] predicted the experimental database.
Maqbool et al. [50]	o, |, 1.224 and 1.70 mm diameter and 245 mm heated length, Ammonia	G=100-500 q"=15-355 t_{sat}= 23, 33 and 43 °C	Two-phase frictional pressure drop increased with mass flux, vapor quality and decreasing channel size, while it was reduced with increase in saturation temperature. A new correlation (modified Tran [23]) was proposed for estimation of the two-phase frictional pressure drop in small vertical channels.

o Circular section, □ Rectangular section, □ □ Multiple parallel channels, − Horizontal, | Vertical, G [kg/m^{2}s], q" [kW/m^2], p [bar], x [-]

2.3 Dryout/Critical Heat Flux

Two-phase heat transfer is strongly influenced by the imposed operating conditions. In a two-phase system, a liquid starved heating surface will show a drastic decrease in the heat transfer coefficient, resulting in a sharp increase in wall surface temperature in heat flux controlled devices (e.g. electronic chips, fuel cells, spacecraft payloads, fuel elements in nuclear reactors [62]). Surpassing such critical limits may leads toward catastrophic failure of the device. This occurrence is also sometimes known as heat flux at burnout. Different definitions and terminology exist in literature for addressing the above mentioned phenomenon. Some researchers use "Critical Heat Flux (CHF)" while others call it "Dryout" to avoid confusion with physical burnout of the test section. For this study, the term "Dryout" has been used, based on our experimental results, we believe that the dryout condition was not the consequence of a high local heat flux but rather of the gradual thinning of a liquid film travelling on the tube wall. Furthermore, it should also be mentioned that physical burnout of the test section was not reached during our experiments. The importance of this parameter in the design of practical devices and prediction assessment is clear from being the maximum safe operating limit.

Depending on the boiling scheme, dryout conditions can be approached both in sub-cooled and saturated cases. For saturated cases where $x_e > 0$, this normally happens at low mass velocity with a slight degree of sub-cooling and with large l/d channels [63]. Different triggering mechanisms can control this process. The operating conditions, flow regimes, governing mechanisms and nomenclature for saturated and sub-cooled boiling cases are summarized below.

Low heat flux ⟶ Annular flow regime ⟶ Depletion of liquid layer ⟶ Dryout

High heat flux ⟶ Inverted annular flow regime ⟶ vapor layer formation ⟶ Departure from nucleate boiling (DNB)

Liquid starved conditions first appear close to the outlet of the test section and travel towards the inlet with a slight increase of applied heat flux. This can easily be traced based on significantly high wall temperature and a drastic fall in the heat transfer coefficient at dryout inception conditions.

The complex nature of driving physical mechanisms is quite clearly reflected in the empirical correlations cited in the literature. The majority of these correlations are based on channel dimensions (diameter and heated length), physical properties (density and viscosity ratios, heat of vaporization), and operating conditions (mass flux, degree of sub-cooling).

The trends observed for the effects of various operating parameters on dryout heat flux are summarized in Figure 2.2. These results are graphical representations and are not to scale. Each subfigure shows the variation of one parameter of interest (mass flux, diameter, saturation temperature, heated length, etc.), with all other conditions remaining unaltered. In general, heat flux at dryout is reported to increase with mass flux and with decrease in heated length. For sub-cooling, some authors have reported an increase in CHF with sub-cooling, while others have found an insignificant effect. There is no general consensus for the effect of operating pressure. However, some recent studies have shown that the linear increase in dryout heat flux with mass flux is valid only at low mass flux conditions ($G<600$ kg/m^{2}s), whereas a noticeable effect of saturation temperature appears at high mass flux conditions ($G>600$ kg/m^{2}s) [9] [62].

The experimental results for the saturated CHF of R134a and R245fa in small horizontal circular tubes were reported by Tibiriça et al. [62]. The experiments were carried out with a stainless steel tube (2.20 mm in diameter and 154 and 361 mm heated length), at 25, 31 and 35 ^{o}C saturation temperature with 100-1500 kg/m^{2}s and 4-10 K degree of sub-cooling. The authors reported an increase in CHF with mass flux and sub-cooling and with reduced heated length. The increased saturation temperature was reported to decrease the

CHF values. Under similar imposed operating conditions, the CHF values of R245fa were about 10% higher than those of R134a. This was explained by the difference in heat of vaporization for these two fluids. The correlation from Katto-Ohno [28] satisfactorily predicted the experimental database.

Revellin and Thome [64] conducted a theoretical study to investigate the parametric effects on CHF of water and four refrigerants in micro-channels. The authors used a theoretical model based on complete evaporation of the thin liquid film on the heating surface. Their model showed an increase in CHF with increasing mass flux, sub-cooling, and tube size, and with decreasing heated length and operating pressure.

Ong and Thome [9] reported experimental findings on the CHF of three refrigerants (R134a, R245fa and R236a) in small vertical tubes (1.03, 2.20 and 3.04 mm internal diameter). The experiments were carried out at 25, 31 and 35 ^{o}C saturation temperature with 100-1500 kg/m^{2}s. The experimental findings revealed an increase in CHF with increasing mass flux. For G<500 kg/m^{2}s, there was no effect of tube size on CHF, which then increased with shrinking tube size up until the threshold limit of 0.79 mm (experimental results from Wojtan et al. [63] were also considered). CHF was reduced with an increase in saturation temperature for R134a and R236fa, while remaining unaffected by varying degree of sub-cooling (about 24 K). Among the three tested gases, R245fa showed the highest values for CHF—an effect that was explained by its high heat of vaporization under similar operating conditions. A new correlation (modified Katto-Ohno [28]) for prediction of saturated CHF was proposed based on a combined database from Ong and Thome [9], Wojtan et al. [63] and Park for R134a, R245fa and R236fa, respectively.

Experimental results on dryout for four refrigerants (R134a, R123, Solkatherm SES36 and ethanol) in small single vertical tubes were reported by Mikielewicz et al. [65]. The experiments were carried out with uniformly heated silver tubes (1.15 and 2.30 mm internal diameter and 380 mm length), at 17-76 ^{o}C saturation temperature, with 40-900 kg/m^{2}s (specific details for each fluid can be found in [65]). Using infrared camera to detect the critical length of the test section, the authors reported reduced critical length and critical vapor quality with high heat fluxes. They further reported that CHF increased with mass velocity and tube size. Decreased critical vapor quality was found with increase in mass flux, and this effect was more prominent in the larger tube.

Maqbool et al. [2] reported experimental findings on dryout of propane in uniformly heated vertical mini-channels (1.224 and 1.70 mm in diameter and 245 mm heated lengths). Their experiments were conducted at 23, 33 and 43 ^{o}C saturation temperatures, and five mass fluxes in the span of 100-500 kg/m^{2}s were tested. The authors reported an increase in the dryout heat flux value with an increase of mass flux and tube cross sectional area, whereas an insignificant effect of varying operating pressure was reported. Dryout completion was observed at higher vapor quality (at constant mass flux conditions) for higher saturation temperature cases. The experimental data was well-predicted by correlations from Katto-Ohno [28] and Callizo et al. [66].

Experimental investigation on dryout under non-uniform heating of a micro-channel was done by Del-Col and Bortolin [67]. The authors used R134a, R32 and R245fa in a 0.96 mm diameter copper tube. The test tube was heated by circulating hot water in counter flow arrangement. In this case, the wall temperature was limited by the secondary fluid temperature, so dryout completion was confirmed from the standard deviation for the collected sample of data (temperature fluctuates widely in the dried region). The experiments were carried out at 31 ^{o}C saturation temperature with mass velocities in the range of 200-900 kg/m^{2}s. The authors reported depletion of the thin liquid film on the heating surface to cause dryout. Furthermore, from the analysis of vapor quality, it was speculated that dryout occurred in the annular flow regime. Experimental results were reported for dryout vapor quality and for average values for heat flux at dryout. The authors reported an increase in average dryout heat flux with the increase of mass flux and with reduced heated length of tube for the three tested refrigerants. The experimental dataset was satisfactorily predicted by the theoretical correlation of Revellin and Thome [64].

Ali and Palm [1] reported experimental findings on dryout of R134a in small vertical tubes (1.224 and 1.70 mm in diameter and 220 mm heated length). The experiments were carried out by uniformly heating stainless steel tubes, with operating parameters of G=50-600 kg/m^{2}s at 27 and 32 ^{o}C saturation temperature. The authors reported an increase in heat flux at dryout incipience and completion conditions with increasing mass flux. An extended intermittent region (dryout incipience-completion) was reported with the smaller tube under similar operating conditions, and dryout completion occurred at low vapor qualities ($x<0.55$ at G=600 kg/m^{2}s). With the increase of mass flux, dryout completion shifted to lower vapor quality, while annular flow conditions were assumed for both tubes. It was further reported that dryout heat flux increased with increasing cross sectional area. The experimental results for dryout completion were satisfactorily predicted by Bowring's correlation [68].

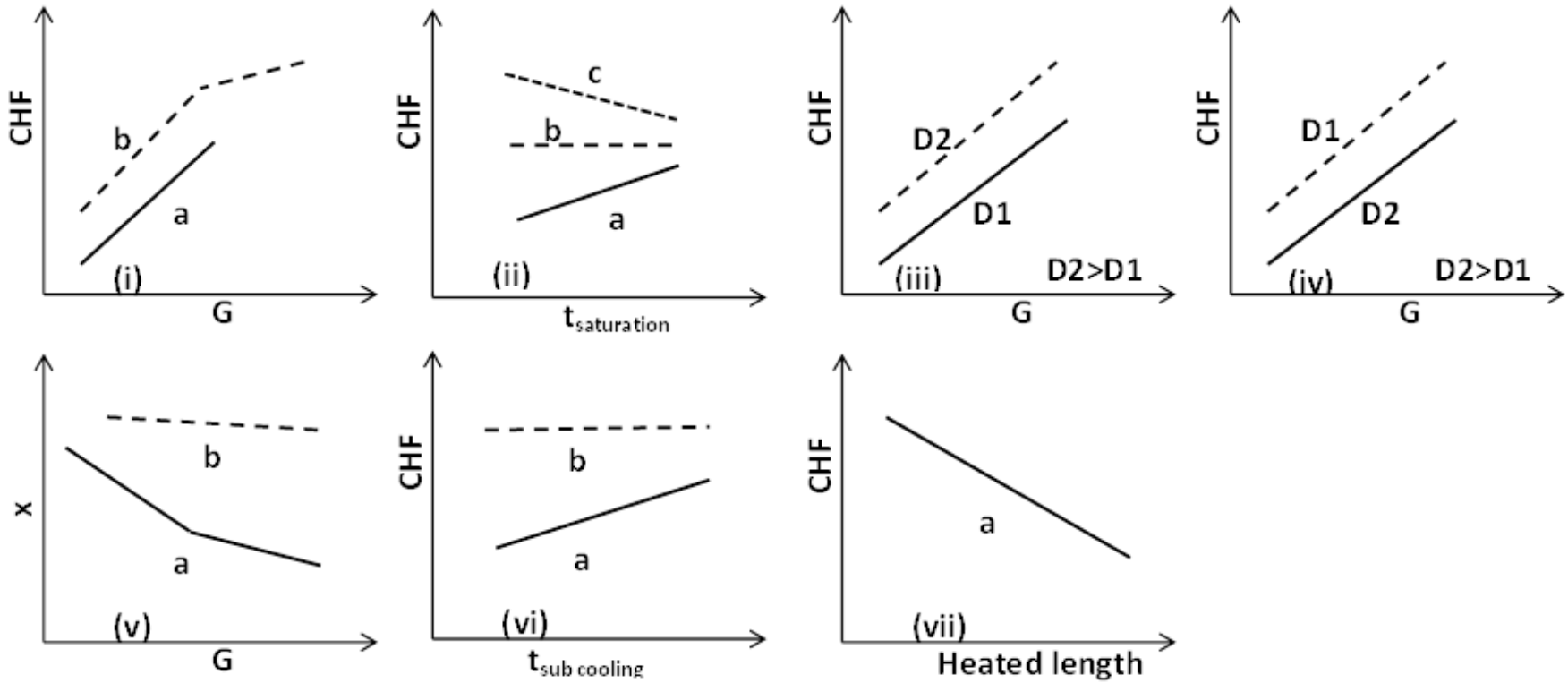

Figure 2.2 Schematic diagrams for the effects of operating parameters (Not to scale)

Table 2-3 Summary of CHF studies from the literature

Author	**Channel geometry, orientation and heating technique**	**Channel dimensions, operating medium**	**Surface characteristics R_a**	**Operating conditions**	**Remarks**
Ali and Palm [1]	o, |, Stainless steel tubes, Joules Heating	1.224 and 1.7 mm tubes with 220 mm heated length, R134a	2.55 and 0.2	G=50-600 t_{sat}=27, 32 Dryout at saturated conditions	Heat flux at dryout increased with increasing mass flux and tube diameter, whereas no clear effect of system pressure was reported. Correlations from Katto-Ohno [28] and Callizo [66] satisfactorily predicted the database. (i, ii, iii and v)
Kosar and Peles [69]	□□, ─, machined on silicon wafer, Joules heating	5 channels, 200 μm wide and 264 μm deep, R123		G=290-1118 p=2.27-5.20	CHF increased with increasing mass flux. CHF increased with increasing system pressure, reaching a peak and then declining again. The Katto-Ohno correlation [28] predicted the database. A new correlation was proposed to predict the effect of pressure. (i and ii)
Bowers and Mudawar [70]	o o, ─, Joules Heating	2.54 mm (3 channels) and 510 μm (17 channels), R113		G<500 kg/m^{2}s $t_{sub\ cool}$=10-32 K p=1.38	Significant effect of mass flux and sub-cooling were reported. Higher CHF values were noticed with mini-channel with 2.54mm internal diameter. A CHF correlation was proposed. (i and vi (a))
Wojtan et al. [63]	o, |, Stainless steel tubes, Joules Heating	0.5 and 0.8 mm tubes with 20-70 mm heated length, R134a and R245fa		G=400-1600 t_{sat}=30 and 35 ^oC $t_{sub\ cooling}$=2-15 K	CHF increased with increasing mass flux and reduced heated length. CHF for the larger tube was higher than for the smaller one under similar operating conditions. CHF remained unaffected by variations in sub-cooling (4-12 ^oC). At low mass flux (G<1000), CHF was not affected by variations in saturation temperature (30 and 35 ^oC). (i, ii(b), iii, vii)
Tibiriça et al. [71]	o, ─, flattened stainless steel tube	Two tubes with different aspect ratios but equivalent diameter of 2.2 mm, R134a and R245fa	0.8	G=100-1200 t_{sat}=31 ^oC	The authors introduced the concept of equivalent heated length. Using this parameter, the performance of the circular tube was comparable to the flattened one. Furthermore, no significant effect of variations in the aspect ratio of the channel was observed. The correlation developed for circular tubes worked reasonably well for flattened tubes.

Tibiriça et al. [62]	o, ─, stainless steel tube	2.20 mm in diameter with 154 and 361 mm heated length, R134a and R245fa	0.827	G=100-1500 t_{sat}=25, 31 and 35 ^{o}C x_{crit}=0.55-1	CHF linearly increased with increases in mass flux and reduced heating length (at fixed inlet sub-cooling) for all tested cases. CHF was reduced with increasing saturation temperature. About 10% higher CHF values were observed with R245fa. The correlation from the Katto-Ohno predicted the experimental database. (i, vii)
Ong and Thome [9]	o, ─, stainless steel tube	1.03, 2.20 and 3.04 mm in diameter, R134a, R245fa and R236fa		G=100-1400 t_{sat}=25, 31 and 35 ^{o}C	CHF increased with increasing mass flux and decreasing tube diameter. CHF decreased with increasing saturation temperature, while remaining unaffected by variations in sub-cooling. (i, ii (c) and iv)
Mikielewicz et al. [65]	o, |, silver tube, Joules heating	1.15 and 2.3 mm in diameter and 380 mm length, SES36, R123, R134a and ethanol		G=40-900 $t_{sub\ cooling}$=2-45 K t_{sat}=17-76 ^{o}C (different with different fluids)	Dryout heat flux increased with increasing mass flux and tube diameter. (i and iii)
Maqbool et al. [2]	o, |, stainless steel tube, Joules heating	1.224 and 1.70 mm in diameter and 245 mm heated length, R290	0.21 and 2.55 (for 1.224 mm tube)	G=100-500 t_{sat}=23, 33 and 43 $t_{sub\ cooling}$ about 1 K	CHF increased with increasing mass flux and tube diameter. CHF remained unaffected by variations in saturation temperature. (i, ii (b) and iii)
Del Col and Bortolin [67]	o, ─, copper tube, Indirect heating	0.96 mm in diameter with 67.5-202.5 mm heated length, R134a, R245fa and R32	1.30	G=100-900 pr=0.05-0.34 t_{sat}=27-32 ^{o}C $t_{sub\ cooling}$=3-6 K	CHF increased with increasing mass flux and decreased heated length. R32 showed higher CHF values compared with R134a. (i and vii)

o (Circular/tube), □ (Rectangular), □□ (Parallel channel), ─ (Horizontal), \| (Vertical), G [kg/m^{2}s], q" [kW/m^2], p [bar], x [-], t [^{o}C]

Chapter 3. Experimental Approach

In this study, experiments were carried out using a closed refrigerant loop with heating and cooling provisions. This setup was originally designed by Owhaib [72] and was utilized by Maqbool et al. [15] and Ali & Palm [1] for their experimental campaigns. For this study, heat transfer and fluid flow characteristics of low GWP refrigerants were investigated using a modified test section in the same experimental apparatus.

This chapter begins with description of the experimental setup and related instrumentation. The calculation procedures for parameters of interest (heat transfer coefficient, single phase friction factor, vapor quality, etc.) are then given. Next, the procedure adopted for estimation of uncertainty in experimental results is explained, followed by the presentation of the single-phase heat transfer results.

3.1 Experimental Setup

The experimental setup is schematically depicted in Figure 3.1. The entire loop was fabricated using stainless steel tubing with swagelok tube fittings. The refrigerant flow through the loop was maintained using a gear pump (ISMATEC MCP-Z) that circulated sub-cooled refrigerant from the condenser to the test section through a mass flow meter and particle filter. A stainless steel tube (1.60 mm inside diameter and 245 mm heated length) in a vertical orientation was used as the test object and experiments were carried out under upward flow conditions. The apparatus was equipped with instruments for measuring flow rate, absolute and differential pressures, wall and bulk temperatures. A 2 μm filter was used before the inlet of the test section to prevent its clogging by any small particles. Eight uniformly spaced type-T thermocouples were attached to the outer periphery of test section using a thermally conducive epoxy, in order to record the wall temperature. The bulk temperatures at the inlet and outlet locations were measured with insertion type counterparts. The system pressure was measured with the help of an absolute pressure sensor, whereas a differential pressure sensor was used to record the pressure drop across the test section. To control the inlet conditions, a preheater coil (coil wrapped around the periphery and heated by Joule's effect) was used prior to the filter. The test section was uniformly heated with DC electricity and a water-cooled plate type heat exchanger was used as a condenser. The system pressure was controlled by regulating the water flow rate in the condenser and with the help of refrigerant tank, as shown in Figure 3.1. This tank was connected to the main loop and was kept in a temperature regulated bath. The system's mass flow was adjusted by varying the speed of the gear pump, and a Coriolis type mass flow meter was used for measuring the flow rate. The whole setup was insulated to minimize thermal loss, with special attention given to the test section. Synthetic rubber-based flexible interlaced foam supplied by Armacell Gmbh "Armaflex" (with k=0.042 W/mK) was used for insulation purpose. Details for the instruments (make, range, accuracy) can be seen in section 3.3.

3.1.1 Test Section

For this study, the fluid flow and heat transfer characteristics of four refrigerants (R134a, R152a, R600a and R1234yf) were investigated within a metallic (AISI 316 stainless steel) test section. This test section (d_i=1.60 mm, d_o=2.0 mm, l_h=245 mm) was heated by applying DC electricity directly to the test tube. To electrically isolate the test section from other components, and to allow for visual observation, similarly sized glass tubes were used before the inlet and at the outlet of the test section.

The inside diameter of the test section was estimated by the weight difference of water in the filled and empty tube. A highly accurate analytical balance (Mettler Toledo AX205, 10 μg resolution) was used for this estimation. In the first step, the empty test section was weighed. The test section was then filled with distilled water and weighed again. From the known density and weight of fluid, the volume of water was estimated. The inside diameter was then calculated by considering its cylindrical shape. This procedure was repeated several times and the average value was used as the tube diameter.

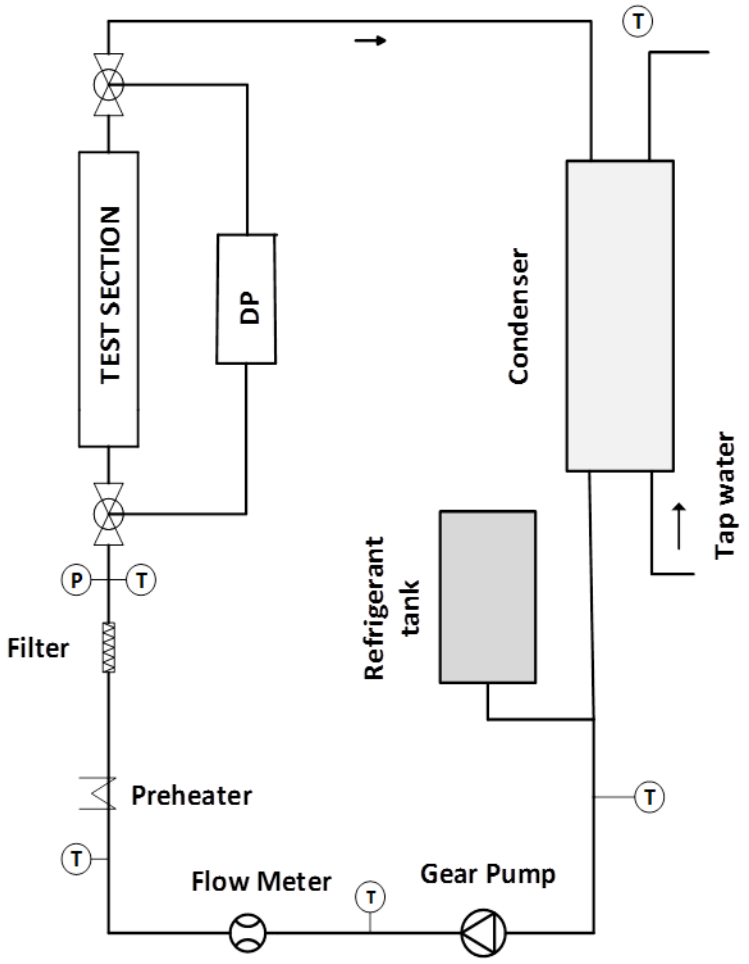

Figure 3.1 Schematic diagram of the setup

Figure 3.2 shows local positions of thermocouples used for wall temperature measurement. The roughness characteristics of the heating surface may have an influence on heat transfer performance due to the effect on the bubble nucleation process. The inner surface of a small sample taken from the same tube as the test section was scanned using Talysurf PGI 800 (Taylor Hobson). The measurement was performed by axial movement on the sample (about 3.5 mm length) at three circumferential locations. The obtained roughness profile is shown in Figure 3.3, and the key roughness parameters are summarized in Table 3-1.

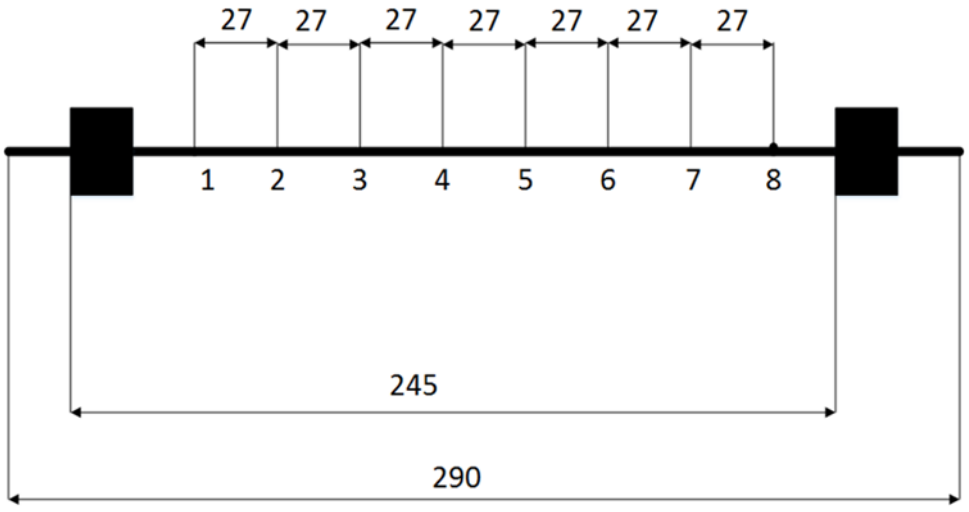

Figure 3.2 Placement of thermocouple along the test section, all dimensions are in millimeter.

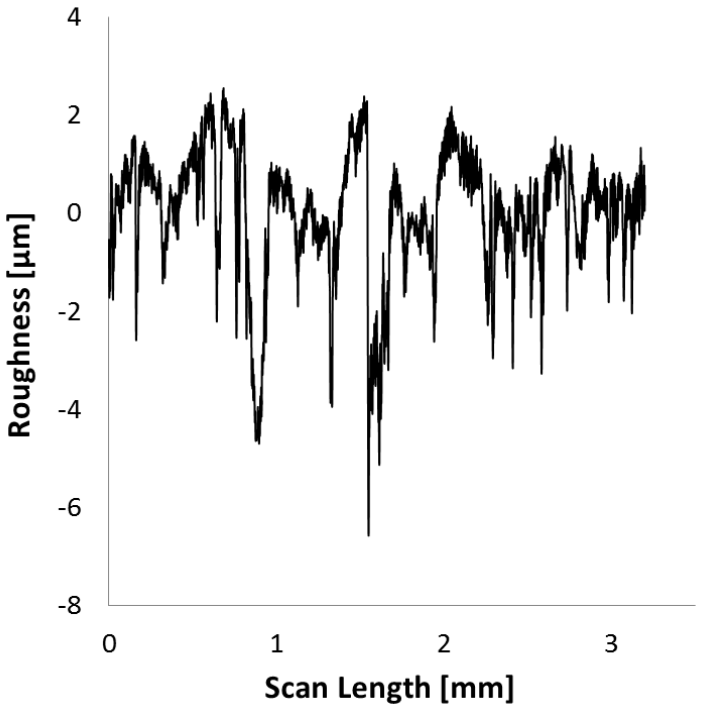

Figure 3.3 Roughness profile of the heating surface

Table 3-1 Roughness characteristics of the heating surface

Parameter	Description	Formula	Value [μm]
R_a	Arithmetic average of absolute values	$R_a = \frac{1}{n}\sum_{i=1}^{n}\lvert X_i\rvert$	0.95
R_v	Maximum valley depth	$R_v = \min_i X_i$	6.44
R_p	Maximum peak height	$R_p = \max_i X_i$	2.69

3.2 Data Acquisition

For electronic data acquisition, signals from the instrumentation were acquired using an Agilent data logger (34970A) along with multiplexers (34901A) from Agilent Technologies. The data was recorded for steady-state conditions (with the exception of boiling incipience and dryout conditions). A custom written HP VEE program running on a desktop computer was used for controlling the data acquisition process. The data collection frequency was within 0.3-0.5 Hz, and data were collected for about 5 minutes. The average value for the collected sample was considered as the nominal value for the data point. The refrigerant property data were calculated using REFPROP 9 developed by NIST [73]. About 2% uncertainty was assumed in the refrigerant property data.

3.3 Measurement Instruments

3.3.1 Temperature Measurement

All temperature measurements in this study were taken using high quality t-type thermocouples (TT-T-30, Omega Engineering INC) that come with a positive copper wire and a negative constantan wire. These thermocouples were fixed on the outer wall of the test section using a special thermally conductive and electrically isolative epoxy (OMEGABOND 101). The fluid temperatures at the inlet and outlet positions were measured using stainless steel sheathed thermocouples (TMQSS-020U-12 from Omega). These were calibrated in the lab and after calibration error was less than ±0.1 °C. The systematic error due to conversion from voltage to temperature was less than 0.001 °C, while the error due to the resolution of the data logger was 0.024 °C (Agilent Technologies). Thus, the overall uncertainty in temperature readings was conservatively estimated to be ±0.1 °C.

3.3.2 Pressure Measurement

The test apparatus was equipped with a high performance absolute pressure transducer (PDCR 4060, 0-20 bars with 0-100 mV output) from Druck, GE Corp. The accuracy of the instrument, as stated by the manufacturer, is 0.04% of full-scale value and this includes non-linearity, hysteresis and repeatability effects. This sensor was placed after the preheater and before the inlet of the test section, as shown in Figure 3.1. A differential pressure sensor, also from Druck (PTX 5072, 0-500 mbar, 4-20 mA output), with accuracy up to 0.04% of full-scale value, was used for measurement of pressure drop across the test section. For the differential pressure sensor, a 2 mm stainless steel tube was used as pressure line for connecting the pressure tap to the transducer on both the high and low pressure sides. These tubes were cooled (or heated) by tap water flowing through a concentric plastic tube on the outer periphery to ensure liquid (or vapor) refrigerant in the pressure lines. Both pressure transducers were calibrated routinely by DRUCK DPI 603 to verify their

performance during the testing period. Negligible errors were associated with the data logger (0.004% for PDCR 4060 and 0.008% for PTX 5072). Therefore, conservative estimates for uncertainty were ±10 mbar for absolute pressure and ±1 mbar for differential pressure readings.

3.3.3 Mass Flow

A Coriolis effect mass flow meter (Micro-Motion DS006) was used for measurement of refrigerant flow rate. For the test span of this study, flow rate was varied within 0.2-1 g/s. As can be seen in Figure 3.4, the accuracy of the flow meter increased with increasing flow rate and in the worst case, was about ±1%. The maximum systematic uncertainty associated with the data logger was estimated to be ±1 %, whereas the uncertainty stemming from the conversion of current to flow rate was about 0.04%. Therefore, a conservative estimate for overall uncertainty was ± 3%.

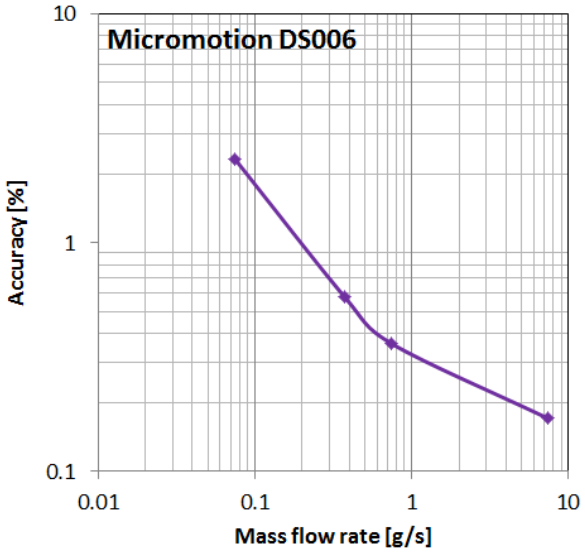

Figure 3.4 Accuracy of mass flow meter

3.3.4 Power Input

The test section was heated using a high current and low voltage DC power supply (Manson SPS-9600). The heat input to the test section was measured by product of current intensity and voltage drop across the test section. The intensity of power was controlled by the Agilent data logger. The stated accuracy for the power supply was ± (1% +1 count). An accurate digital voltmeter (Gw-Instek GDM 8246, 0.02% accuracy) was used for separate and more accurate measurement of the voltage.

3.4 Data reduction for Single Phase flow

The heat flux applied to the test section was calculated as

$$q'' = \frac{Q}{A_h} = \frac{V \cdot I}{\pi d l_h} \tag{3.1}$$

The inside wall temperature at any location can be calculated from the measured outside temperature using a one dimensional conduction equation with heat generation in cylinders:

$$t_{wall\ in,z} = t_{wall\ out,z} + \frac{Q}{4\pi K l_h}\left(\frac{\varphi(1-\ln\varphi)-1}{\varphi-1}\right) \tag{3.2}$$

Where $\varphi = \frac{d_{out}{}^2}{d_{in}{}^2}$. The bulk fluid temperature at any axial location was calculated using the inlet temperature and heat added to the test section, as follows:

$$t_{fluid,z} = t_{in} + z\frac{q^{"}\pi d}{\dot{m}C_p}. \tag{3.3}$$

The single-phase heat transfer coefficient was calculated as

$$\alpha = \frac{q^{"}}{t_{wall\ in,z} - t_{fluid,z}} \tag{3.4}$$

The experimental single-phase friction factor was calculated using the Darcy Weisbach equation from the measured pressure drop after subtracting minor losses (at entrance and at exit, due to change of cross-section):

$$f = \frac{\Delta p \cdot 2 \cdot \rho \cdot d}{G^2 l} \tag{3.5}$$

The experimental values for the friction factor obtained from the mini-channel of this study were compared with well-known correlations from literature. The Hagen-Poiseuille equation [74] [75] was used for laminar flow while the Blasius equation [76] was used for the turbulent flow regime,

$$f_{lam} = \frac{64}{Re} \tag{3.6}$$

$$f_{turb} = \frac{0.3164}{Re^{0.25}} \tag{3.7}$$

3.5 Data reduction for Two-Phase flow

The local heat transfer coefficient at any axial location during the two-phase flow was calculated by

$$\alpha_z = \frac{q^{"}}{t_{wall\ in,z} - t_{sat,z}} \tag{3.8}$$

Where $t_{wall\ in,\ z}$ is the inner wall temperature and $t_{sat,z}$ is the local saturation temperature at location z. The local saturation temperature was calculated using inlet pressure and pressure drop across the test section. For pressure drop, a linear profile was considered along the test section.
The vapor quality at any location was calculated using the inlet conditions and heat added to the fluid, as follows:

$$x_z = \frac{q^{"}\pi d(z-z_o)}{A_c G h_{lg}} \tag{3.9}$$

Where A_c is the cross sectional area of the test tube and z_o is the location where saturated conditions were approached, calculated as

$$z_o = \frac{\dot{m} C_p (t_{sat} - t_{in})}{q'' \pi d} \tag{3.10}$$

In case of two-phase flow, the pressure drop measured by the differential pressure sensor combines the contributions of single-phase pressure drop, pressure drop due to minor losses (entrance, exit etc.) and two-phase pressure drop.

$$\Delta p_{measured} = \Delta p_{minor\ losses} + \Delta p_{single\ phase} + \Delta p_{two\ phase} \tag{3.11}$$

Two-phase pressure drop ($\Delta p_{two\ phase}$) is a combination of frictional, accelerational and gravitational effects.

$$\Delta p_{two\ phase} = \Delta p_{frictional} + \Delta p_{accelerational} + \Delta p_{gravitational} \tag{3.12}$$

3.6 Uncertainty Analysis

The quality and reliability of any measured or derived quantity is reflected in its associated level of uncertainty. An uncertainty level basically defines the range within which a measured or derived quantity is believed to be correct. Therefore experimental results must always be presented with an estimate of uncertainty [77].

The elemental sources of error are broadly grouped into "Random" and "Systematic" errors. Random errors (also known as Type A uncertainty) are statistical in nature and are estimated using statistical techniques from a large sample (n>10) of a measured quantity. Systematic errors, sometimes referred as bias error (also known as Type B uncertainty), are not statistical in nature and can be estimated from calibration tables, previous experiments or from personal knowledge about the behavior of an instrument.

As per The International Bureau of Weight and Measures BIPM, the combined uncertainty in a measured or derived quantity from two types of uncertainties (types A and B) can be calculated using the root sum square (RSS) method as follows:

$$u_{\bar{x}} = \sqrt{(s_{\bar{x}})^2 + (w_{\bar{x}})^2} \tag{3.13}$$

Where *u* is the combined/overall uncertainty and *s* and *w* are the type A and type B uncertainties, respectively.

Equation 3.13 gives a value for uncertainty at the 68% (within 1σ) confidence level. However, estimates for uncertainty are normally required at a higher confidence level. The combined uncertainty at the 95% confidence level is obtained by multiplying $u_{\bar{x}}$ with the coverage factor of 2.

In many practical cases, the desired quantity is not directly measureable but can be estimated from several individual measurable quantities through a set of equations.

$$y = f(\bar{x}_1, \ldots\ldots\ldots \bar{x}_i, \ldots\ldots\ldots \bar{x}_n) \tag{3.14}$$

The standard uncertainty of quantity *y* is the positive square root of the estimated variance obtained from

$$u_y{}^2 = \sum_{i=1}^{n} \left(\frac{\partial f}{\partial \bar{x}_i}\right)^2 u_{\bar{x}_i}{}^2 + 2\sum_{i=1}^{n-1}\sum_{j=i+1}^{n} \frac{\partial f}{\partial \bar{x}_i}\frac{\partial f}{\partial \bar{x}_j} u_{\bar{x}_i,\bar{x}_j} \tag{3.15}$$

This is based on a first-order Taylor series approximation and is known as the law of propagation of uncertainty.

With all x_i considered as independent variables, the standard uncertainty of quantity y for type A and type B will become [78], respectively:

$$s^2{}_y = \sum_{i=1}^{n} \left[\left(\frac{\partial f}{\partial \bar{x}_i}\right)^2 s^2{}_{\bar{x}_i}\right] \tag{3.16}$$

$$w^2{}_y = \sum_{i=1}^{n} \left[\left(\frac{\partial f}{\partial \bar{x}_i}\right)^2 w^2{}_{\bar{x}_i}\right] \tag{3.17}$$

The overall combined uncertainty in the derived quantity y can finally be calculated using root sum square method as follows:

$$U_y = k\sqrt{s^2{}_y + w^2{}_y} \tag{3.18}$$

Where k is the coverage factor. For this study, calculations were done for 95% confidence level (k=2).

For this thesis, uncertainty computations were carried out following Moffat's procedure [79]. In this sequential perturbation method (SPM), each individual variable was sequentially perturbed to estimate its influence on the derived quantity y. The combined uncertainty is then calculated as follows:

$$u_y{}^2 = \sum_{i=1}^{n} \left[\frac{\partial f}{\partial \bar{x}_i}\right]^2 u^2{}_{\bar{x}_i} \approx \sum_{i=1}^{n} \left[f\left(\bar{x}_i + u_{\bar{x}_i}\right) - f(\bar{x}_i)\right]^2 \tag{3.19}$$

SPM is simple to implement and can easily identify the main parameters contributing to overall uncertainty. The maximum values for uncertainty in various experimental parameters are summarized in Table 3-2.

Table 3-2 Summary of uncertainty analysis

Parameter	Uncertainty
Tube diameter	± 0.007 mm
Mass flux	± 3.5 %
Wall temperature	± 0.1 °C
Saturation temperature	± 0.2 °C
Absolute pressure	± 10 mbar
Differential pressure	± 1 mbar
Heat flux	± 4 %
Heat transfer coefficient	< 14 %
Vapor quality	± 7%

3.7 Single-Phase Results

In addition to surface characterization (Figure 3.3), the test setup was validated by conducting single-phase heat transfer and pressure drop experiments. These tests were done before conducting the boiling experiments and their results were compared with well-known correlations from the literature.

3.7.1 Single-Phase Heat Transfer

For the single-phase experiments, boiling was inhibited by adjusting heat flux so that sub-cooling was always > 7 °C. The experimental results for the single-phase heat transfer coefficients of R1234yf and R134a are shown in Figure 3.5. These results were compared with correlations from Gnielinski [80] (Dittus-Boelter [81] and Yu et al. [82] were also used) for the turbulent flow regime. As can be noticed from Figure 3.5 the Nusselt number slightly increased with increase in Reynolds number in the laminar region. For fully developed laminar flow under constant heat flux conditions, the Nusselt number should be 4.36. The observed deviation in the laminar region could be due to the entrance effects as flow was not fully developed. Figure 3.6 shows a significant entrance effect, with an increase in Reynolds number for the test section. The observed increase in heat transfer coefficient/Nusselt number in laminar region matched well with predictions of correlation from Choi et al. [83]. In the turbulent region, the experimental results can be satisfactorily predicted using Gnielinski's correlation [80] for the conventional channels (15% max uncertainty for single phase experiments).

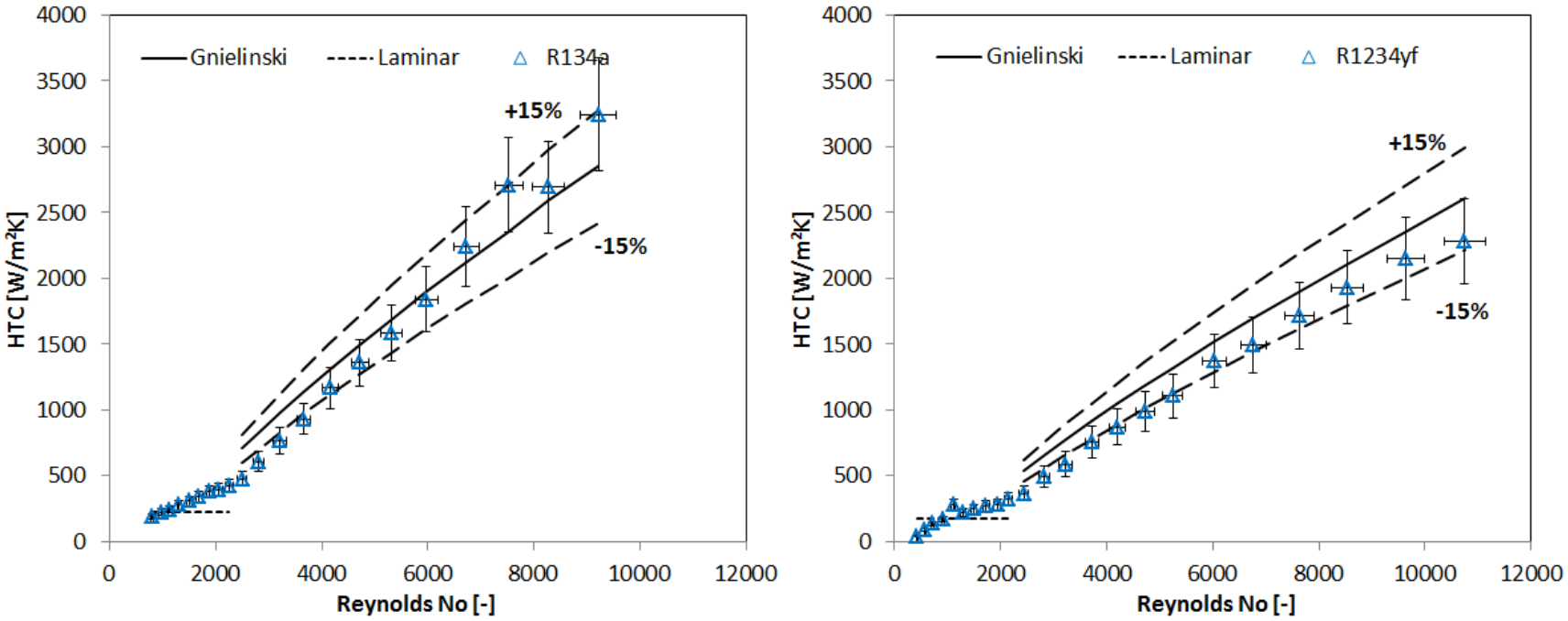

Figure 3.5 Single-phase average heat transfer coefficients with Reynolds Number for R1234yf and R134a

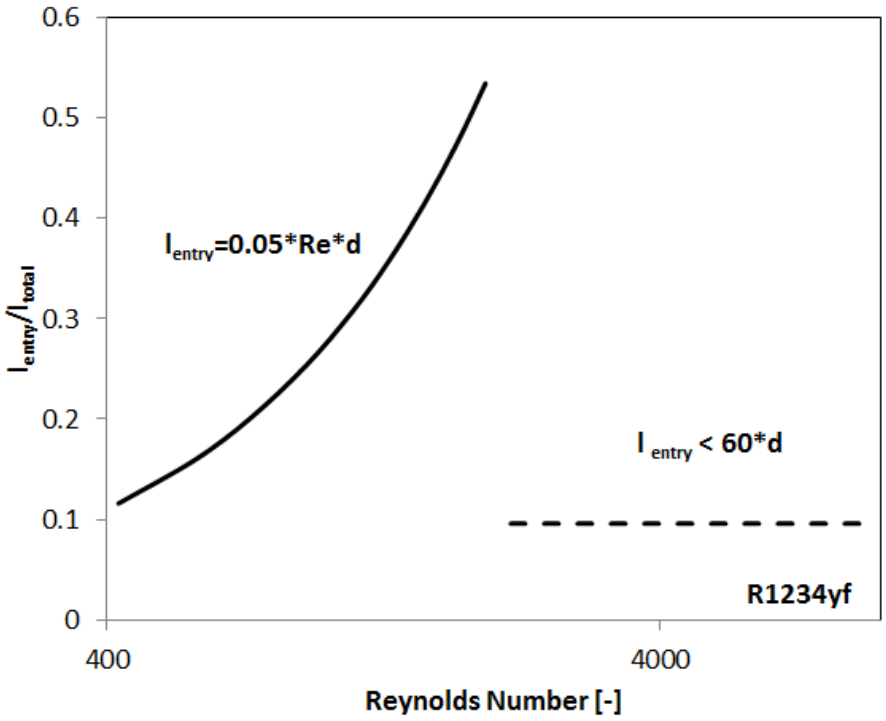

Figure 3.6 Hydrodynamic entry length for fully developed laminar and turbulent regions within test section

3.7.2 Single-Phase Pressure Drop

The experimental results for single-phase pressure drop for R1234yf, R134a and R600a, in the form of frictional factors (with Darcy- Weisbach equation), are shown in Figure 3.7. All minor losses (at entrance and at outlet, changes of cross-section) were subtracted from the measurement made by the differential pressure sensor. In all cases, the Hagen-Poiseuille [74] [75] and Blasius correlations [76] were used to compare the experimental findings. The critical value of the Reynolds number (transition from laminar to turbulent regime) was about 2000. Under similar operating conditions, the highest pressure drop was observed with R600a while the lowest values were noted with R1234yf. This could be explained by differences in their thermophysical properties (see Table 3-3). For all test cases, the experimental values were slightly higher than the predictions from the correlations.

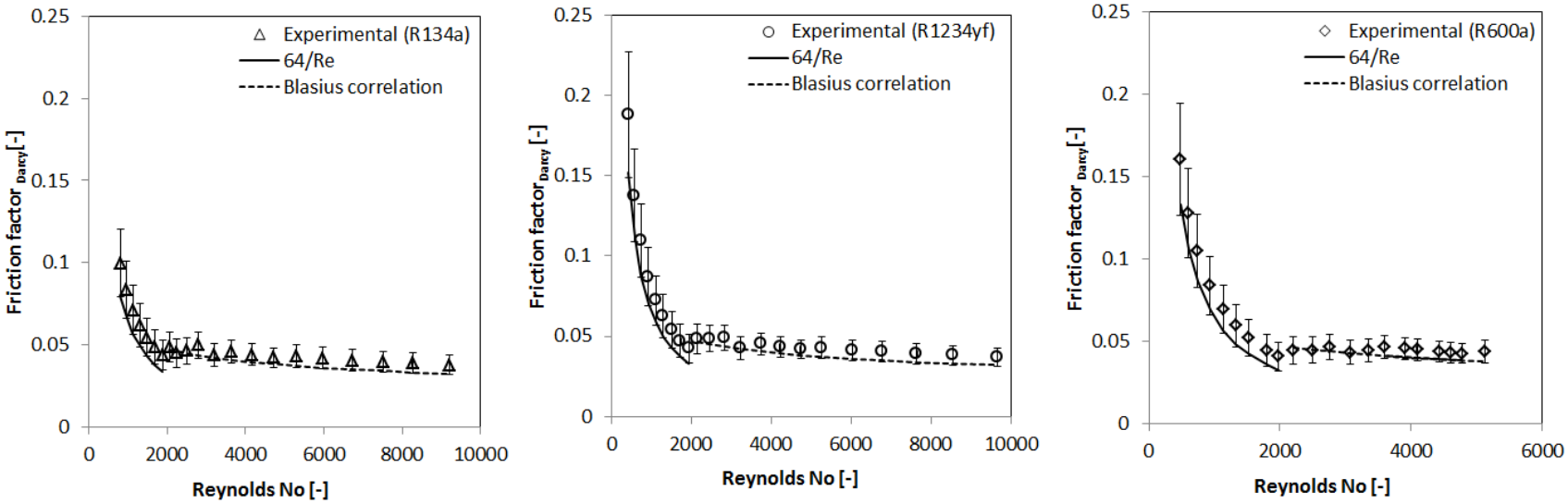

Figure 3.7 Single-phase frictional factor versus Reynolds number for R1234yf, R134a and R600a

Table 3-3 Thermophysical properties for four refrigerants of this study, table also includes property data for previous work (R717, R290, R245fa and R22 [15] [14] [16]) all for 27 °C saturation temperature

Refrigerant	p	ρ_l	ρ_g	h_{lg}	k_l	k_g	μ_l	μ_g	σ
	[bar]	[kg/m^3]	[kg/m^3]	[kJ/kg]	[mW/m.k]	[mW/m.k]	[µPa-s]	[µPa-s]	[mN/m]
R134a	7.059	1199.1	34.34	175.94	80.27	14.02	190.10	11.77	7.81
R152a	6.325	894.37	19.58	276.91	97.12	15.03	159.31	10.14	9.46
R600a	3.716	548.13	9.64	326.71	88.54	17.04	147.99	7.54	9.87
R1234yf	7.217	1084.5	40.16	143.74	62.96	14.16	151.82	12.39	5.91
R290	10.014	489.21	21.71	332.18	92.78	19.26	95.13	8.34	6.74
R245fa	1.595	1333.1	9.17	189.13	87.47	13.052	397	10.32	13.78
R22	11.014	1182.8	46.73	180.73	82.57	11.52	160.78	12.61	7.79
R717	10.666	599.75	8.28	1157.32	479.8	26.42	129.15	9.89	24.19

The agreement of the single-phase heat transfer and pressure drop results with classical correlations from the literature, as shown in Figure 3.5-3.6, confirms the accuracy of the setup and instrumentation.

Chapter 4. Experimental Results for Flow Boiling Heat Transfer

This chapter provides the experimental results for saturated flow boiling heat transfer characteristics. The operating conditions used for each refrigerant are summarized in Table 4-1. The experiments were carried out by varying applied heat flux under constant mass flux and inlet conditions. First, the thermophysical properties of refrigerants will be described, followed by the parametric effects (heat flux, mass flux, vapor quality, operating pressure) on flow boiling heat transfer, and a comparison of the data with empirical correlations from the literature. Detailed results for boiling heat transfer characteristics of R152a, R600a and R1234yf can be found in Paper 1, 2, and 3 respectively appended at the end.

Table 4-1 Operating conditions for saturated flow boiling heat transfer experiments

Refrigerant	**Data Source**	**Diameter [mm]**	**Heated length [mm]**	**Saturation temperature [^{o}C]**	**Mass flux [kg/m^{2}s]**	**$\Delta t_{sub,\,in}$ [K]**	***x*** **[-]**	**R_a [μm]**
R1234yf	This study	1.60	245	27 and 32	100-500	1-1.5	Until dryout	0.95
R134a	This study	1.60	245	27 and 32	100-500	1-1.5	Until dryout	0.95
R152a	This study	1.60	245	27 and 32	100-500	1-1.5	Until dryout	0.95
R600a	This study	1.60	245	27 and 32	50-350	1-1.5	Until dryout	0.95
R717	Maqbool et al. [15]	1.70 and 1.224	245	23, 33 and 43	100-500	1-2	Until dryout	2.55 0.21[2]
R290	Maqbool et al. [2]	1.70	245	23, 33 and 43	100-500	1-2	Until dryout	2.55
R134a, R245fa and R22	Callizo [16]	0.64	213	30, 35	185-535	1	Until dryout	0.77

4.1 Flow boiling heat transfer

In this study, experiments were conducted at 27 and 32 ^{o}C saturation temperature with five mass fluxes in the 100-500 kg/m^{2}s (50-350 kg/m^{2}s for R600a) range. A cold drawn, seamless, vertical, stainless steel tube (1.60

[2] For 1.224 mm test section

mm inside diameter, 2.00 mm outside diameter with 245 mm heated length, R_a=0.95 μm) was the test piece for all four experimental campaigns. Figure 4.1 shows thermophysical properties and important dimensionless numbers obtained for R600a, R152a and R1234yf, with R134a as a reference case at 27 °C saturation temperatures. For all refrigerants, an increase in saturation temperature resulted in lower liquid density, heat of vaporization, thermal conductivity and surface tension values. Pamitran et al. [84] reported higher HTCs for fluids with high saturation temperature and low viscosity values. Increased saturation temperature results in reduced density and viscosity ratios (liquid/vapor). A reduced density ratio results in reduced vapor velocity, which could be translated into less suppression of nucleate boiling. The liquids which tend to wet the surface will have less risk of the thin film breaking on the heating surface and consequently dryout may be delayed to higher vapor qualities. Compared with R134a, Isobutane had quite low (about 50%) operating pressure, low viscosity, and significantly high heat of vaporization and surface tension. R152a showed similar characteristics with slightly lower values than R600a.

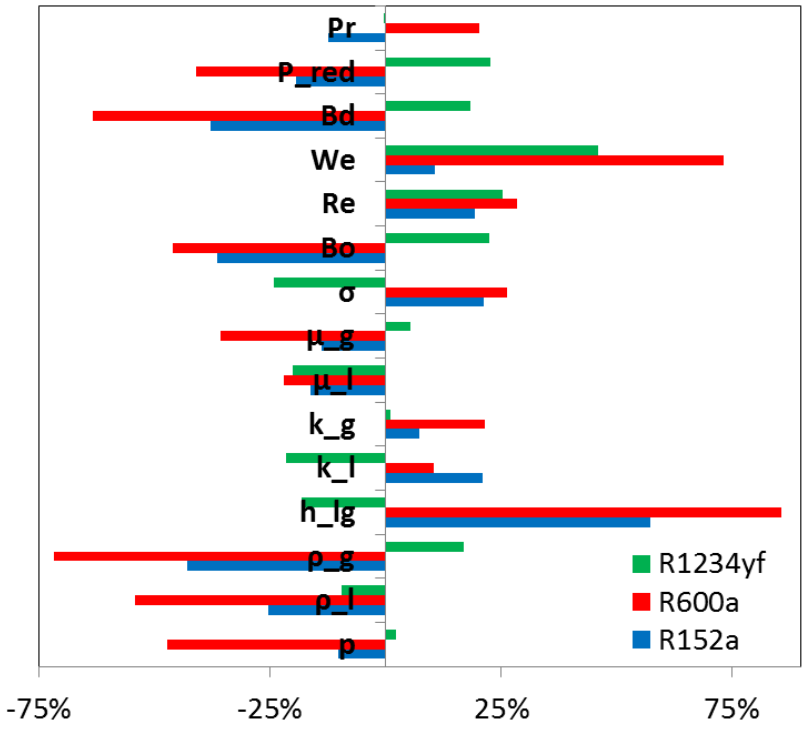

Figure 4.1 Thermo-physical properties and important dimensionless numbers for R1234yf, R152a and R600a, as compared with R134a (Dimensionless numbers were calculated for G=500 kg/m²s and q"=50 kW/m², where Boiling number (Bo), Bond Number (Bd), operating pressure (p), reduced pressure (p_red), Prandtl Number (Pr))

Reduced vapor density will enhance the degree of expansion associated with the phase change process. Bubble departure diameter may increase, whereas departure frequency may be reduced with an increase in surface tension [40].

4.1.1 Boiling curves

All experiments were carried out with a gradual increase of applied heat flux, and data was recorded for stable conditions. Figure 4.2 shows representative boiling curves, in which heat flux is plotted against degree of wall superheat (t_{wall}-t_{sat}). These curves are based on temperature readings from the final thermocouple on the test

section, located at 220 mm from the inlet. The entire boiling span is covered in these figures. In some cases, tests were repeated with descending heat fluxes and no hysteresis effects were noticed. For all cases dryout conditions can be seen on right hand side, where a slight increase in heat flux results in sharp rise in wall superheat due to the liquid-starved condition on the wall. For each mass flux, heat flux on the completion of dryout and the corresponding degree of wall superheat is shown by the final point of each plot. The high heat of vaporization for R600a and R152a helped to sustain significant high heat fluxes. With R152a, a temperature overshoot of about 20 K was observed before incipience of boiling.

4.1.2 Effect of heat flux

The influence of heat flux on heat transfer performance is shown in Figure 4.3a, in which local heat transfer coefficients for R134a and R1234yf are given, along with local vapor quality. The local heat transfer coefficients were calculated by accounting for pressure drop, which was assumed to vary linearly along the test section[3]. For each refrigerant, the local HTCs for three applied heat fluxes are shown; other operating conditions (mass flux, saturation temperature and inlet conditions) remained constant. The strong effect of heat flux on heat transfer is clearly reflected in these plots, with high HTCs occurring at higher heat fluxes and a similar trend was observed for all four refrigerants (see appended papers). In all cases, a dip/ditch in HTC at the third thermocouple can be seen. This is believed to be due to an attachment related problem with the thermocouple in which the contact was not as good as with the other thermocouples. In the same set of figures, it can be seen that the effect of vapor quality was insignificant, with variation of HTC remaining within the degree of uncertainty of the calculation. Detailed results for each individual refrigerant can be seen in paper appended with this thesis.

4.1.3 Effect of mass flux

Figure 4.3b shows the local heat transfer coefficient with local vapor quality, under constant applied heat flux conditions for various mass flow rates. The depicted results show the 27 ^{o}C saturation temperature case, the corresponding heat flux for each sub case is mentioned accordingly. The lack of effect of mass flux is clearly reflected through the duplication of similar heat transfer results with varying mass fluxes. Similar trends were also noticed at other operating conditions (heat fluxes and saturation temperature).

4.1.4 Effect of saturation temperature

The effect of operating pressure is shown in Figure 4.4, which shows the local HTCs for two operating pressures under constant applied heat flux for each refrigerant. As can be seen in the figure, an increase in saturation pressure increased the heat transfer performance for all test cases, with the maximum increment observed with R152a. Increased saturation temperature results in reduced surface tension and lower viscosity and density ratios (liquid/vapor). The increased vapor density results in reduced vapor velocity, which translates into reduced suppression of nucleate boiling, consequently resulting in enhanced heat transfer at higher operating pressures.

[3] Trends from empirical correlations (among others Homogenous model [13], correlations from Tran et al. [23] and Friedel [57]) agrees well with this consideration.

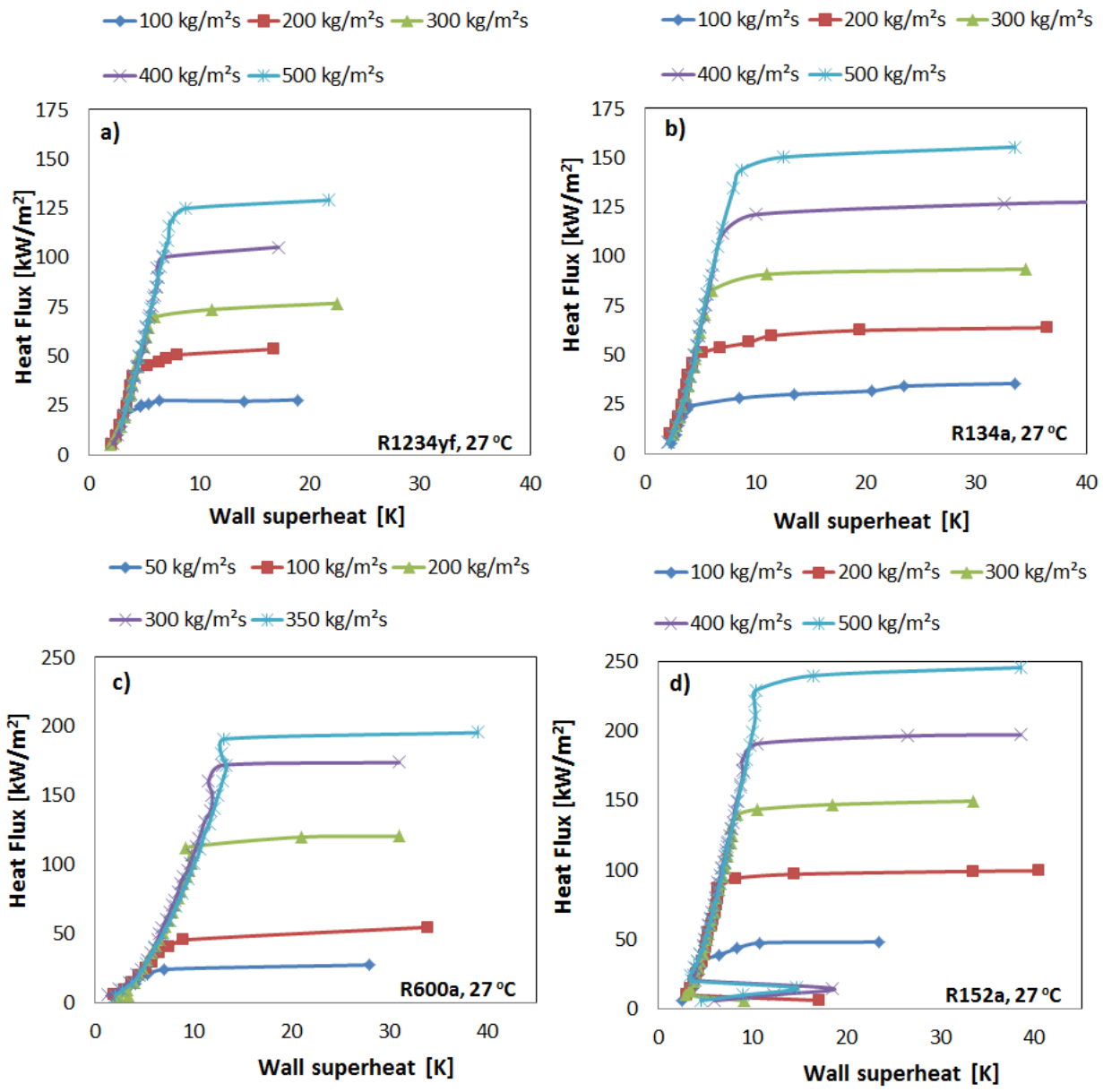

Figure 4.2 Heat flux versus wall superheat for R134a (a), R1234yf (b), R600a (c), and R152a (d) at 27 °C saturation temperature

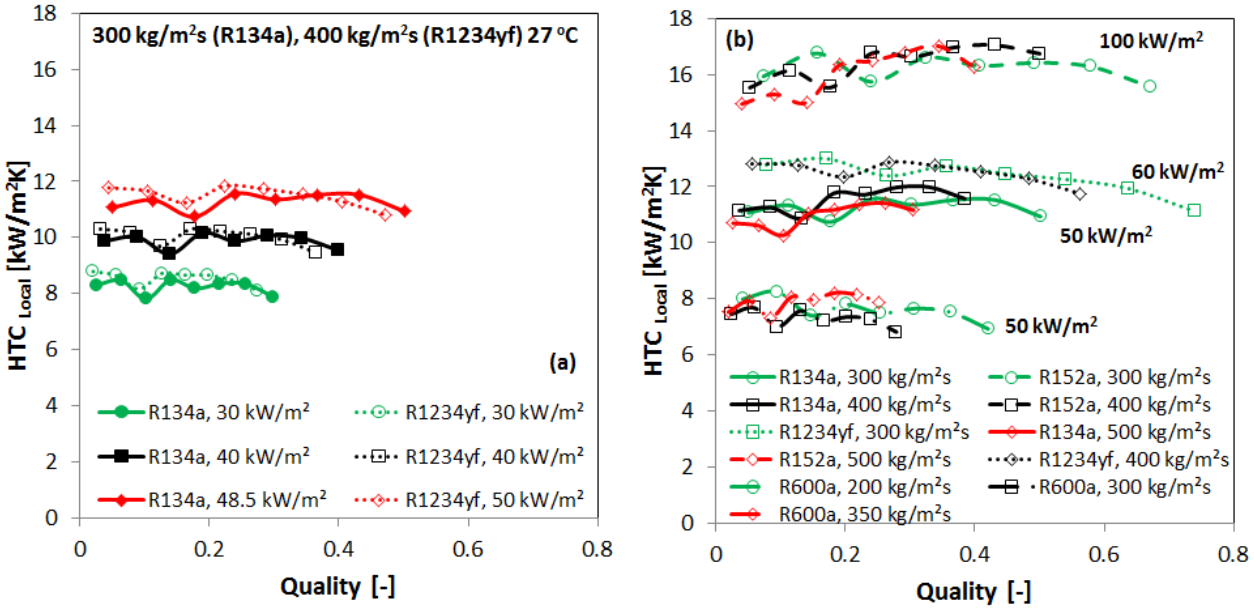

Figure 4.3 Local heat transfer coefficient versus vapor quality for R134a, R1234yf, R152a and R600a

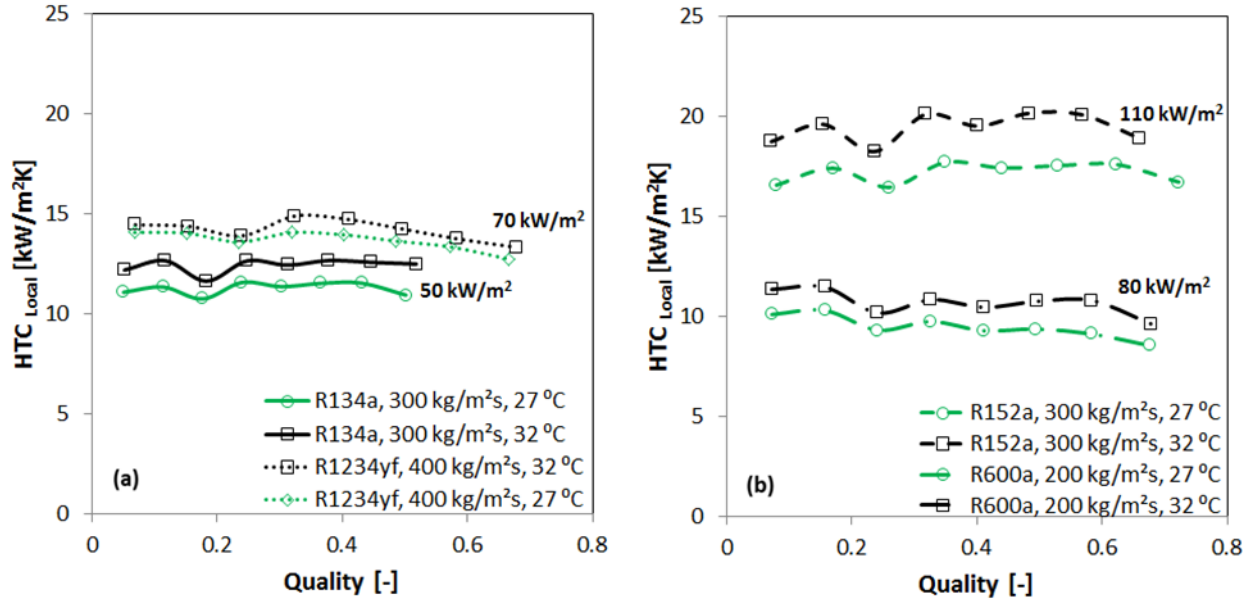

Figure 4.4 Local heat transfer coefficient versus vapor quality at two operating pressures for R134a, R1234yf, R152a and R600a

Comparative thermal performance of the four refrigerants in this study, along with previous results for R717, R290, R245fa and R22 [15] [14] [16], are shown in Figure 4.5, with local HTCs plotted against local vapor quality. These results refer to three different test sections (one from this study, one from Maqbool et al. [15] and one from Callizo [16]) with different geometrical and surface characteristics, as summarized in Table 4-1.

Under similar operating conditions (saturation temperature and heat flux), similar thermal performance can be noticed with R134a, R152a and R1234yf, (Figure 4.5a) whereas significantly lower HTCs can be seen with R600a. Results for R134a from Figure 4.5a can also be compared with R717 and R290 shown in Figure 4.5b, the channel size and operating conditions are quite comparable. Under similar operating conditions R290 showed higher HTCs than R717, while R717 showed slightly lower values than those obtained with R134a. Higher HTCs with R290 could be due to its good thermophysical properties (high thermal conductivity and low surface tension). Figure 4.5b also shows lower heat transfer results with R22, whereas R245fa showed almost identical performance to R134a. Del-Col et al. [20] also reported similar heat transfer performance for R1234yf compared with R134a. Those experiments were conducted under non-uniform heating conditions in which a secondary fluid in counter flow arrangement was used for heating the test section. In contrast, Mortada et al. [38] reported higher heat transfer results with R1234yf under similar operating conditions (maximum 40% deviation in local values was reported). Hamdar et al. [3] reported a strong influence of heat flux on HTCs for saturated boiling of R152a in a 1x1 mm horizontal mini-channel. Copetti et al. [21] reported higher heat transfer coefficients for R600a than R134a under similar operating conditions, but it should be mentioned that the test section had different surface characteristics (R_a=2.05 µm versus 0.95 µm for the current study) and had small heated length (185 mm test section versus 245 mm for the current study).

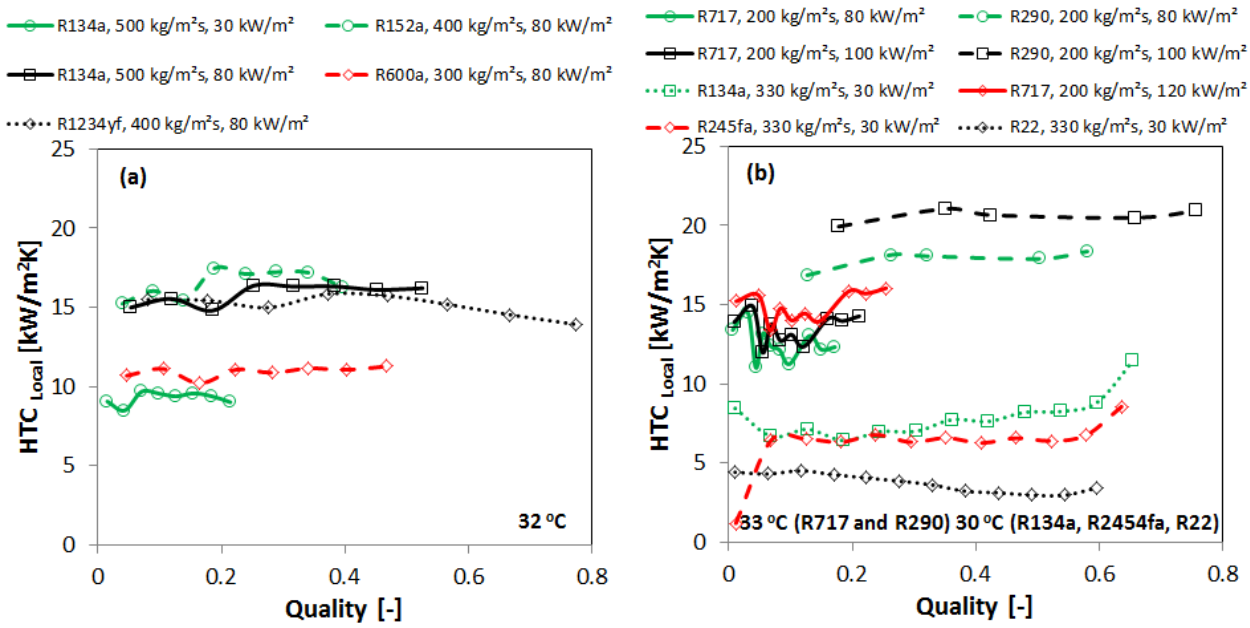

Figure 4.5 Local HTCs plotted against vapor quality for (a) R134a, R152a, R600 and R1234yf (1.60 mm tube at 27 °C saturation temperature), and (b) R717 [15] and R290 (1.70 mm tube) [14] and R134a, R22 and R245fa (0.64 mm tube) [16]

The parametric trends observed in this study, the strong influence of heat flux and system pressure, and the lack of effect of mass flux and vapor quality on heat transfer performance are consistent with those reported by Saisorn et al. [32] for R134a in a 1.75 mm horizontal channel, Tran et al. [19] for R12 and R113 in small circular and rectangular tubes, and Del-Col et al. [20] for R1234yf in a non-uniformly heated 1 mm horizontal tube. However, some researchers have identified different trends in which a strong effect of heat flux was only noticed at lower vapor quality conditions and HTCs increased thereafter with vapor quality and mass flux. Among others, such trends have been reported by Copetti et al. [21], Pamitran et al. [84] and Mortada et al. [38].

The experimental trends observed in this study are consistent with what can be expected from conventional nucleate boiling experiments. However, As per Thome and Consolini [85] and also based on previous

visualization studies from our lab [26] [39], nucleation was only active at low vapor qualities and in the close vicinity of inlet of the test section. So nucleation was not occurring along the whole channel length and such trends for heat transfer could be explained and predicted by the evaporation of thin liquid film around the elongated vapor bubble in compact channels. The empirical models/correlations for nucleate boiling only relate the boiling heat transfer coefficient with heat flux without physically modeling the boiling process. We believe that trends reported in this study just have similarity with what would conventionally be expected from nucleate boiling process and in reality this similarity is coming from the bubble formation and evaporation of thin liquid film processes.

4.1.2 Comparison with correlations

Flow boiling in mini/micro-channels is complex interplay of fluid transport properties and imposed operating conditions. Many empirical correlations have been proposed in the literature for modeling evaporative heat transfer in small channels; however, the majority of these have been obtained using the author's own databases, so they are only applicable to a narrow range and lack generalizability.

Experimental data from this study was compared to often-cited macro and micro-scale correlations from the literature. While a brief summary for comparison of our experimental data is given in following paragraphs, the expressions and applicability range for correlations can be seen in the appendix. Predictions for average and local heat transfer coefficients (best worked cases) are shown in Figure 4.6 and Figure 4.7, respectively, and a statistical summary for all tested correlations is given in Table 4-2. Mean absolute error (MAE) and percentage of data within ±30% of experimental values were considered for this comparison. MAE is a measure of deviation of predicted values from experimental ones and is defined as follows,

$$\mathrm{MAE} = \frac{1}{\mathrm{N}}\left(\sum_{\mathrm{i}=1}^{\mathrm{N}} \frac{\left|\mathrm{X}_{\mathrm{Predicted_i}} - \mathrm{X}_{\mathrm{Experimental_i}}\right|}{\mathrm{X}_{\mathrm{Experimental_i}}}\right) * 100$$

Data-points before incipience of boiling and after incipience of dryout were neglected in this exercise.

Cooper's pool boiling correlation [24] was chosen, as some authors [86] [50] have reported satisfactory predictions using this correlation when it is applied to flow boiling in narrow channels. Experimental results for average heat transfer coefficients are shown in Figure 4.6. As can be seen, this correlation mostly under-predicted the experimental data (with the exception of R600a), with quite coherent predictions. Slightly better predictions were achieved by changing the leading multiplier.

Experimental results for average heat transfer coefficients were also compared with predictions made by the correlation from Lazarek and Black [87]. This correlation was developed from a refrigerant-based database collected from a small channel, in which nucleate boiling was reported as the dominant heat transfer mechanism. This correlation gave quite scattered predictions for all fluids, with data mostly under-predicted, especially in low vapor quality conditions.

Average HTCs were also compared with the correlation from Tran et al. [19]. This correlation had coherent predictions for R152a and R134a, although the data were highly under-predicted. For R1234yf, almost all data-points were captured within ±30% limit with slight scatter. Scattered predictions were observed for Isobutane, with the data mostly under-predicted. In contrast with the correlation from Lazarek and Black, this correlation gave nearly similar predictions over the entire tested vapor quality range.

The experimental results for local HTCs were compared with macro-scale correlations from Chen [88], Gungor and Winterton [89] and Liu and Winterton [31], whereas the Mikielewicz [90], Mahmoud and Karayiannis [91] models were employed for the micro side. The correlations from Gungor and Winterton [89] and Liu and Winterton [31] are different variants of Chen's original correlation [88] using nucleate and

convective boiling terms. Cooper's pool boiling correlation [24] is recommended to account for the nucleate pool boiling contribution and convection effects are addressed by using Dittus-Boleter equation [81]. The correlation from the Mahmoud and Karayiannis [91] gave good predictions for all four refrigerants, and good predictions for R134a, R152a and R1234yf were obtained with the correlations from Chen [88], Gungor and Winterton [89] and Mikielewicz [90], as can be seen in Figure 4.7. Micro-scale correlation from Mahmoud and Karayiannis [92] was developed from R134a based database.

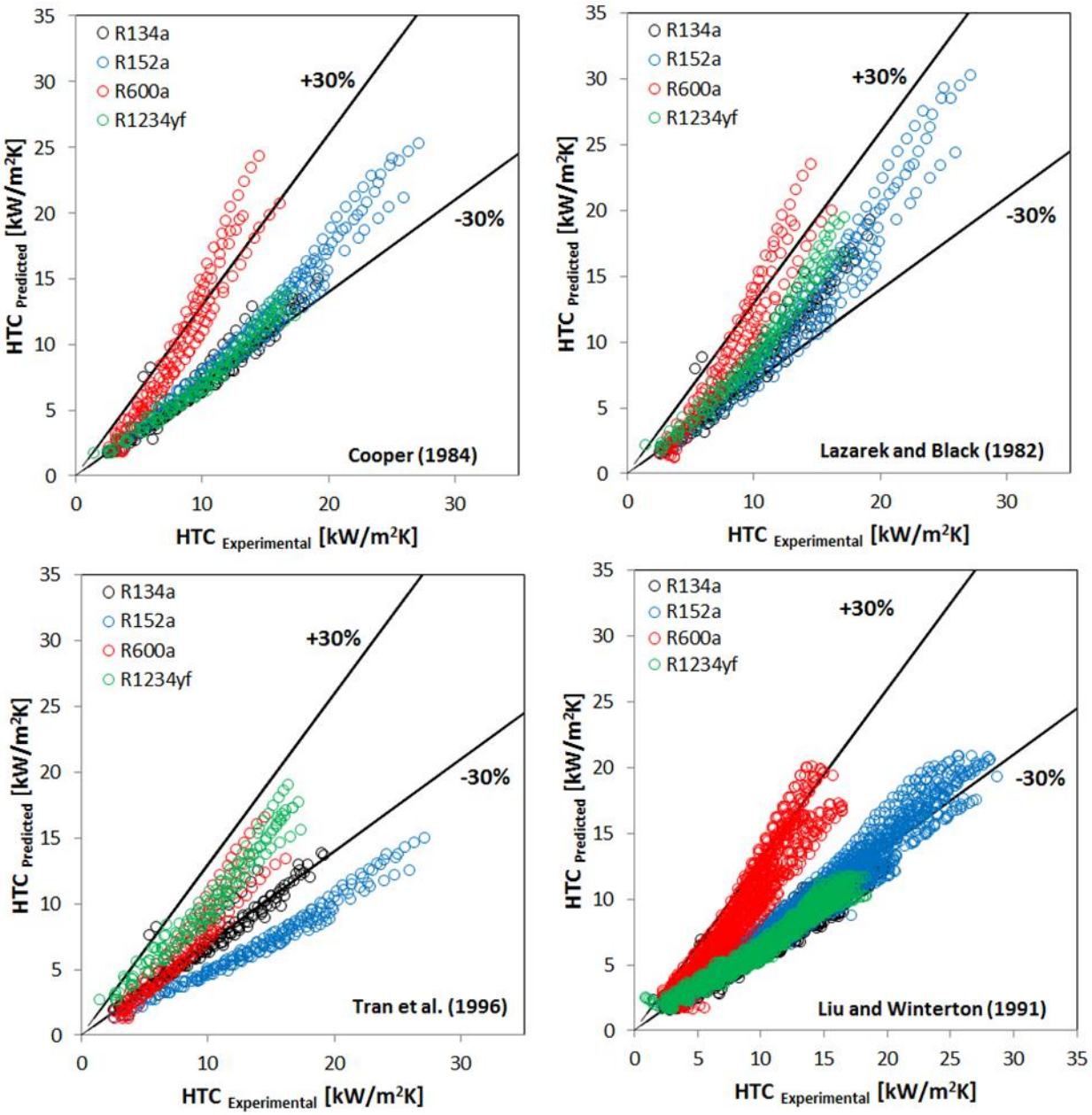

Figure 4.6 Comparison of experimental data with correlations from Cooper [24], Lazarek and Black [87], Tran et al. [19] and with Liu and Winterton [31].

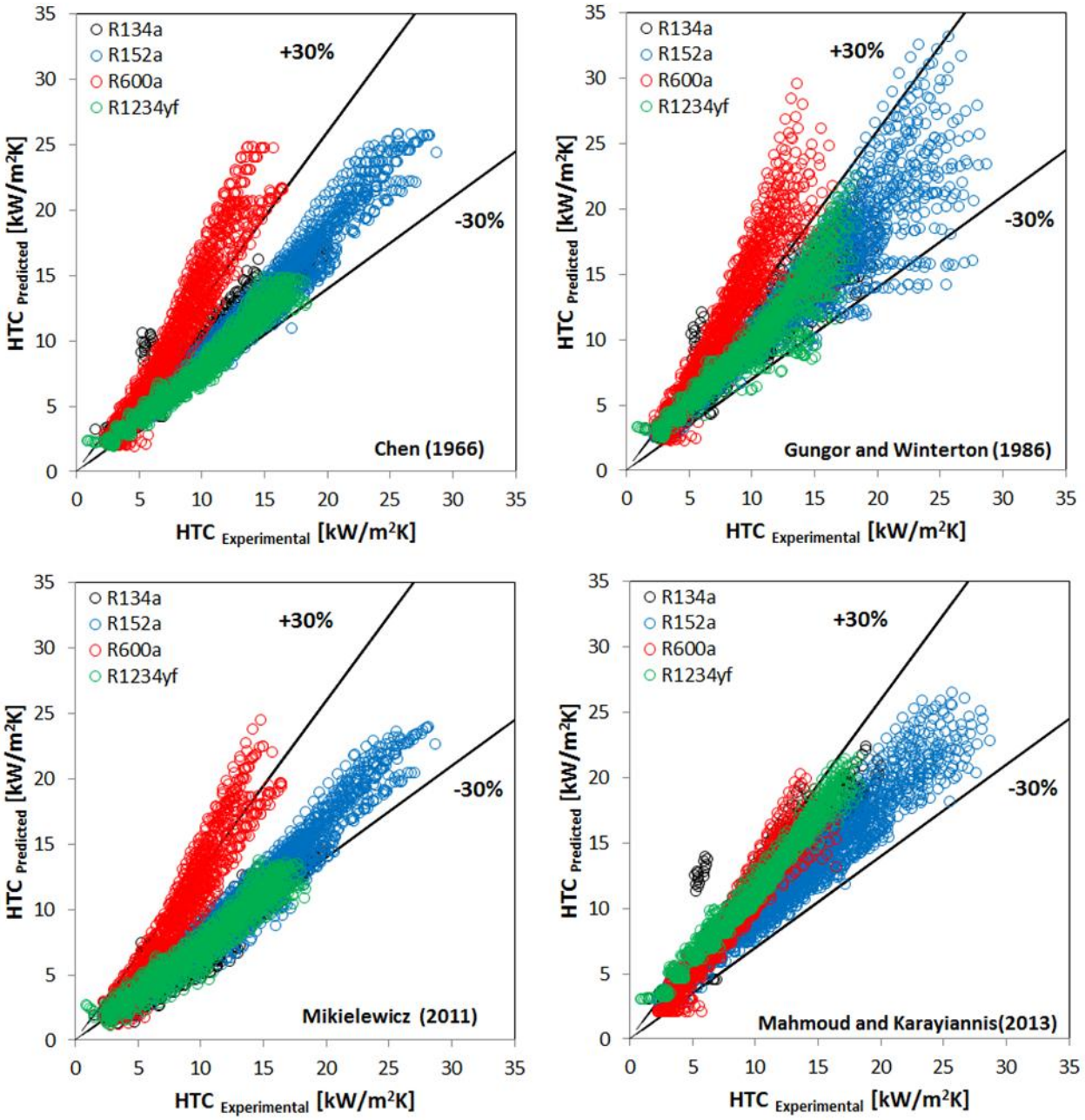

Figure 4.7 Comparison of experimental local heat transfer coefficients with correlations from Chen [88], Gungor and Winterton [89], Mikielewicz [90] and Mahmoud and Karayiannis [91]

Table 4-2 Summary of comparisons with correlations from the literature

Correlation	**MAE**	**Percentage of data in ± 30%**	**Data points**
Cooper [24]	26.10	59.77	619
Lazarek and Black [87]	19.50	78.77	619
Tran et al. [19]	30.75	44.74	619
Chen [88]	18.86	86.80	4952
Liu and Winterton [31]	30.09	41.76	4952
Gungor and Winterton [89]	17.05	82.12	4952
Mahmoud and Karayiannis [92]	13.27	98.60	4952
Mikielewics [90]	26.20	66.05	4952
Li and Wu [11]	26.78	65.85	4952
Kandlikar [93]	20.25	78.09	4952

Chapter 5. Experimental Results for Two-Phase Frictional Pressure Drop

Frictional pressure drop is an important parameter that helps in selecting the properly sized components and pump for any practical installation. Additionally, it can be helpful in the selection of proper operating conditions for a device operating under two-phase conditions. A summary of operating conditions for the two-phase frictional pressure drop is given in Table 5-1.

Table 5-1 Summary of operating conditions

Refrigerant	**Diameter [mm]**	**Heated length [mm]**	**Saturation temperature [°C]**	**Mass flux [kg/m²s]**	**$\Delta t_{sub,\ in}$ [K]**	***x*** **[-]**	**R_a [μm]**
R1234yf	1.60	245	27 and 32	100-500	1-1.5	Until dryout	0.95
R134a	1.60	245	27 and 32	100-500	1-1.5	Until dryout	0.95
R152a	1.60	245	27 and 32	100-500	1-1.5	Until dryout	0.95
R600a	1.60	245	27 and 32	50-350	1-1.5	Until dryout	0.95

The pressure drop data collected from the differential pressure sensor ($dp_{measured}$) includes contributions from single-phase, two-phase and end effects for the pressure drop, as seen in equation 5.1. The pressure drop at the ends (contraction at inlet and expansion at outlet) and single-phase pressure drop were estimated as per the standard procedures explained by Maqbool et al. [50]. The two-phase pressure drop (dp_{tp}) was calculated by subtracting all other contributions from the measured pressure drop (Eq. 5.2).

$$dp_{measured} = dp_{end\ effects} + dp_{sp} + dp_{tp} \tag{5.1}$$

$$dp_{tp} = dp_{frictional} + dp_{gravitational} + dp_{accelerational} \tag{5.2}$$

The two-phase pressure drop was further subdivided into two-phase frictional, two-phase accelerational ($dp_{accelerational}$) and two-phase gravitational components ($dp_{gravitational}$) (Equation 5.2).

The gravitational pressure drop is due to the position of test channel and its gradient form can be calculated as

$$\left(\frac{dp}{dz}\right)_{gravitational} = [\alpha\rho_g + (1-\alpha)\rho_l]g\sin\emptyset \tag{5.3}$$

Where α is the void fraction, as per homogenous model [13],

$$\alpha = \left[1 + \left(\frac{1-x}{x}\right)\left(\frac{\rho_g}{\rho_l}\right)^{2/3}\right]^{-1} \tag{5.4}$$

The accelerational pressure drop is due to the momentum variation of the liquid and vapor phases resulting from specific volume enhancement during the evaporation process. The accelerational pressure gradient was calculated as follows:

$$\left(\frac{dp}{dz}\right)_{accelerational} = G^2\left[\frac{v_g x^2}{\alpha} + \frac{v_l(1-x)^2}{(1-\alpha)}\right] \tag{5.5}$$

Finally, the two-phase frictional pressure drop ($dp_{frictional}$) was calculated by subtracting the accelerational and gravitational components from the two-phase pressure drop (dp_{tp}).

5.1 Experimental Results

The experimental results for the two-phase frictional pressure drop of R134a, R1234yf, R600a and R152a are shown in Figure 5.1. The results depicted are of the 27 °C saturation temperature case; similar trends with slightly lower values were observed at the higher operating pressure. For each case (mass flux) experiments were conducted with gradual increase of heat flux and pressure drop results are shown with exit vapor quality. As can be seen in Figure 5.1, frictional pressure drop increased with mass flux and vapor quality. Increasing mass flux eventually results in an increase in velocity that augments the frictional and accelerational components of pressure drop. The increase in pressure drop with vapor quality can be explained by the increase in specific volume at higher vapor quality, which results in increased average vapor velocity and higher pressure drop. In all cases a peak for pressure drop was observed at about 85% vapor quality and this was not affected with change in mass flux. These trends are consistent with those reported by Ali et al. [48] and Maqbool et al. [50]. The single-phase pressure drop value for each refrigerant is also shown in Figure 5.1.

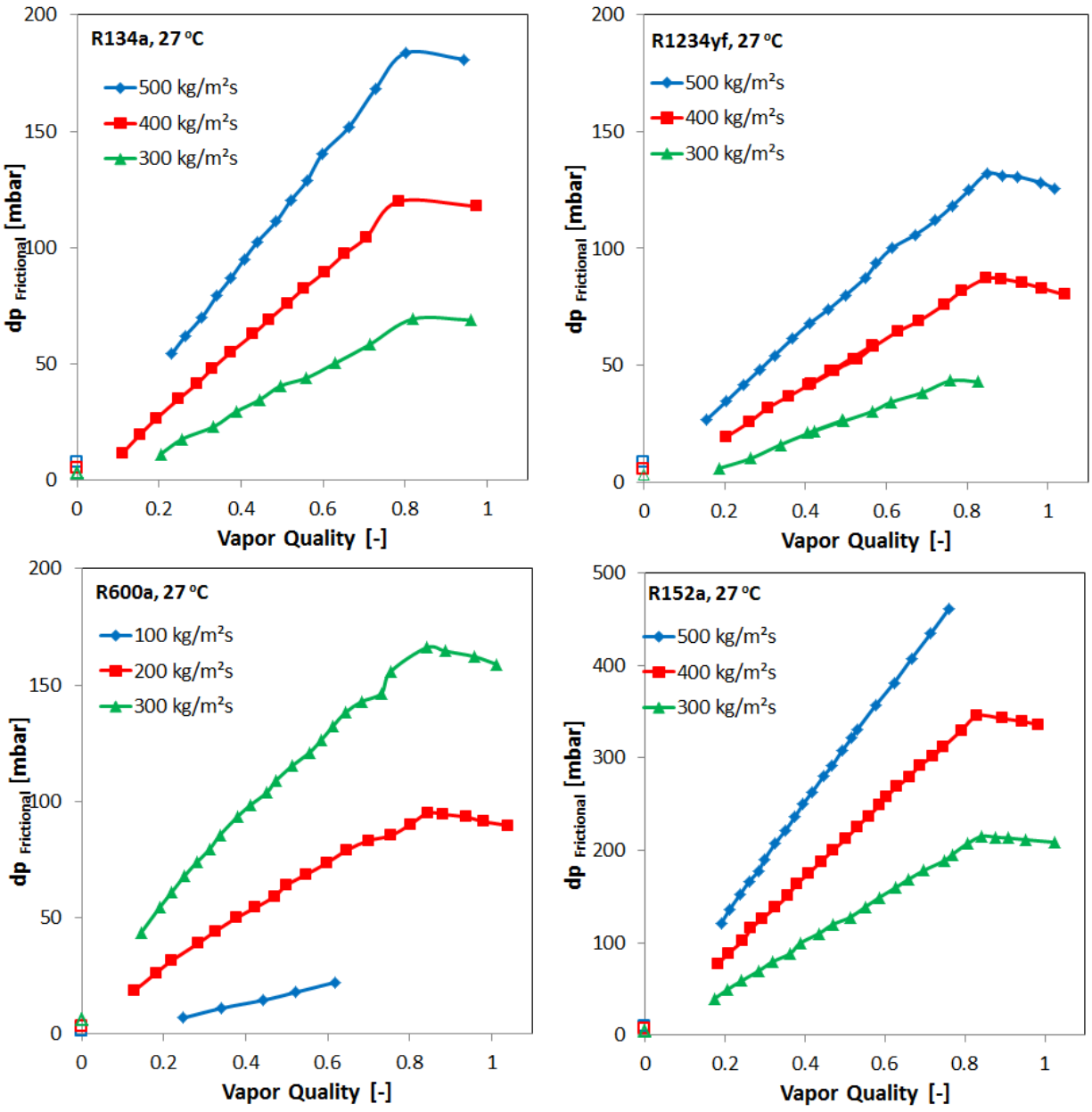

Figure 5.1 Two-phase frictional pressure drop versus exit vapor quality for R134a, R152a, R600a and R1234yf

The effect of saturation temperature on two-phase pressure drop can be seen in Figure 5.2, which shows the frictional pressure drop results for R1234yf at two saturation temperatures. An increase in saturation temperature resulted in lower values for the two-phase frictional pressure drop. Reduced vapor velocity (increased vapor density) and liquid viscosity at higher saturation temperature results in lower pressure drop values.

Figure 5.2 also shows the two-phase results for all four refrigerants at 27 °C saturation temperature. Under similar operating conditions, R152a and R600a showed higher pressure drop/pumping power than R134a, an effect that can partially be explained by the different thermo-physical properties of these refrigerants (Figure 4.1). Under similar operating conditions (saturation temperature), R152a and R600a have lower vapor density than R134a. This results in higher vapor velocity and vapor shear at the liquid vapor interface, which consequently increases pressure drop.

R134a showed high values for frictional pressure drop compared to R1234yf. This finding is consistent with those of Del-Col et al. [94], they reported 10-12% lower pressure drop with R1234yf (compared to R134a) and explained this through the higher operating pressures of R1234yf under similar operating conditions. In our experiments, we noticed that frictional pressure drop of R1234yf was about 30% less than that of R134a.

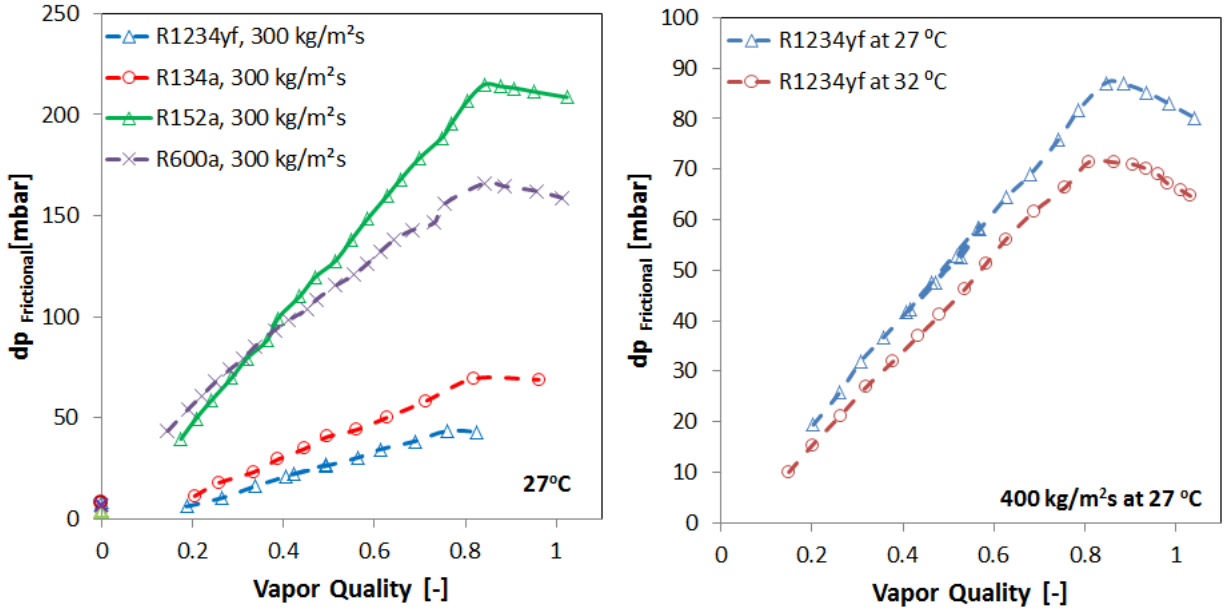

Figure 5.2 Two-phase frictional pressure drop versus exit vapor quality

5.2 Comparison with correlations

Experimental results for two-phase frictional pressure drop were compared with well-known macro and micro-scale correlations from the literature. See appendix for formulation and applicability range of correlations. Figure 5.3 graphically presents the scatters obtained from the best worked correlations. A brief statistical summary for all tested correlations is given in Table 5-2. For the prediction of pressure drop with the correlations, pressure gradients were calculated by dividing the test section into ten equal parts. Overall pressure drop was then calculated through the summation of these local gradients. Correlations for estimation of pressure drop can broadly be grouped into homogenous and separated flow models. The homogenous model considers flow as single-phase with mean fluid properties, whereas the separated flow model considers the contributions from each phase separately using suitable multipliers.

The experimental results were compared with the macro-scale model proposed by Jung and Radermacher [95]. This is based on the separate flow model approach and was developed from a refrigerant-based database where pure fluids and their mixtures were tested. Comparison of our data with this correlation showed good

coherent predictions for all tested refrigerants, however under-predictions with R152a and over-predictions with R134a, R600a and R1234yf are clearly visible.

The Grönnerud correlation [96] which was originally developed from refrigerant based database collected from conventional channels was also tested. This is also based on separate flow model and in this case two phase multiplier depends on Froude number. Comparison of our data with this correlation shows reasonable predictions for R134a, R600a and R1234yf whereas data was highly under-predicted for R152a. While more data-points were captured within ±30% error limit with this correlation, more coherent predictions were observed with correlation from Jung and Radermacher [95].

The experimental data was also compared with micro-scale correlation from Mishima and Hibiki [49]. This correlation was developed from the analysis of air-water flow in small pyrax tubes (1-4 mm in diameter). This correlation is modified version of Lockhart and Martinelli correlation [60], the effect of channel size is considered with modified Chisholm parameter [55]. Comparison of our data showed good coherent predictions with this correlation at low heat flux conditions, thereafter data was highly under-predicted.

Another correlation was proposed by Wang and coworkers [97]. They conducted a visualization study with refrigerants (R22, R134a and R407c) by using 6.5 mm horizontal tube. This is also modified form of Lockhart and Martinelli correlation, for wavy annular flow regime the two-phase multiplier was not effected by variation in mass flux. Comparison of our data with this correlation shows good predictive capability, however data for R152a was highly under-predicted as can be seen in Figure 5.3.

The experimental results were also compared with predictions from the homogenous model [13]. These results, (not shown in Figure 5.3), were calculated by following McAdams's definition [98] for homogenous viscosity. The correlation underestimated the experimental data for all four refrigerants.

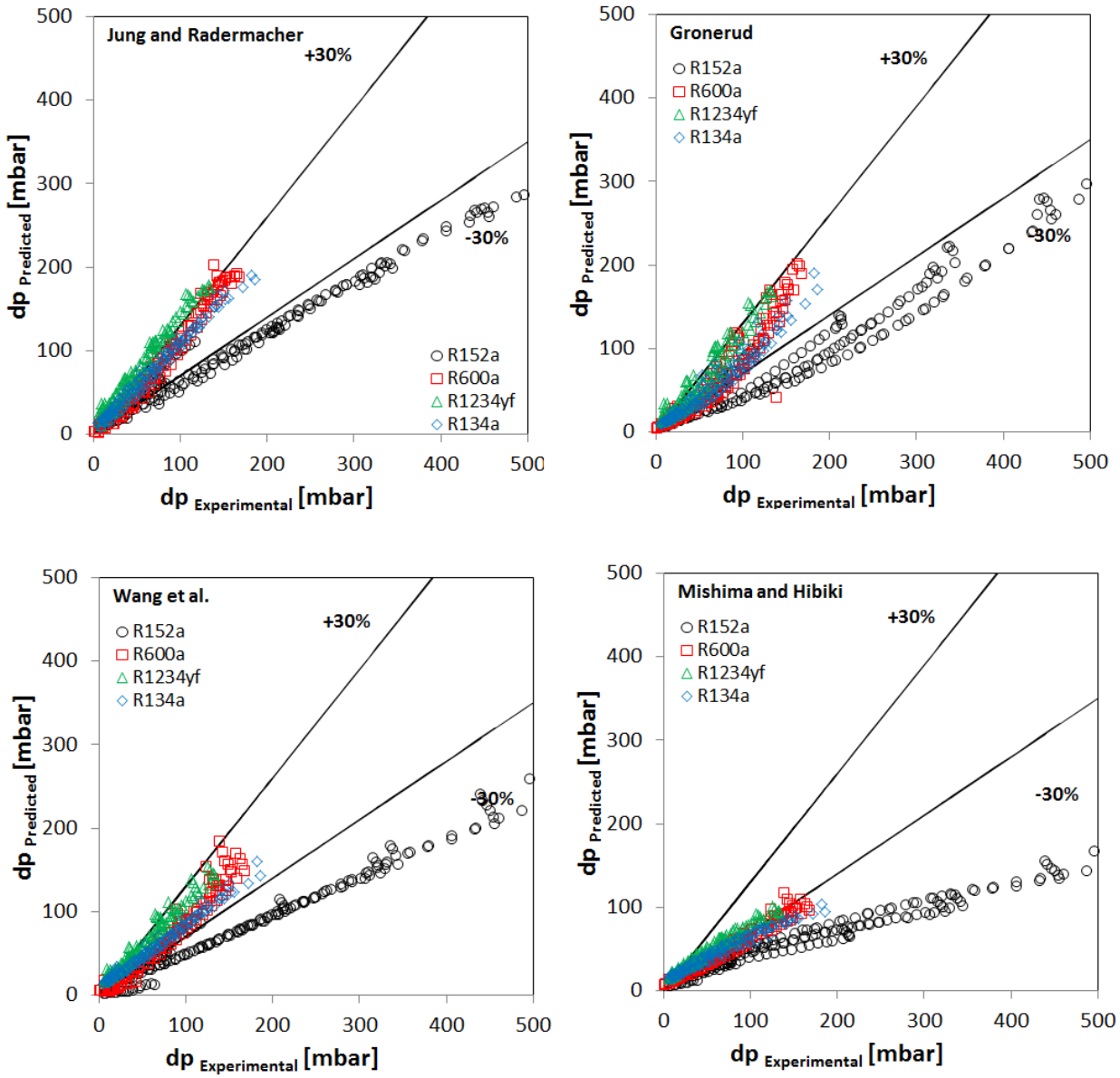

Figure 5.3 Comparison of experimental frictional pressure drop with correlations from the literature

Table 5-2 Statistical summary for comparison with correlations

Correlation	**MAE**	**Percentage of data within ± 30%**
Homogenous Model [13]	55.24	9.04
Lockhart and Martinelli [60]	50.97	40.95
Friedel [57]	36.70	36.71
Müller-Steinhagen and Heck [51]	40.70	0
Jung and Radermacher [95]	33.72	45.94
Mishima and Hibiki [49]	39.45	38.19
Yang and Webb [99]	47.76	19.37
Tran et al. [23]	45.23	47.78
Hwang and Kim [59]	55.67	36.96
Sun and Mishima [100]	40.29	32.28
Li and Wu [101]	44.08	35.05
Zhang et al. [52]	53.80	16.05
Grönnerud [96]	31.20	52.76
Wang et al. [97]	35.25	53.50

Chapter 6. Experimental Results for Dryout Heat Flux

Heat transfer/thermal performance of the two-phase system heavily relies on imposed operating conditions. In a two-phase system, a liquid starved surface results in drastically reduced heat transfer coefficients. Furthermore, the situation becomes even worse in heat flux controlled applications where surface temperatures sharply rise, leading to possible catastrophic failure of the device. With the aforementioned circumstance in mind, it is therefore very important to know the safe and effective operating limits. This chapter summarizes the experimental results on dryout for the four refrigerants tested along with previous data from our lab [2] [66] [1] on R290, R22 and R245fa. The detailed operating conditions and test section characteristics are summarized in Table 6-1. Detailed results with each medium can separately be found in Paper 1, Paper 2 and Paper 3 for R152a, R600a and R1234yf respectively, whereas Paper 4 has discussion on combined dryout database collected at KTH (Four refrigerants of this study +previous data).

Table 6-1 Summary of operating conditions for dryout experiments

Refrigerant	Data source	Diameter [mm]	Heated length [mm]	Saturation temperature [°C]	Mass flux [kg/m²s]	$\Delta t_{sub,\,in}$ [K]	R_a [μm]
R1234yf	This study	1.60	245	27 and 32	100-500	1-1.5	0.95
R134a	This study+ Callizo [16]	0.64, 1.6	245 and 213	27 and 32	50-600	1-1.5	0.95, 0.77[4]
R152a	This study	1.60	245	27 and 32	100-500	1-1.5	0.95
R290	Maqbool et al. [2]	1.224 and 1.70	245	23, 33 and 43	100-500	1-1.5	0.21[5], 2.55
R600a	This study	1.60	245	27 and 32	50-350	1-1.5	0.95
R22	Callizo [16]	0.64	213	25 and 30	170-525	1-1.5	0.77
R245fa	Callizo [16]	0.64	213	30	200-335	1-1.5	0.77

6.1 Dryout detection criteria

In heat flux controlled applications, dry patches can easily be traced from a significantly high degree of wall superheat in the dried region. The dryout conditions first appear close to the outlet of test section and travel upstream toward the inlet side with increased heat flux. The surface/wall temperature fluctuates a great deal in the dried region; thus standard deviation of the collected temperature data is another criterion that indicates

[4] For 0.64 mm tube, where heated length was 213 mm
[5] For 1.70 mm tube

dryout. In this study, boiling curves (Figure 6.1) based on temperature reading from the final thermocouple were used to identify the initiation and completion of dryout. Dryout incipience is the point at which the normal trend changes in a boiling curve following the nucleate boiling regime. At this point, the heater surface is intermittently dry and wet with the passage of incoming fluid streams. As the process continues, slightly higher heat fluxes lead to the dryout completion region, where wall temperature sharply rises. For this study, dryout completion was defined by $t_{wall\ superheat} > 15$ °C and an electrical relay was used to switch off the power supply when surface temperature crossed the 70 °C limit. This preserved the functionality of the test section for next test run.

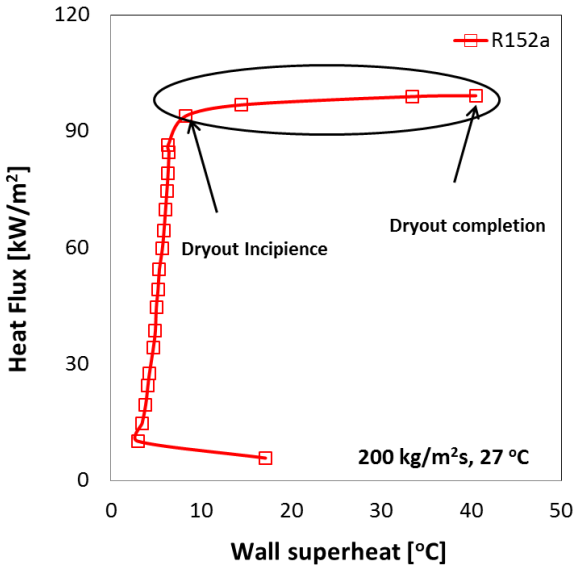

Figure 6.1 Criteria for identification of dryout incipience and completion

The local wall temperatures and heat transfer coefficients at dryout conditions are shown in Figure 6.2. The depicted results are of R1234yf, for five mass fluxes at 27 °C saturation temperature. A sharp increase in wall temperature and drastic decrease in the heat transfer coefficient at the final thermocouple location clearly indicates the dried region.

Figure 6.3 shows heat flux at dryout incipience and completion versus vapor quality at the final thermocouple location. For each case, the two points are connected with a straight line, with dryout incipience heat flux occurring at lower vapor quality.

Experimental results for vapor quality (for four refrigerants of this study) at the incipience of dryout were compared with S2 regime of the dryout model proposed by Mori et al. [102] and its modified version from Wojtan et al. [103] and is shown in Figure 6.4. The appendix contains formulation for these correlations. The comparison of our experimental data shows good agreement with predictions from the original model at high mass flux conditions ($G>200$ kg/m²s), whereas the modified variant highly under-predicted data. Chiapero et al. [104] also reported better predictions for dryout incipience quality with model from Mori et al. [102].

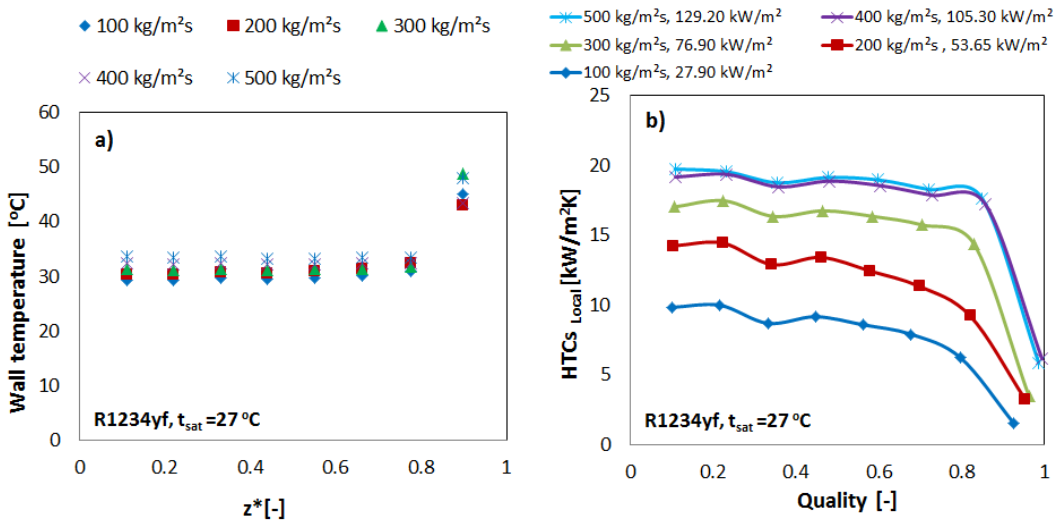

Figure 6.2 Local wall temperatures and HTCs (for R1234yf) on completion of dryout

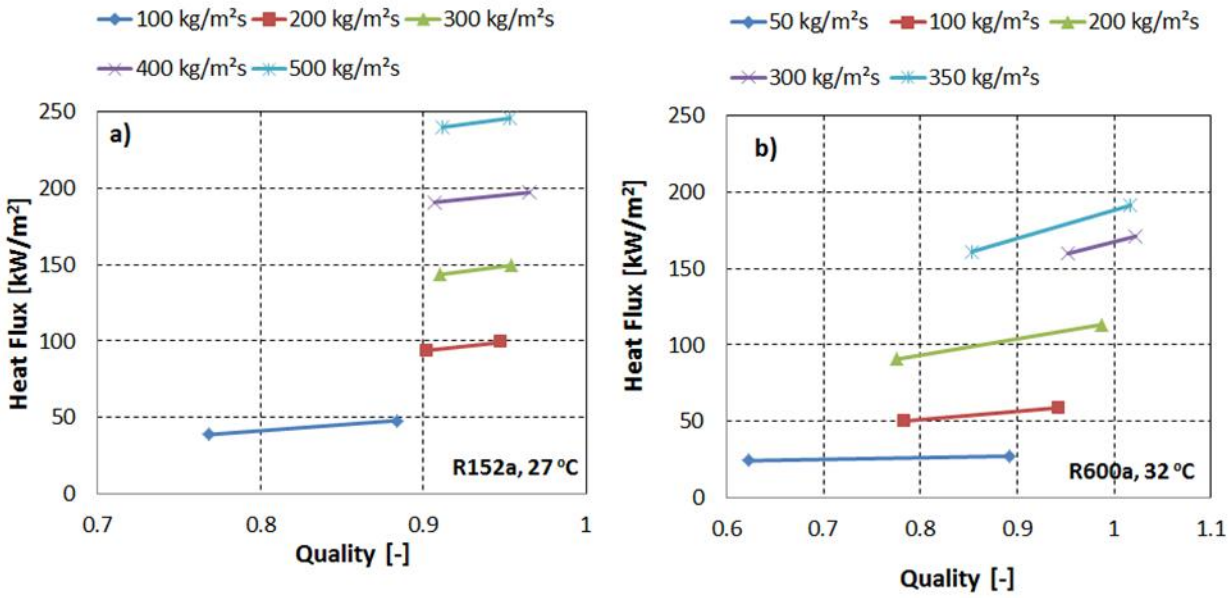

Figure 6.3 Heat flux at dryout incipience and completion versus vapor quality

6.2 Parametric effects on Dryout

6.2.1 Effect of mass flux

The effects of varying mass flux on dryout heat flux (on completion of dryout) are shown in Figure 6.5. For all cases operating conditions (tube size and saturation temperature) are given in the legends. The results from Maqbool et al. [2] and from Callizo [16] are shown in Figure 6.5a, while all other cases (see Table 6-1) are shown in Figure 6.5b. As was expected, dryout heat flux linearly increased with increasing mass flux for all experimental datasets. The linear increase in dryout heat flux suggests an almost constant value for critical

vapor quality (vapor quality at dryout). This can be simply explained as the fact that more heat energy is required to attain a specific vapor fraction/quality.

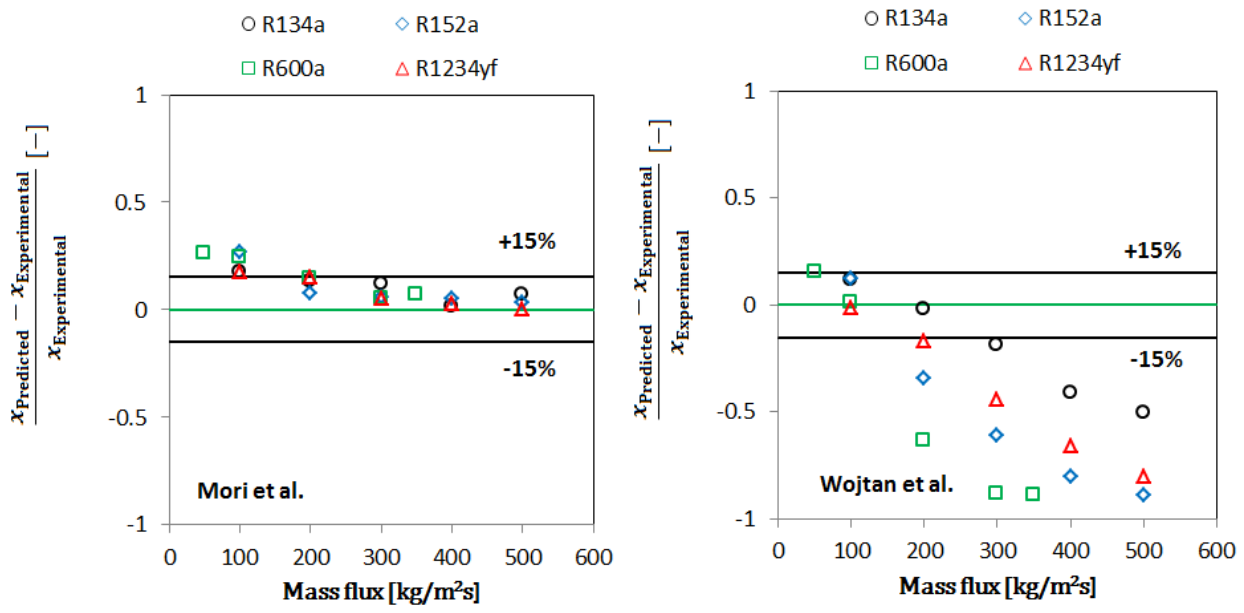

Figure 6.4 Comparison of dryout vapor quality (at dryout incipience conditions) with correlations from Mori et al. [102] and Wojtan et al. [103]

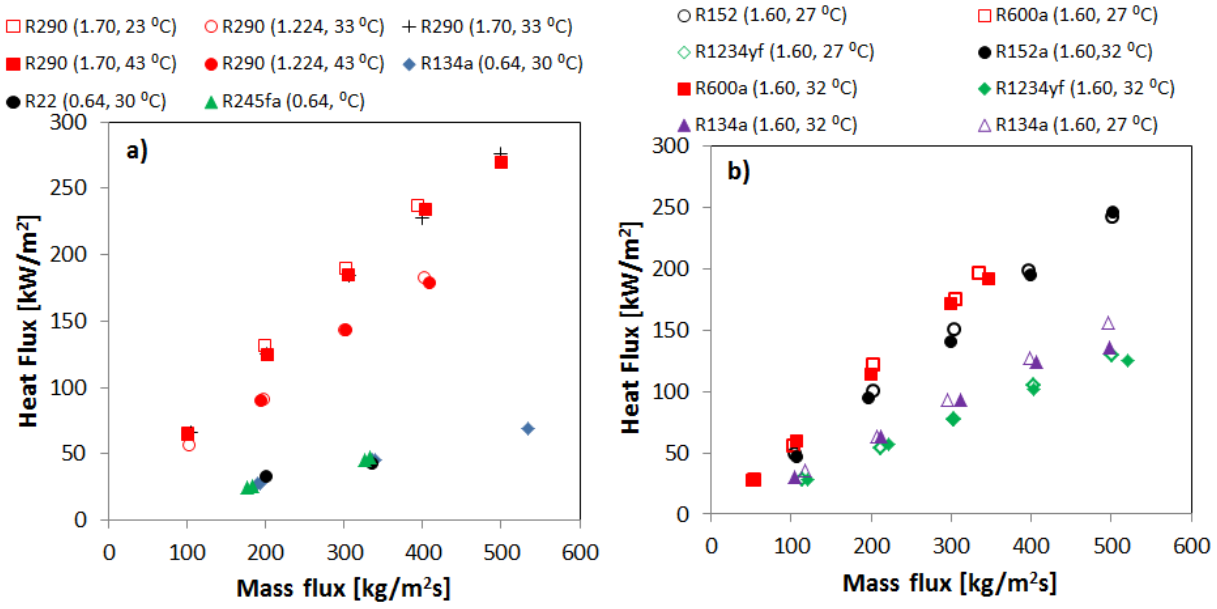

Figure 6.5 Dryout heat flux versus mass flux at different saturation temperatures

6.2.2 Effect of saturation pressure

The effect of varying saturation temperature is also shown in Figure 6.5. The filled symbols refer to the high saturation temperature case. The dryout heat flux remained almost unaffected by varying saturation temperature for the test span. Increased saturation temperature results in reduced heat of vaporization and lower density ratio (liquid/vapor). The reduced heat of vaporization suggests lower values for dryout heat flux at higher saturation temperatures. However, an opposite effect is caused by the reduced density ratio. The reduced density ratio results in reduced vapor velocity (lower suppression of nucleate boiling), which may positively contribute to sustaining the thin liquid film on the heated wall by reducing the droplet entrainment rate into the vapor core, consequently tending to increase dryout heat flux.

Higher values for critical heat flux at high operating pressures have been reported by Wojtan et al. [63]. Their experiments were carried out with R134a and R245fa in 0.5 and 0.8 mm tubes at 30 and 35 ^{o}C saturation temperatures. Reduced critical heat flux at high mass flux (>600 kg/m^{2}s) and at higher saturation temperature has been reported by Ong and Thome [9] and Tibiriça et al. [62]. These trends were reported for high mass flux conditions, with significantly high heat fluxes than those presented in this study.

6.2.3 Critical vapor quality

Vapor quality at the dryout condition is termed as critical vapor quality in the literature. Figure 6.6 shows the trend for critical vapor quality versus mass flux at different operating conditions (see Table 6-1). Critical vapor quality varied in a narrow range, which can be explained by the linear increase in dryout heat flux with mass flux as shown in Figure 6.5. In some cases (see Figure 6.3 and Figure 6.6), vapor quality at complete dryout condition was > 1. This is probably due to the fluctuation in mass flux on the downstream side of the test section. The incoming liquid stream periodically wets the heating surface to the point where the average vapor quality was > 1.

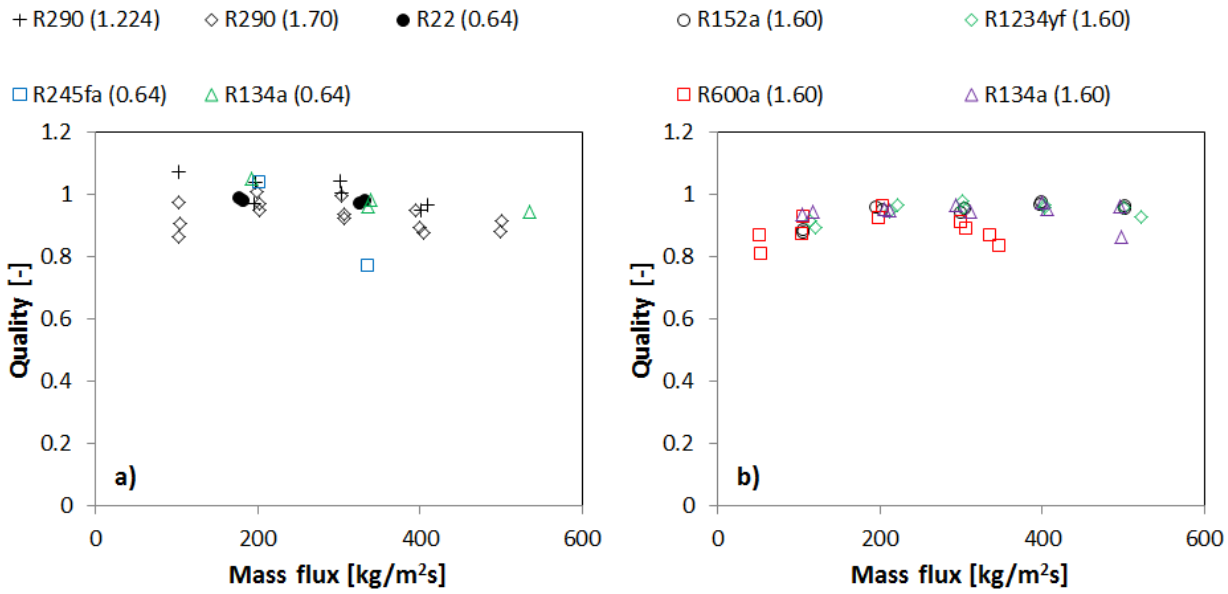

Figure 6.6 Critical vapor quality versus mass flux, (6a) Data from previous studies and (6b) data from this study (see Table 6-1 for details)

6.2.4 Effect of the fluid

As can be seen in Figure 6.5, dryout heat flux has a fluid effect. Under similar operating conditions (mass flux, degree of inlet sub-cooling, saturation temperature, channel size), higher values for dryout heat flux were observed for hydrocarbons, followed by the values for R152a and R134a. The lowest values were recorded for R1234yf. Dryout heat flux for all refrigerants was compared with that of R134a. The proportional difference agreed well with the difference in the heat of vaporization for tested refrigerants. This can also be noticed from almost constant critical vapor qualities as shown in Figure 6.6, occurrence of dryout will follow difference in heat of vaporization for approaching a certain vapor fraction. Ong and Thome [9] also reported the difference in the heat of vaporization as being the contributing factor in the difference in critical heat flux for their experiments with R134a, R236fa and R245fa. Tibiriça et al. [71] additionally reported higher critical heat flux values for fluid with higher surface tension and low reduced pressure. As per Tibiriça et al. [71], high surface tension reduces the interface wave amplitude and liquid droplet entrainment into the vapor core. Thus, fluids with high surface tension may have higher values for dryout heat flux.

6.2.5 Effect of channel size

The effect of channel size can be seen in Figure 6.5a for propane. It was observed that dryout heat flux increased with increasing channel diameter. It should also be mentioned that both tubes had same heated length with different surface characteristics (Ra). Figure 6.6a shows almost similar values for critical vapor quality for both tubes tested with propane, almost similar results for R134a can be noticed from Figure 6.6a and Figure 6.6b. Increase in heat flux at dryout with larger channels can thus be explained by higher heat demands (due to increased mass flow rate in larger channel under constant mass flux conditions) to reach the critical vapor quality values. This trend could also be explained by the presence of slightly reduced shear force in larger channels, which might be favorable for the establishment of the thin liquid layer on the heating surface, consequently resulting in enhanced dryout heat flux values. Similar results have been reported by Mikielewicz et al. [65] and Wojtan et al. [63]. However, Ong and Thome [9] reported an increase in critical heat flux with decreasing channel size until a threshold size is reached (0.79 to 1.03 mm in their case), after which critical heat flux decreased with further reduction in the tube size. However it should be mentioned, their observed trend was also having influence from varying heated length. The effective heated length was not fixed for all those channels. A close observation revealed indeed CHF increased with reduction in l/d, this is an expected trend and can be seen from many correlations.

6.3 Comparison with correlations from the literature

The experimental results for dryout heat flux were compared with predictions using well-cited macro and micro-scale correlations from the literature. The formulations for correlations can be found in the appendix. The predictions for best worked cases are graphically presented in Figure 6.7 to Figure 6.9, while a statistical summary for all tested correlations is given in Table 6-2. Two statistical parameters—mean absolute error (MAE) and percentage of data within ± 25% were used for this comparison. All plots (Figure 6.7-Figure 6.9) shows departure of predicted values from experimental ones $\left[\frac{q''_{\text{Predicted}} - q''_{\text{Experimental}}}{q''_{\text{Experimental}}} * 100\ [\%]\right]$ plotted against mass flux.

The Katto-Ohno correlation [28] has been widely cited in the literature for prediction of saturated critical heat flux in the single channel configuration. This correlation was originally developed from a conventional channels-based (d>3 mm) database; however, satisfactory predictions for mini/micro-channel have been reported using its modified form, as reported by Wojtan et al. [63] and Ong and Thome [9]. Comparison of our data with this correlation shows good predictive capability, as most of the data points were captured

within ±25% of their experimental values. However, the data was mostly under-predicted, especially at high mass flux conditions, as can be seen in Figure 6.7.

Bowring's correlation [68] was developed from a water-based dataset collected from large tubes. As with the Katto-Ohno correlation [28], Bowring's correlation [68] worked well at low mass fluxes, whereas under-predictions were noted at moderate and high mass fluxes.

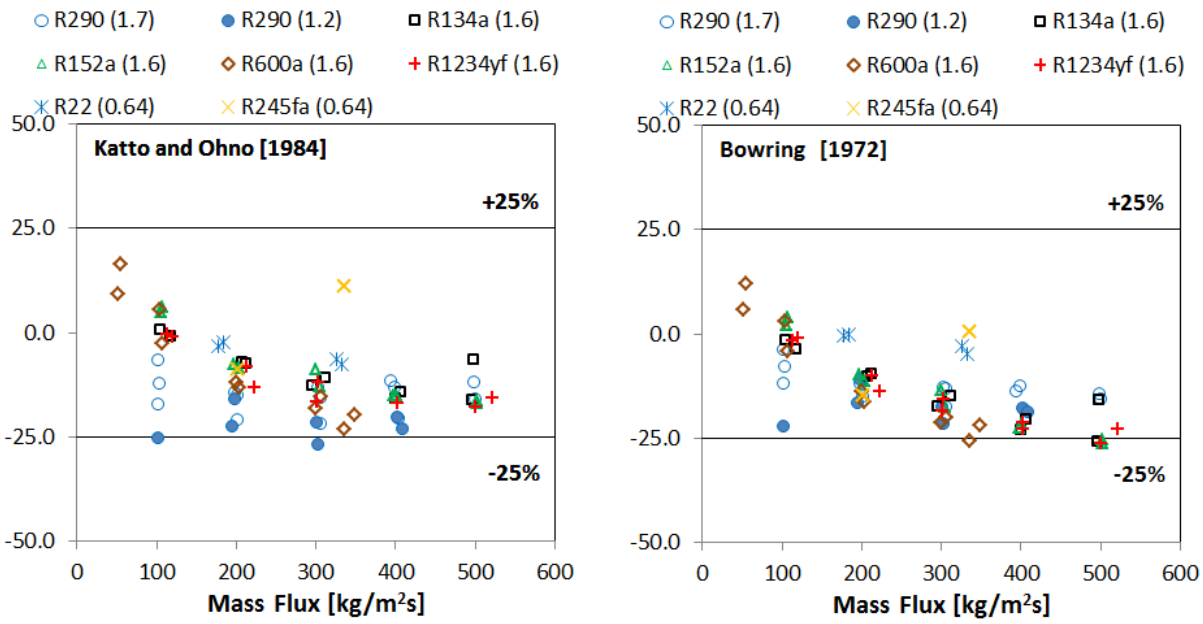

Figure 6.7 Dryout heat flux comparison with macro scale correlations from literature

Prediction results from the micro-scale correlations are shown in Figure 6.8. Modified versions of the Katto-Ohno model [28] have been proposed by Wojtan et al. [63] and Callizo et al. [66], based on micro-scale databases with R134a, R245fa and R22. The leading constants and exponents were modified in these versions. A comparison with our data showed good predictive ability of Callizo's model [66], whereas scattered predictions were obtained with Wojtan's recommendation [63]. In using Callizo's recommendation, all data points were predicted to be within ±25% error span, with 9% MAE value (whereas only 40% points were captured by Wojtan's version [63]).

Mikielewicz et al. [65] proposed another micro-scale correlation for estimation of saturated dryout heat flux values in single mini-channels. This correlation was developed from a Solkatherm SES 136, R123, R134a and ethanol-based database. The predictions showed that the data was well traced at low mass flux conditions (with the exception of hydrocarbons), after which the data was mostly under-predicted (at moderate and high mass fluxes).

Another correlation for estimation of saturated critical heat flux was proposed by Wu et al. [105]. This correlation was developed from a large database (629 data points) from water and refrigerants. This correlation accounts for exit vapor quality in addition to geometrical parameters such as (l_h/d_h) and mass velocity. This correlation gave good predictions, with > 80% data points captured within the ±25% limit. However, the data was mostly under-predicted. Predictions could be further refined by replacing the leading multiplier with 0.70 instead of 0.60 in the original correlation (Figure 6.8 shows predictions from original correlation and Figure 6.9 with the modified version). With its modified form, this correlation captured >95% of data points within the ± 25% error limit, and about 7.50% MAE.

Based on above mentioned experimental results (linear increase in mass flux and almost constant critical vapor quality) a new simple correlation for prediction of dryout heat flux has been proposed. This relies on heat demand to attain critical vapor quality conditions and could be used for estimation of dryout heat flux values for single mini-channels.

$$\frac{q''_{CHF}}{Gh_{lg}} = 0.27 \cdot \left(\frac{d}{l}\right) \tag{6.1}$$

This correlation satisfactorily predicted all experimental data within ±25%.

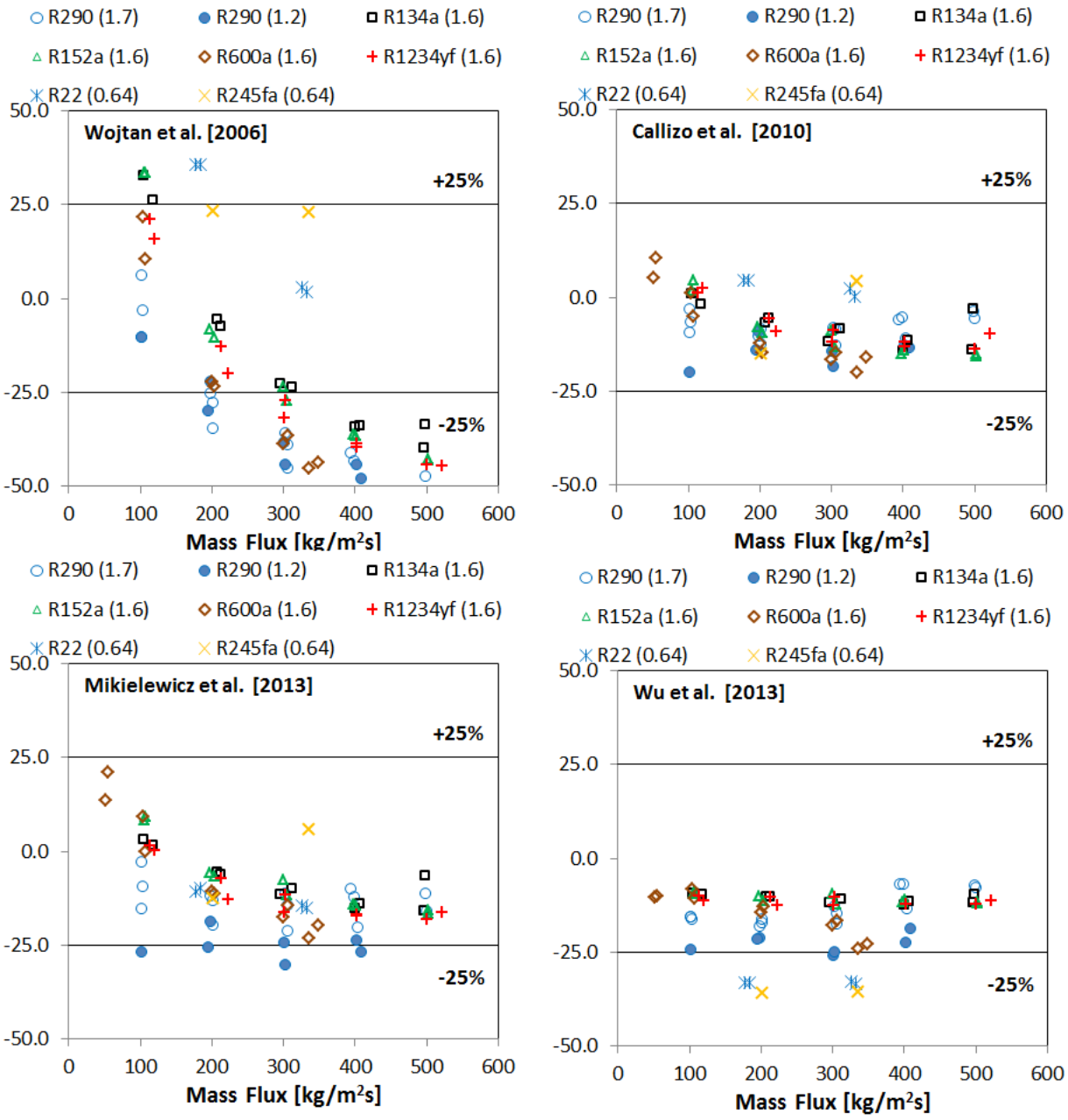

Figure 6.8 Dryout heat flux comparison with micro-scale correlations from the literature

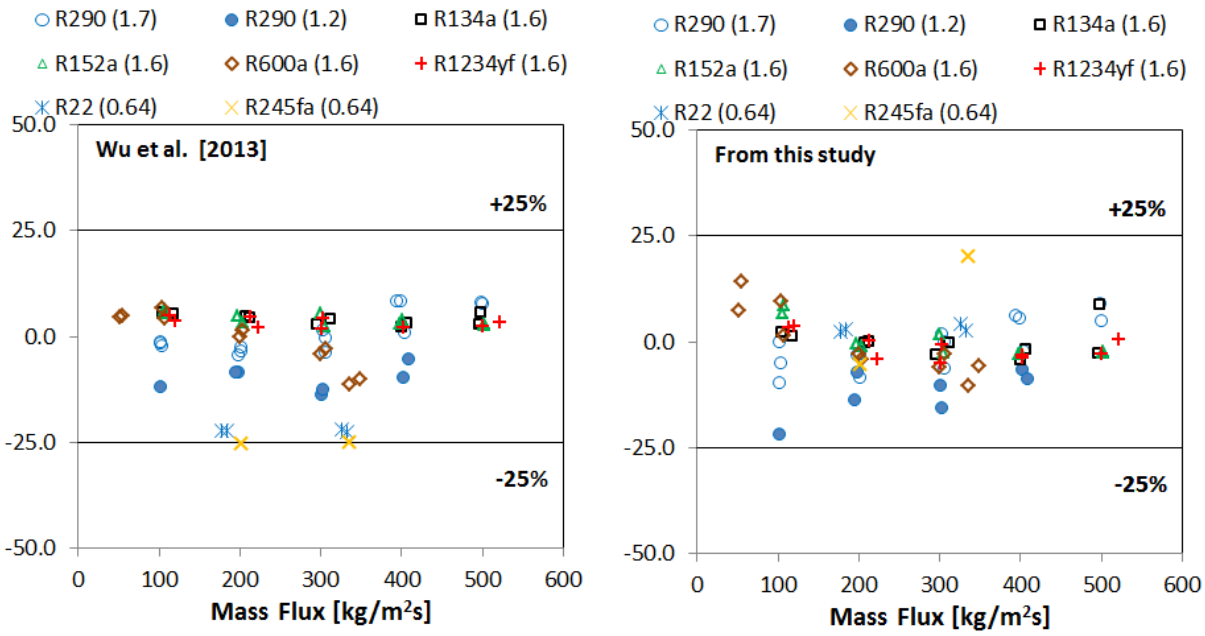

Figure 6.9 Dryout heat flux comparison with modified Wu's correlation [105] and newly proposed correlation from this study

Table 6-2 Summary of comparison with correlations from the literature

Correlation	MAE/Percentage of data ± 25%	Applicability range
Macro-scale correlations		
Katto-Ohno [28]	12.66/97.22	Developed from a large database including water, nitrogen, helium, R12, R22 and R113 in large tubes
Bowring [68]	13.36/93.05	Developed from a wide database of water in large tubes
Zhang et al. [106]	27.15/37.50	Developed from an experimental database on saturated flow boiling of water in small diameter tubes (0.33-6.2 mm)
Shah [107]	29.55/29.16	Developed from a large database (water and non-aqueous fluids) from 23 independent sources
Micro-scale correlations		
Wu et al. [105]	17/81.94	Saturated flow boiling critical heat flux for micro-channels (experimental database had refrigerants, water and nitrogen)
Mikielewicz et al. [65]	13.94/95.83	Developed from a database of SES 36, R134a, R123 and Ethanol in 1.15 and 2.3 mm silver circular channels
Ong and Thome [9]	23.38/59.72	Revised version of Wojtan's correlation [63] Developed from a database including R134a, R245fa, R236fa and data from single and multi-channels
Callizo et al. [66]	09.15/100	Modified form of Katto-Ohno correlation [28] based on experiments with R134a, R245fa & R22 in a vertical circular 640 μm test section
Wojtan et al. [63]	30.55/40.27	Revised version of Katto-Ohno correlation [28] Least square curve fitting for R134a and R245fa in 0.5 and 0.8 mm circular channels
New from this study	5.4/100	For Single vertical mini-channels, developed from refrigerant based database.

Chapter 7. Conclusions and Future Recommendations

7.1 Conclusions

For boiling heat transfer, strong effect of heat flux and system pressure was noticed, with an insignificant effect of vapor quality and mass flux (for $x < 0.85$) for all four refrigerants in this study.

Under similar operating conditions, R1234yf and R152a showed nearly comparable heat transfer results to R134a, whereas ammonia R22 and R600a showed lower values for heat transfer coefficients. R290 shows better thermal performance than R134a. Different thermal behavior from these mediums is due to different thermophysical properties.

Trends observed in this study have similarity with what could be expected from nucleate boiling. Channel confinement restricts radial growth for the vapor bubbles, consequently elongated bubble and annular regimes predominates the flow. We believe that trends reported in this study just have similarity with what would conventionally be expected from nucleate boiling process and in reality this similarity is coming from the bubble formation and evaporation of thin liquid film processes.

Among macro-scale models, the correlations from Chen [88] and Gungor and Winterton [89] showed good predictions (with the exception of R600a), whereas the micro-scale model from Mahmoud and Karayiannis [91] quite satisfactorily predicted the entire database for this study.

Under similar operating conditions, R152a, and R600a showed higher frictional pressure drop than R134a whereas R1234yf showed lower values than R134a, and effect can partially be explained by the difference in thermo-physical properties.

For almost all cases a peak in pressure drop curve was observed at about 85% vapor quality and this was not influenced by mass flux.

None of tested correlations (frictional pressure drop) worked well for R152a, although comparatively better predictions were noticed with correlation from Wang et al. [97] and Grönnerud [95].

Dryout heat flux increased with tube size and mass flux, while remained mostly unaffected by variations in saturation temperature.

Critical vapor quality (experimental value) varied in a narrow range, suggesting that dryout was triggered by complete evaporation of the thin liquid film on the heating surface. Experimental results for vapor quality at incipience of dryout agreed well with correlation from Mori et al. [102] whereas the same was highly under-predicted with Wojtan's model [103].

Under similar operating conditions (mass flux, saturation temperature, test section, degree of sub-cooling), the hydrocarbons (R290 and R600a) showed the highest values for dryout heat flux, followed by R152a and R134a, with the lowest values recorded for R1234yf. The proportional difference among these fluids agreed well with differences in their heat of vaporization.

Among the macro-scale correlations, satisfactory predictions were obtained using the Katto-Ohno correlation [28], whereas reasonable prediction for the entire test span were observed with modified version of Wu's micro-scale model [105].

A new, simple correlation for prediction of dryout heat flux has been proposed. This is based on simple energy balance method to reach the critical vapor quality conditions. This model accurately predicted whole database of this study.

7.2 Future recommendations

Experiments could be repeated with an indirect heating approach to clarify the details of heat transfer and dryout characteristics after incipience of dryout or after transition from annular to mist flow region. It is not possible to explore these minute details under heat flux controlled conditions.

This study was not focused on any specific application. Experiments targeting specific applications (e.g. heating load or cooling demand) and using commonly used components (e.g. a compact evaporator with number of parallel channels) would thus be beneficial and appealing.

Use of advanced tools, a high-speed visualization study, or infrared thermometry could be helpful in defining transition limits for various flow regimes and for analysis other important parameters (such as dried length).

A broader range of operating conditions (system pressure, inlet conditions, channel configuration and characteristics) should also be tested.

Nomenclature

A_c	Cross sectional area [m^2]
A_h	Heat surface area [m^2]
C_p	Specific heat capacity [J/kg K]
d	Hydraulic diameter of channel [m]
F	Convective boiling enhancement factor [-]
f	Friction factor [-]
g	Gravitational acceleration [m/s^2]
G	Mass Flux [kg/m^2s]
h_{lg}	Heat of vaporization [kJ/kg]
I	Current supplied [A]
k	Thermal conductivity [W/mK]
l_h	Heated length of test section [m]
$\dot{m}$	Mass flow rate [kg/s]
p	Pressure [bar]
p_r	Reduced pressure [-]
Q	Heat supplied [W]
q"	Heat flux [kW/m^2]
Ra	Average roughness value [μm]
S	Nucleate boiling suppression factor [-]
t	Temperature [^oC]
v	Specific volume [m^3/kg]
V	Voltage [V]
x	Vapor quality [-]
z	Axial location [m]
z_o	Subcooled/Single phase length [m]
Δp	Pressure drop [mbar]

Subscripts

CHF	Critical heat flux
CB	Convective boiling
D	Based on diameter
D-B	Dittus-Boelter correlation
di	Dryout Incipience
dc	Dryout completion
f_{fl}	Fluid surface parameter
Fluid,z	Fluid at location z
g	Gas phase
go	Gas only
l	Liquid phase
lam	Laminar flow condition
lh	Based on heated length
lo	Liquid only

Nb	Nucleate/Pool boiling
sat	Saturation condition
tp	Two-phase
turb	Turbulent flow conditions
Wall,z	Wall on location z

Dimensionless groups

Bd	Bond No $\left[\frac{(\rho_l-\rho_g)gd^2}{\sigma}\right]$
Bo	Boiling No $\left[\frac{q''}{Gh_{lg}}\right]$
Co	Confinement No $\left[\sqrt{\frac{\sigma}{g(\rho_l-\rho_g)d^2}}\right]$
Eo	Eötvös No $\left[\frac{(\rho_l-\rho_g)gd^2}{8\sigma}\right]$
Nu	Nusselt No $\left[\frac{h\cdot d}{k}\right]$
Pr	Prandtl No $\left[\frac{\mu\cdot C_p}{k}\right]$
Re	Reynolds No $\left[\frac{Gd}{\mu}\right]$
We	Weber No $\left[\frac{Gd}{\rho\sigma}\right]$

Greek letters

α	Heat transfer coefficient [kW/m^{2}K]
σ	Surface Tension [N/m]
ϱ	Density [kg/m^3]
μ	Dynamic viscosity [N.s/m^2]

Bibliography

[1] R. Ali and B. Palm, "Dryout characteristics during flow boiling of R134a in vertical circular minichannels," *International Journal of Heat and Mass Transfer,* vol. 54, pp. 2434-2445, 2011.

[2] M. H. Maqbool, B. Palm and R. Khodabandeh, "Experimental investigation of dryout of propane in uniformly heated single vertical mini-channels," *Experimental Thermal and Fluid Science,* vol. 37, pp. 121-129, 2012.

[3] M. Hamdar, A. Zoughaib and D. Clodic, "Flow boiling heat transfer and pressure drop of pure HFC-152a in a horizontal minichannel," *International Journal of Refrigeration,* vol. 33, pp. 566-577, 2010.

[4] B. Agostini, M. Fabbri, J. E. Park, L. Wojtan, J. R. Thome and B. Michel, "State of the Art of High Heat Flux Cooling Technologies," *Heat Transfer Engineering,* vol. 28, pp. 258-281, 2007.

[5] S. S. Mehendale, R. K. Shah and A. M. Jacobi, "Fluid flow and heat transfer at micro and meso scales with applications to heat exchanger design," *Applied Mechanics Reviews,* vol. 53, pp. 175-193, 2000.

[6] S. G. Kandlikar and W. J. Grande, "Evolution of Microchannel Flow Passages—Thermohydraulic Performance and Fabrication Technology," *Heat Transfer Engineering,* vol. 24, no. 1, pp. 3-17, 2003.

[7] P. A. Kew and K. Cornwell, "Correlations for the prediction of boiling heat transfer in small diameter channels," *Applied Thermal Engineering,* vol. 17, pp. 705-715, 1997.

[8] K. A. Triplett, S. M. Ghiaasiaan, S. I. Abdel-Khalik and D. L. Sadowski, "Gas liquid two-phase flow in microchannels Part 1: Two Phase Flow Patterns," *International Journal of Multiphase Flow,* vol. 25, pp. 377-394, 1999.

[9] C. L. Ong and J. R. Thome , "Macro-to-microchannel transition in two-phase flow: Part 2 – Flow boiling heat transfer and critical heat flux," *Experimental Thermal and Fluid Science,* vol. 35, no. 6, pp. 873-886, 2011.

[10] T. Harirchian and S. V. Garimella, "A comprehensive flow regime map for microchannel flow boiling with quantitative transition criteria," *International Journal of Heat and Mass Transfer,* vol. 53, pp. 2694-2702, 2010.

[11] W. Li and Z. Wu, "A general criterion for evaporative heat transfer in micro/mini-channels," *International Journal of Heat and Mass Transfer,* vol. 53, pp. 1967-1976, 2010.

[12] A. Ullmann and N. Brauner, "The prediction of flow pattern maps in minichannels," *Multiphase Science and Technology,* vol. 19, pp. 49-73, 2007.

[13] J. G. Collier and J. R. Thome, Convective boiling and condensation, Third ed., Oxford University press, 1994, p. 176.

[14] M. H. Maqbool, B. Palm and R. Khodabandeh, "Investigation of two phase heat transfer and pressure drop of propane in a vertical circular minichannel," *Experimental Thermal and Fluid Science,* vol. 46, pp. 120-130, 2103.

[15] M. H. Maqbool, B. Palm and R. Khodabandeh, "Boiling heat transfer of ammonia in vertical smooth mini-channels: Experimental results and predictions," *International Journal of Thermal Sciences,* vol. 54, pp. 13-21, 2012.

[16] C. M. Callizo, "Flow boiling heat transfer in single vertical channels of small diameter," Doctoral Thesis in Energy Technology, Stockholm, 2010.

[17] S. Saitoh, C. Dang, Y. Nakamura and E. Hihara, "Boiling heat transfer of HFO-1234yf flowing in a smooth small diameter horizontal tube," *International Journal of Refrigeration,* vol. 34, pp. 1846-1853, 2011.

[18] S. Saitoh, H. Diaguji and E. Hihara, "Correlation for boiling heat transfer of R134a in horizontal tubes including effect of tube diameter," *International Journal of Heat and Mass Transfer,* vol. 50, pp. 5215-5225, 2007.

[19] T. N. Tran, M. W. Wambsganss and D. M. France, "Small circular and rectangular channel boiling with two refrigerants," *International Jouranl of Multiphase Flow,* vol. 22, pp. 485-498, 1996.

[20] D. Del-Col, S. Bortolin, D. Torresin and A. Cavallini, "Flow boiling of R1234yf in a 1 mm diameter channel," *International Journal of Refrigeration,* vol. 36, pp. 353-362, 2013.

[21] J. B. Copetti , M. H. Macagnan and F. Zinani, "Experimental study on R-600a boiling in 2.6 mm tube," *International Journal of Refrigeration,* vol. 36, pp. 325-334, 2013.

[22] S. G. Kandlikar and P. Balasubramanian, "An extension of the flow boiling correlation to transition, laminar and deep laminar flows in minichannels and microchannels," *Heat Transfer Engineering,* vol. 25, pp. 86-93, 2004.

[23] T. N. Tran, M. C. Chyu and M. W. Wambsganss, "Two-phase pressure drop of refrigerants during flow boiling in small channels: an experimental investigation and correlation development," *International Journal of Refrigeration,* vol. 26, pp. 1739-1754, 2000.

[24] M. G. Cooper, "Saturation Nucleate pool boiling, a simple correlation," in *1st UK National conference on Heat Transfer*, Leeds, 1984.

[25] R. Ali, B. Palm and M. H. Maqbool, "Flow Boiling Heat Transfer Characteristics of a Minichannel up to Dryout Condition," *Journal of Heat Transfer ,* vol. 133, pp. 081501-10, 2011.

[26] R. Ali and B. Palm, "Study of Flow Boiling characteristics of a microchannel using high speed visualization," *ASME Journal of Heat Transfer,* vol. 135, pp. 81501-08, 2013.

[27] C. B. Tibiriça, G. Ribatski and J. R. Thome, "Flow Boiling Characteristics for R1234ze(E) in 1.0 and 2.2 mm circular channel," *Journal of Heat Transfer,* vol. 134, pp. 1-8, 2012.

[28] Y. Katto and H. Ohno, "An improved version of the generalized correlation for critical heat flux for forced convective boiling in uniformly heated vertical tubes," *International Journal of Heat and Mass Transfer,* vol. 27, no. 9, pp. 1641-1648, 1984.

[29] J. B. Copetti, M. H. Macagnan, F. Zinani and N. L. F. Kunsler, "Flow boiling heat transfer and pressure drop of R-134a in a mini tube: an experimental investigation," *Experimental Thermal and Fluid Science,* vol. 35, pp. 636-644, 2011.

[30] L. Saraceno, G. P. Celata, M. Furrer, A. Mariani and G. Zummo, "Flow boiling heat transfer of refrigerant FC-72 in microchannels," *International Journal of Thermal Sciences,* vol. 53, pp. 35-41, 2012.

[31] Z. Liu and R. H. S. Winterton, "A general correlation for saturated and subcooled flow boiling in tubes and annuli, based on nucleate pool boiling equation," *International Journal of Heat and Mass Transfer,* vol. 34, no. 11, pp. 2759-2766, 1991.

[32] S. Saisorn, J. Kaew-On and S. Wongwises, "Flow pattern and heat transfer characteristics of R134a refrigerant during flow boiling in a horizontal circular mini channel," *International Journal of Heat and Mass Transfer,* vol. 53, no. 19-20, pp. 4023-4038, 2010.

[33] A. S. Pamitran, K.-I. Choi, J.-T. Oh and H.-K. Oh, "Forced convective boiling heat transfer of R-410A in horizontal minichannels," *International Journal of Refrigeration,* vol. 30, pp. 155-165, 2007.

[34] B. Agostini, J. R. Thome, M. Fabbri, B. Michel, D. Calmi and U. Kloter, "High heat flux flow boiling in silicon multi-microchannels –Part 1 Heat transfer characteristics of refrigerant R236fa," *International Journal of Heat and Mass Transfer,* vol. 51, pp. 5400-5414, 2008.

[35] C. Huh and M. H. Kim, "Pressure Drop, Boiling Heat Transfer and Flow Patterns during flow boiling in a single microchannel," *Heat Transfer Engineering,* vol. 28, pp. 730-737, 2007.

[36] S. In and S. Jeong, "Flow boiling heat transfer characteristics of R123 and R134a in a micro-channel," *International Journal of Multiphase Flow,* vol. 35, pp. 987-1000, 2009.

[37] R. Yun, J. H. Heo and Y. Kim, "Evaporative heat transfer and pressure drop of R410A in microchannels," *International Journal of Refrigeration,* vol. 29, pp. 92-100, 2006.

[38] S. Mortada, A. Zoughaib, C. Arzano-Daurelle and D. Clodic, "Boiling heat transfer and pressure drop of R-134a and R1234yf in minichannels for low mass fluxes," *International Journal of Refrigeration,* vol. 35, pp. 962-973, 2012.

[39] C. Martin-Callizo, B. Palm, W. Owhaib and R. Ali, "Flow boiling visualization of R134a in a vertical channel of small diameter," *ASME Journal of Heat Transfer,* vol. 132, pp. 1-8, 2010.

[40] L. Consolini and J. R. Thome, "Micro-channel flow boiling heat transfer of R-134a, R-236fa, and R245fa," *Microfluid Nanofluid,* vol. 6, pp. 731-746, 2009.

[41] B. Agostini and A. Bontemps, "Vertical flow boiling of refrigerant R134a in small channels," *International Journal of Heat and Fluid Flow,* vol. 26, pp. 293-306, 2005.

[42] S. S. Bertsch, E. A. Groll and S. V. Garimella, "Effects of heat flux, mass flux, vapor quality, and saturation temperature on flow boiling heat transfer in microchannels," *International Journal of Multiphase Flow,* vol. 35, pp. 142-154, 2009.

[43] S. Bortolin, D. Del Col and L. Rossetto, "Flow Boiling of R245fa in a Single Circular Microchannel," *Heat Transfer Engineering,* vol. 32, pp. 1160-1172, 2011.

[44] G. P. Celata, S. K. Saha, G. Zummo and D. Dossevi, "Heat transfer characteristics of flow boiling in a single horizontal microchannel," *International Journal of Thermal Sciences,* vol. 49, pp. 1086-1094, 2010.

[45] K.-I. Choi, A. S. Pamitran, C.-Y. Oh and J.-T. Oh, "Boiling heat transfer of R-22, R-134a, and CO2 in horizontal smooth minichannels," *International Journal of Refrigeration,* vol. 30, pp. 1336-1346, 2007.

[46] J. Wu, T. Koettig, C. Franke, D. Helmer, T. Eisel, F. Haug and J. Bremer, "Investigation of heat transfer and pressure drop of CO2 two-phase flow in a horizontal mini-channel," *International Journal of Heat and Mass Transfer,* vol. 54, pp. 2154-2162, 2011.

[47] C. B. Tibiriça and G. Ribatski, "Two-Phase Frictional Pressure Drop and flow boiling heat transfer for R245fa in a 2.32 mm tube," *Heat Transfer Engineering,* vol. 32, pp. 1139-1149, 2011.

[48] R. Ali, B. Palm and M. H. Maqbool, "Experimental investigation of two-phase pressure drop in a microchannel," *Heat Transfer Engineering,* vol. 32, no. 13-14, pp. 1126-1138, 2011.

[49] K. Mishima and T. Hibiki, "Some characteristics of air-water two-phase flow in small diameter vertical tubes," *International Journal of Multiphase Flow,* vol. 22, pp. 703-712, 1996.

[50] M. H. Maqbool, B. Palm and R. Khodabandeh, "Flow boiling of ammonia in vertical small diameter tubes: Two phase frictional pressure drop results and assessment of prediction methods," *International Journal of Thermal Sciences,* vol. 54, pp. 1-12, 2012.

[51] H. Müller-Steinhagen and K. Heck, "A simple friction pressure drop correlation for two-phase flow in pipes," *Chemical Engineering Prvoess,* vol. 20, pp. 197-308, 1986.

[52] W. Zhang, T. Hibiki and K. Mishima, "Correlations of two-phase frictional pressure drop and void fraction in mini-channel," *International Journal of Heat and Mass Transfer,* vol. 53, pp. 453-465, 2010.

[53] R. Yun and Y. Kim, "Two Phase pressure drop of CO2 in mini tubes and microchannels," *Microscale Thermophysical Engineering ,* vol. 8, pp. 259-270, 2004.

[54] C. B. Tibiriça, J. D. Da-Silva and G. Ribatski, "Experimental Investigation of flow boiling pressure drop of R134a in a microscale horizontal smooth tube," *ASME Journal of Thermal Science and Engineering Applications,* vol. 3, pp. 011006-1-011006-8, 2011.

[55] D. Chisholm, "Pressure gradients due to friction during the flow of evaporating two-phase mixtures in smooth tubes and channels," *International Journal of Heat and Mass Transfer,* vol. 16, pp. 347-358, 1973.

[56] K. Pehlivan, I. Hassan and M. Vaillancourt, "Experimental study on two-phase flow and pressure drop in millimeter sized channel," *Applied Thermal Engineering,* vol. 26, pp. 1506-1514, 2006.

[57] L. Friedel, "Improved friction pressure drop correlations for horizontal and vertical two phase pipe flow," in *European Two-phase meeting*, Ispra-Italy, 1979.

[58] F. Madrid, N. Caney and P. Marty, "Study of a Vertical Boiling Flow in rectangular mini-channel," *Heat Transfer Engineering,* vol. 28, pp. 753-760, 2007.

[59] Y. W. Hwang and M. S. Kim, "The pressure drop in microtubes and the correlation development," *International Journal of Heat and Mass Transfer,* vol. 49, pp. 1804-1812, 2006.

[60] R. W. Lockhart and R. C. Martinelli, "Proposed correlation of data for isothermal two-phase, two-component flow in pipes," *Chemical Engineering Progress,* vol. 45, pp. 39-48, 1949.

[61] K.-I. Choi, A. S. Pamitran, J.-T. Oh and K. Saito, "Pressure drop and heat transfer during two-phase flow vaporization of propane in horizontal smooth minichannels," *International Journal of Refrigeration,* vol. 32, pp. 837-845, 2009.

[62] C. B. Tibiriça, S. Szczukiewicz, G. Ribatski and J. R. Thome, "Critical Heat Flux of R134a and R245fa inside small diameter tubes," *Heat Transfer Engineering,* vol. 34, pp. 492-499, 2013.

[63] L. Wojtan, R. Revellin and J. R. Thome, "Investigation of saturated critical heat flux in a single, Uniformly heated microchannel," *Experimental Thermal and Fluid Science,* vol. 30, no. 8, pp. 765-774, 2006.

[64] R. Revellin and J. R. Thome, "Critical Heat Flux During Flow Boiling in Microchannels: A parametric study," *Heat Transfer Engineering,* vol. 30, pp. 556-563, 2009.

[65] D. Mikielewicz, J. Wajs, M. Glinski, A. Baset and R. S. Zrooga, "Experimental investigation of dryout of SES 36, R134a, R123 and ethanol in vertical small diameter tubes," *Experimental Thermal and Fluid Science,* vol. 44, no. 1, pp. 556-564, 2013.

[66] C.-M. Callizo, R. Ali and B. Palm, "Dryout incipience and critical heat flux in saturated flow boiling of refrigerants in a vertical uniformly heated microchannel," in *Sixth International ASME conference on Nanochannels, microchannels and minichannels*, Darmstadt, 2008.

[67] D. Del Col and S. Bortolin, "Investigation of dryout during flow boiling in a single microchannel under non uniform axial heat flux," *International Journal of Thermal Sciences,* vol. 57, pp. 25-36, 2012.

[68] R. W. Bowring, "A simple but accurate round tube uniform heat flux correlation over the pressure range 0.7-17 MN/m2," Winfrith, 1972.

[69] A. Kosar and Y. Peles, "Critical Heat Flux of R-123 in silicon based microchannels," *Journal of Heat Transfer,* vol. 129, pp. 844-8514, 2007.

[70] M. B. Bowers and I. Mudawar, "High flux boiling in low flow rates, low pressure drop mini-channel and micro-channel heat sinks," *International Journal of Heat and Mass Transfer,* vol. 37, pp. 321-332, 1994.

[71] C. B. Tibiriçá, G. Ribatiski and J. R. Thome, "Saturated flow boiling heat transfer and critical heat flux in small horizontal flattened tubes," *International Journal of Heat and Mass Transfer,* vol. 55, pp. 7873-7883, 2012.

[72] W. Owhaib, "Experimental heat transfer, pressure drop and flow visualization of R134a in a vertical mini/micro tubes," Doctoral Thesis in Energy Technology, KTH, Stockholm, 2007.

[73] NIST, "National Institute of Standard and Technology," Refprop Version 9.0, Boulder Colorado, 2010.

[74] G. Hagen, "Über die Bewegung des Wassers in engen zylindrischen Röhren," *Pogg. Ann. ,* vol. 46, pp. 423-442, 1839.

[75] J. Poiseuille, "Rècherches expèrimentelles sur le movement des liquids les tubes de très petits diameters," *C. R. Acad. Sci.,* vol. 11, pp. 961-967, 1840.

[76] H. Blasius, "Das Ähnlichkeitsgesetz bei Reibungsvorgängen in Flüssigkeiten," in *Forsch Arb. Ing-Wesen Heft*, Berlin, 1913.

[77] J. Holman, Experimental Methods for Engineers, McGraw-Hill, 2000.

[78] S. J. Kline and F. A. McClintock, "Describing uncertainties in single sample experiments," *Mech Eng,* vol. 75, p. 1953, 3-8.

[79] R. J. Moffat, "Describing the uncertainties in experimental results," *Experimental Thermal and Fluid Science,* vol. 1, pp. 3-17, 1988.

[80] V. Gnielinski, "New equation for heat and mass transfer in turbulent pipe and channel flow," *International Chemical Engineering,* vol. 16, pp. 359-368, 1976.

[81] F. W. Dittus and L. M. K. Boelter, "Heat transfer in automobile radiators of the tubular type," *International Communication in Heat and Mass Transfer,* vol. 12, pp. 3-22, 1985.

[82] D. Yu, R. Warrington, R. Barron and T. Ameel, "An experimental and theoritical investigation of fluid flow and heat transfer in microtubes," in *4th ASME/JSME Thermal Engineering Conference*, Hawaii, 1995.

[83] S. B. Choi, R. F. Barron and R. O. Warrington, "Fluid flow and heat transfer in microtubes," in *Microchannel sensors, Actuators and Systems ASME DSC*, Atlanta, 1991.

[84] A. S. Pamitran, K.-I. Choi, J.-T. Oh and Nasruddin, "Evaporation heat transfer coefficient in single circular small tubes for flow natural refrigerants of C3H8, NH3 and CO2," *International Journal of Multiphase flow,* vol. 37, pp. 794-801, 2011.

[85] J. R. Thome and L. Consolini, "Mechanisms of boiling in Micro-channels: Critical Assessment," *Heat Transfer Engineering ,* vol. 34, pp. 288-297, 2010.

[86] Z. Y. Bao, D. F. Fletcher and B. S. Haynes, "Flow boiling heat transfer of Freon R11 and HCFC123 in narrow passages," *International Journal of Heat and Mass Transfer,* vol. 43, pp. 3347-3358, 2000.

[87] G. Lazarek and S. H. Black, "Evaproative heat transfer, pressure drop and critical heat flux in a small veratical tube with R-113," *International Journal of Heat and Mass Transfer,* vol. 25, pp. 945-960, 1982.

[88] J. C. Chen , "A correlation for boiling heat transfer to saturated fluids in convective flow," *Industrial Engineering and Chemistry,* vol. 5, pp. 322-329, 1966.

[89] K. E. Gungor and R. H. S. Winterton, "A general correlation for flow boiling in tubes and annuli," *International Journal of Heat and Mass Transfer,* vol. 29, pp. 351-358, 1986.

[90] D. Mikielewicz, "A new method for deterimation of flow boiling heat transfer coefficient in conventional-diameter channels and minichannels," *Heat Transfer Engineering,* vol. 31, no. 4, pp. 276-287, 2010.

[91] M. M. Mahmoud and T. G. Karayiannis, "Heat transfer correlation for flow boiling in small to micro tubes," *International Journal of Heat and Mass Transfer,* vol. 66, pp. 553-574, 2013.

[92] M. M. Mahmoud and T. G. Karayiannis, "A statistical correlation for flow boiling heat transfer in micro tubes," in *3RD European Conference on Microfluidics*, Heidelberg, 2012.

[93] S. G. Kandlikar, "A general correlation for saturated two phase flow boiling heat transfer inside horizontal and vertical tubes," *Journal of Heat Transfer, Transactions of ASME,* vol. 112, pp. 219-228, 1990.

[94] D. Del Col, D. Torresin and A. Cavallini, "Heat transfer and pressure drop during condensation of the low GWP refrigerant R1234yf," *International Journal of Refrigeration,* vol. 33, pp. 1307-1318, 2010.

[95] D. S. Jung and R. Radermacher, "Prediction of pressure drop during horizontal annular flow boiling of pure and mixed refrigerants," *International Journal of Heat and Mass Transfer,* vol. 32, pp. 2435-2446, 1989.

[96] R. Grönnerud, "Investigation of liquid hold-up, flow resistance and heat transfer in circulation type evaporators, Part IV: Two phase flow resistance in boiling," *Bull. Inst. Froid [Annex 1972-1] ,* 1979.

[97] C. C. Wang, C. S. Chiang and D. C. Lu , "Visual observation of two-phase flow pattern of R-22, R134a and R407C in a 6.5 mm smooth tube," *Experimental Thermal and Fluid Science,* vol. 15, pp. 395-405, 1997.

[98] W. McAdams, W. Woods and L. C. Heroman, "Vaporization inside horizontal tubes, II. Benzen-Oil mixture," *Transacton of ASME,* vol. 64, pp. 193-200, 1942.

[99] C. Y. Yang and R. L. Webb, "Friction pressure drop of R-12 in small hydraulic diameter extruded aluminum tubes with and without micro-fins," *International Journal of Heat and Mass Transfer,* vol. 39, pp. 801-809, 1996.

[100] L. Sun and K. Mishima, "Evaluation analysis of prediction methods for two-phase flow pressure drop in mini-channels," *International Journal of Multiphase Flow,* vol. 35, pp. 47-54, 2009.

[101] W. Li and Z. Wu, "A general correlation for adiabatic two-phase pressure drop in micro/mini-channels," *International Journal of Heat and Mass Transfer,* vol. 53, pp. 2732-2739, 2010.

[102] S. Mori, Y. Yoshida, K. Ohishi and Y. Kokimoto, "Dryout quality and post dryout heat transfer coefficient in horizontal evaporator tubes," in *3rd European Thermal Science Conference*, 2000.

[103] L. Wojtan, T. Ursenbacher and J. R. Thome, "Investigation of flow boiling in horizontal tubes: part i – a new diabatic two-phase flow pattern map," *International Journal of Heat and Mass Transfer,* vol. 48, pp. 2955-2969, 2005.

[104] E. M. Chiapero, M. Fernandino and C. A. Dorao, "Experimental results on boiling heat transfer coefficient, frictional pressure drop and flow patterns for R134a at a saturation temperature of 34 °C," *International Journal of Refrigeration,* vol. 40, pp. 317-327, 2014.

[105] Z. Wu, W. Li and S. Ye, "Correlations for saturated critical heat flux in microchannels," *International Journal of Heat and Mass Transfer,* vol. 54, pp. 379-389, 2011.

[106] W. Zhang, T. Hibiki, K. Mishima and Y. Mi, "Correlation of critical heat flux for flow boiling of water in mini-channels," *International Journal of Heat and Mass Transfer,* vol. 49, pp. 1058-1072, 2006.

[107] M. M. Shah, "Improved general correlation for critical heat flux during upflow in uniformly heated vertical tubes," *Heat and Fluid Flow,* vol. 8, pp. 326-335, 1987.

[108] H. K. Forster and N. Zuber , "Dynamics of vapor bubble and boiling heat transfer," *A.I.Ch.E,* vol. 1, no. 4, pp. 531-535, 1955.

[109] W. Yu, D. M. France and M. W. Wambsganss, "Two phase pressure drop, boiling heat transfer and critical heat flux to water in a small diameter horizontal tube," *International Journal of Multiphase Flow,* vol. 28, pp. 927-941, 2002.

[110] Z. Anwar, B. Palm and R. Khodabandeh, "Flow boiling heat transfer and dryout characteristics of R152a in a vertical minichannel," *Experimental Thermal and Fluid Science,* vol. 53, pp. 207-217, 2014.

List of Figures

List of Tables

Appendix

This section contains brief information on correlations for boiling heat transfer, pressure drop, dryout incipience quality and dryout heat flux. Applicability range and expressions of correlations are given in following paragraphs.

Correlations for prediction of saturated flow boiling heat transfer

Micro-scale correlations

Brief descriptions of the correlations utilized for the prediction of saturated flow boiling heat transfer are given below.

Cooper [24]

Originally proposed for estimation of pool boiling heat transfer performance.

$$\alpha = 55 p_r^{0.12-0.4343 \ln R_a} (-0.4343 \ln p_r)^{-0.55} M^{-0.5} q''^{0.67}$$

Lazarek and Black [87]

The experimental database used for developing this correlation showed a strong influence of heat flux on heat transfer coefficients, with insignificant effects of vapor quality and mass flux. The experimental database was collected with R113 in a 3.1 mm diameter tube with 123 and 246 mm heated length (G=125-750 kg/m²s, 1.3-4.5 bar). The experimental Nusslet numbers were not influenced by variation of *x*. Using least square regression, the following functional form was proposed:

$$Nu = 30 Re_l^{0.857} Bo^{0.714}$$

Tran et al. [19]

Tran et al. [19] reported experimental findings for flow boiling of R12 in similarly sized circular and rectangular mini-channels (d~2.40 mm and 0.9 m length). Other operating parameters were mass flux 48-832 kg/m²s and vapor quality up to 94%. The authors observed similar trends and heat transfer performance from both geometries. Nucleate boiling was reported as the dominant heat transfer mechanism for wall superheat > 2.75 °C, whereas convection dominance was observed for wall superheat < 2.75 °C. From their findings, the authors proposed the following functional form for prediction of saturated flow boiling heat transfer from compact channels:

$$\alpha = (8.4 * 10^5) \cdot (Bo^2 We_d)^{0.3} \cdot \left(\frac{\rho_l}{\rho_g}\right)^{-0.4}$$

An insignificant contribution from mass flux in this correlation can be noted from the combination of exponents for the two dimensionless numbers considered. Furthermore, to accommodate for the dominance of the surface tension effect in small channels, the Weber No (We) was used, whereas fluid-related effects were adjusted through the presence of the density ratio term.

Li and Wu [11]

Based on experimental results from 18 published datasets, Li and Wu [11] proposed another correlation for prediction of saturated boiling heat transfer coefficients from mini/micro-channels. The consolidated database contained data from both multi and single channel configurations (3700 data points) under wide operating conditions with various fluids (water, natural and synthetic refrigerants) and channel dimensions (0.16-3.1 mm). The analysis of combined database revealed liquid flow laminarization and small Bond numbers in the compact channels. The functional form of proposed correlation is as follows:

$$\mathrm{Nu} = 334\mathrm{B_o}^{0.3}\left(\mathrm{B_d} * \mathrm{Re_l}^{0.36}\right)^{0.4}$$

It should also be mentioned that the data points at very low vapor quality (x<0.10) and after incipience of dryout were not considered for the authors regression analysis.

Kandlikar and Balasubramanian [22]

Kandlikar and Balasubramanian [22] observed liquid flow laminarization in mini/micro-channels and revised Kandlikar's original macro-scale correlation [93]. With this correlation, the fully developed laminar region is considered for Re < 1600, whereas the fully developed turbulent region is considered for Re > 3000, with transition in between. For the transition region, a linear interpolation was suggested for predicting heat transfer coefficient.

$$\alpha = \text{Larger of } \begin{cases} \alpha_{\mathrm{NB}} \\ \alpha_{\mathrm{CB}} \end{cases}$$

$$\alpha_{\mathrm{NB}} = 0.6683 \cdot \mathrm{Co}^{-0.2}(1-x)^{0.8} \cdot \alpha_{\mathrm{lo}} + 1058 \cdot \mathrm{Bo}^{0.7}(1-x)^{0.8} \cdot \mathrm{f_{Fl}} \cdot \alpha_{\mathrm{lo}}$$

$$\alpha_{\mathrm{CB}} = 1.136 \cdot \mathrm{Co}^{-0.9}(1-x)^{0.8} \cdot \alpha_{\mathrm{lo}} + 667.2 \cdot \mathrm{Bo}^{0.7}(1-x)^{0.8} \cdot \mathrm{f_{Fl}} \cdot \alpha_{\mathrm{lo}}$$

$$\alpha_{\mathrm{lo}} = \frac{\mathrm{Re_{lo}Pr_l}\left(\frac{\mathrm{f}}{2}\right)\left(\frac{\mathrm{k_l}}{\mathrm{d}}\right)}{1 + 12.7\left(\mathrm{Pr_l}^{2/3} - 1\right)\left(\frac{\mathrm{f}}{2}\right)} \qquad 10^4 \le \mathrm{Re_{lo}} \le 5 * 10^6$$

$$\alpha_{\mathrm{lo}} = \frac{(\mathrm{Re_{lo}} - 1000)\mathrm{Pr_l}\left(\frac{\mathrm{f}}{2}\right)\left(\frac{\mathrm{k_l}}{\mathrm{d}}\right)}{1 + 12.7\left(\mathrm{Pr_l}^{2/3} - 1\right)\left(\frac{\mathrm{f}}{2}\right)} \qquad 3000 \le \mathrm{Re_{lo}} \le 10^4$$

$$\mathrm{f} = 1.58[\ln(\mathrm{Re_{lo}} - 3.28)]^{-2}$$

Mikielewicz correlation [90]

In this prediction model, two-phase flow is considered as a single liquid phase flow with properties of two-phase flow. The model is based on the theoretical evaluation of energy dissipation for two-phase flow. This model is general in nature and can be used for conventional as well as mini-channels. Furthermore, it can be applied (with some correction) in sub-cooled flow boiling cases.

$$\frac{\alpha_{tp}}{\alpha_{lo}} = \sqrt{{R_{MS}}^{n} + \frac{1}{1+P}\left(\frac{\alpha_{Nb}}{\alpha_{lo}}\right)}$$

$$P = 2.53 * 10^{-3} Re^{1.17} Bo^{0.6} (R_{MS} - 1)^{-0.65}$$

$$R_{MS} = \left[1 + 2\left(\frac{1}{f_1} - 1\right) x\, Co^{m}\right] \cdot (1-x)^{\frac{1}{3}} + x^3 \frac{1}{f_{1z}}$$

$$n = 0.9 \text{ (Turbulent flow) or } 2 \text{ (Laminar flow)}, m = -1 \text{ (for mini} - \text{channels) and } \alpha_{Nb} = \alpha_{Cooper}$$

$$f_1 = \left(\frac{\rho_g}{\rho_l}\right)\left(\frac{\mu_l}{\mu_g}\right)^{0.25} \text{(for turbulent flow)}\ f_1 = \left(\frac{\rho_g}{\rho_l}\right)\left(\frac{\mu_l}{\mu_g}\right) \text{(for laminar flow)}$$

$$f_{1z} = \left(\frac{\mu_g}{\mu_l}\right)\left(\frac{k_l}{k_g}\right)^{1.5}\left(\frac{Cp_l}{Cp_g}\right) \text{ (for laminar flow)}\ f_{1z} = \left(\frac{k_g}{k_l}\right) \text{ (for turbulent flow)}$$

Mahmoud and Karayiannis [91]

Based on statistical analysis of their database, Mahmoud and Karayiannis [91] also proposed a correlation for prediction of saturated flow boiling heat transfer. This correlation was developed from an R134a-based database. Boiling number, Reynolds number, confinement number, thermal conductivity and the channel's geometrical details are required for prediction of the heat transfer coefficient by the following:

$$\alpha = 3320\ \frac{Bo^{0.63} {We_l}^{0.2} {Re_l}^{0.11} k_l}{Co^{0.6} d} \quad \text{for } d = 1.10 - 4.26 \text{ mm}$$

Macro-scale correlations

Chen [88]

Chen's approach for predicting saturated flow boiling heat transfer in a large tube is summarized below. It is an additive approach, where contributions from nucleate and convective boiling terms are considered along with suppression and enhancement factors, respectively. Forster and Zuber's correlation [108] is used to account for the nucleate boiling part, whereas convection effects are addressed with the Dittus-Boelter [81] model.

$$\alpha = S \cdot \alpha_{\text{Forster and Zuber}} + F \cdot \alpha_{lo}$$

$$F = \begin{cases} 1 & \text{For } {}^{1}/_{X_{tt}} \le 0.1 \\ 2.35\left(0.213 + \frac{1}{X_{tt}}\right)^{0.736} & \text{For } {}^{1}/_{X_{tt}} \ge 0.1 \end{cases}$$

$$S = \frac{1}{1 + 0.00000253 {Re_{tp}}^{1.17}}$$

$$\mathrm{Re_{tp}} = \mathrm{Re_l} F^{1.25}$$

$$\alpha_{lo} = \alpha_{D-B}$$

Gungor and Winterton [89]

This macro-scale correlation for predicting boiling heat transfer was developed from a large database (4300 data points with seven fluids) under vertical and horizontal flow conditions and covered sub-cooled as well as saturated boiling regimes. This correlation is further applicable to tube and annular flow conditions. The functional form of this correlation considers contributions from nucleate boiling and forced convective evaporation, with suppression and enhancement factors as given below. The suppression factor is a function of Reynolds number, whereas the enhancement factor is a function of the Martinelli parameter and Boiling number.

$$\alpha = F \cdot \alpha_{CB} + S \cdot \alpha_{NB}$$

$$\alpha_{CB} = 0.023 * \mathrm{Re_l}^{0.8} \mathrm{Pr_l}^{0.4} \frac{k_l}{d} \text{ and } \alpha_{NB} = \alpha_{cooper}$$

$$F = 1 + 24000 \mathrm{Bo}^{1.16} + 1.37 \left(\frac{1}{X_{tt}}\right)^{0.86} \text{ and } S = \frac{1}{1 + 1.15 * 10^{-6} E^2 \mathrm{Re_l}^{1.17}}$$

The above expressions are for vertical flow conditions; refinements/modifications for horizontal flow conditions are given in [89].

Liu and Winterton [31]

Like Gungor and Winterton's correlation [89], this macro-scale model also considers contributions from both boiling mechanisms; however, overall contribution is not simply additive. The functional form of this correlation is given as follows:

$$\alpha^2 = (F \cdot \alpha_{CB})^2 + (S \cdot \alpha_{NB})^2$$

$$F = \left[1 + x \, \mathrm{Pr_l} \left(\frac{\rho_l}{\rho_g} - 1\right)\right]^{0.35}$$

$$S = \left[1 + 0.055 F^{0.1} \mathrm{Re_l}^{0.16}\right]^{-1}$$

$$\alpha_{CB} = \alpha_{Dittus-Boelter} \text{ and } \alpha_{NB} = \alpha_{Cooper}$$

Unlike other correlations, the convective boiling enhancement factor F is a function of the Prandtl number. The pool boiling correlation from Cooper [24] and the convective heat transfer coefficient from Dittus-Boelter [81] are used to account for the nucleate and convective boiling contributions.

Kandlikar correlation [93]

This correlation was developed from a large saturated flow boiling database (5246 data points, involving water and non-aqueous fluids) under horizontal and vertical flow conditions. The correlation considers

contributions from nucleate and convective boiling mechanisms with a fluid-dependent parameter "F_{fl}" as given below.

$$\alpha = \mathrm{Max}[\alpha_{CB}, \alpha_{NB}]$$

$$\alpha_{CB} = [1.136\mathrm{Co}^{-0.9}(25\mathrm{Fr}_{lo})^{c} + 667.2\mathrm{Bo}^{0.7}\mathrm{F}_{fl}]\alpha_{lo}$$

$$\alpha_{NB} = [0.6683\mathrm{Co}^{-0.2}(25\mathrm{Fr}_{lo})^{c} + 1058\mathrm{Bo}^{0.7}\mathrm{F}_{fl}]\alpha_{lo}$$

$$\alpha_{lo} = \alpha_{D-B}$$

Where C=0 for vertical tubes.

Correlations for two-phase frictional pressure drop

Homogenous Model

The homogenous model—sometimes called the zero slip model—assumes the same velocity for liquid and vapor phases. Basically, it considers flow as single phase with mean fluid properties based on vapor quality.

$$\left(\frac{dp}{dz}\right)_{tp} = \frac{2f_{tp}G^2}{d\rho_{tp}}$$

$$\rho_{tp} = \left[\frac{x}{\rho_g} + \frac{1-x}{\rho_l}\right], f_{tp} = \frac{16}{\mathrm{Re}_{tp}} \text{ for } \mathrm{Re} < 2000, f_{tp} = \frac{0.079}{\mathrm{Re}_{tp}^{-0.25}}$$

Lockhart and Martinelli [60]

Lockhart and Martinelli's method is based on the separated flow model with separate liquid and vapor streams and is also sometimes known as the slip flow model. The following procedure is adopted for estimation of two-phase frictional pressure drop.

$$\left(\frac{dp}{dz}\right)_{tp} = \Phi^2{}_l \left(\frac{dp}{dz}\right)_l$$

$$\Phi^2{}_l = 1 + \frac{C}{X} + \frac{1}{X^2}$$

$$C_{vv} = 5, C_{tv} = 10, C_{vt} = 12, C_{tt} = 20$$

$$X^2 = \frac{\left(dp/dz\right)_l}{\left(dp/dz\right)_g}, \left(dp/dz\right)_l = f_l \frac{2G^2(1-x)^2}{d\rho_l}, \left(dp/dz\right)_g = f_g \frac{2G^2x^2}{d\rho_g}$$

Müller-Steinhagen and Heck [51]

This macro-scale model was developed from a large data base (9300 data points from various fluids in 4-392 mm channels) and covers a wide range of operating conditions under horizontal flow conditions.

$$\left(\frac{dp}{dz}\right)_{tp} = \left[\left(\frac{dp}{dz}\right)_{lo} + 2\left\{\left(\frac{dp}{dz}\right)_{go} - \left(\frac{dp}{dz}\right)_{lo}\right\}x\right](1-x)^{1/3} + \left(\frac{dp}{dz}\right)_{go} x^3$$

Jung and Radermacher [95]

This correlation was developed from a refrigerant-based database (R22, R12, R114, R152a pure and their mixtures, 600 data points, 230-720 kg/m^{2}s, 10-45 kW/m^2 and 200-800 kPa) in conventional sized channels. This separated flow model basically relies on the primary assumption of equal static pressure drop for liquid and vapor phases and is therefore well-suited for annular flow conditions.

$$\left(\frac{dp}{dz}\right)_{tp} = \left[\left(\frac{dp}{dz}\right)_{lo}\right]\Phi_{lo}{}^2$$

$$\Phi_{lo}{}^2 = 12.82 X_{tt}{}^{-1.47}(1-x)^{1.8}$$

Tran et al. [23]

This micro-scale correlation is a modified form of Chisholm's original macro-scale correlation [55] , in which surface tension and flow characteristics due to change in scale are addressed using the Confinement Number. This correlation was developed from a refrigerant-based database (R12, R134a and R113) in small circular and rectangular channels.

$$\left(\frac{dp}{dz}\right)_{tp} = \left(\frac{dp}{dz}\right)_{lo}\Phi_{lo}{}^2$$

$$\Phi_{lo}{}^2 = 1 + \left[4.3\frac{\left(\frac{dp}{dz}\right)_{go}}{\left(\frac{dp}{dz}\right)_{lo}} - 1\right][Co \cdot x^{0.875}(1-x)^{0.875} + x^{1.75}]$$

Hwang and Kim [59]

$$\left(\frac{dp}{dz}\right)_{tp} = \left(\frac{dp}{dz}\right)_{l}\Phi_{l}{}^2 \text{ where } \Phi^2{}_l = 1 + \frac{C}{x} + \frac{1}{x^2}$$

$$C = 0.227\left[Re_{lo}{}^{0.452} X^{-0.32} Co^{-0.82}\right]$$

Mishima and Hibiki [49]

This correlation is based on the combination of laminar liquid and laminar vapor flow, where the channels geometrical characteristics are addressed by including hydraulic diameter (surface tension effects, however, are not covered) in the Chisholm constant. This correlation is based on data from small circular channels (1-4 mm in diameter).

$$\left(\frac{dp}{dz}\right)_{tp} = \left(\frac{dp}{dz}\right)_{l} \Phi^2{}_{l}, \text{where } \Phi^2{}_{l} = 21\ (1 - \exp\{-0.333d\})\ d(mm)$$

Yu et al. [109]

$$\left(\frac{dp}{dz}\right)_{tp} = \left(\frac{dp}{dz}\right)_{l} \Phi^2{}_{l}, \text{where } \Phi^2{}_{l} = \left[18.65\ \left(\frac{v_f}{v_g}\right)^{0.5} \left(\frac{1-x}{x}\right) \left(\frac{Re_g{}^{0.1}}{Re_l{}^{0.5}}\right)\right]^{-1.9}$$

Zhang et al. [52]

$$\left(\frac{dp}{dz}\right)_{tp} = \left(\frac{dp}{dz}\right)_{l} \Phi^2{}_{l}, \text{where } \Phi^2{}_{l} = 1 + \frac{C}{x} + \frac{1}{x^2}$$

$$C = 21\ [1 - \exp(-0.142/Co)]$$

Li and Wu [101]

This micro-scale correlation was developed from a large micro-scale database (769 data points collected from 0.148-3.25 mm test channels with 12 working fluids) collected from previous publications. The authors proposed a new transition limit for macro to micro-scale based on $BdRe_l{}^{0.5}$. As reported, surface tension effects can be ignored for cases with Bd>11, whereas a strong effect of surface tension was observed when Bd < 1.5.

$$\left(\frac{dp}{dz}\right)_{tp} = \left(\frac{dp}{dz}\right)_{l} \Phi^2{}_{l}, \text{where } \Phi^2{}_{l} = 1 + \frac{C}{x} + \frac{1}{x^2}$$

$$\text{For } Bd < 1.5\ C = 11.9\ Bd^{0.45}, \text{For } 1.5 < Bd < 11\ C = 109.4\ \left(BdRe_l{}^{0.5}\right)^{-0.56}$$

$$\text{For } Bd > 11 \text{ Beattie and Whalley correlation is recommended.}$$

Sun and Mishima [100]

For Re_l < 2000 and Re_g< 2000

$$\left(\frac{dp}{dz}\right)_{tp} = \left(\frac{dp}{dz}\right)_{l} \Phi^2{}_{l}$$

$$\Phi^2{}_{l} = 1 + \frac{C}{x} + \frac{1}{x^2}$$

$$C = 26\left[1 + \frac{Re_l}{1000}\right]\left[1 - \exp\left(\frac{-0.153}{0.27Co + 0.8}\right)\right]$$

For Re_l > 2000 and Re_g > 2000

$$\left(\frac{dp}{dz}\right)_{tp} = \left(\frac{dp}{dz}\right)_{l} \Phi^2{}_{l}$$

$$\Phi^2{}_l = 1 + \frac{C}{x^{1.19}} + \frac{1}{x^2}$$

$$C = 1.79 \left(\frac{Re_g}{Re_l}\right)^{0.4} \left(\frac{1-x}{x}\right)^{0.5}$$

Yang and Webb

$$\left(\frac{dp}{dz}\right)_{tp} = 0.87\, Re_{tp}{}^{0.12} f_{lo} \frac{G_{eq}{}^2 v_l}{d}$$

$$\text{where } Re_{eq} = \frac{G_{eq} d}{\mu} \text{ and } G_{eq} = G\left[1 - x + x\left(\frac{\rho_l}{\rho_g}\right)^{0.5}\right]$$

Wang et al.

For G>200 kg/m²s

$$\left(\frac{dp}{dz}\right)_{tp} = \left(\frac{dp}{dz}\right)_g \Phi^2{}_g \; where \; \Phi^2{}_g = 1 + 9.4X^{0.62} + 0.56X^{2.45}$$

For G<200 kg/m²s

$$\left(\frac{dp}{dz}\right)_{tp} = \left(\frac{dp}{dz}\right)_l \Phi^2{}_l \; where \; \Phi^2{}_l = 1 + \frac{C}{x} + \frac{1}{x^2}$$

$$C = 4.566 * 10^{-6} X^{0.128} Re_{lo}{}^{0.938} \left(\frac{v_l}{v_g}\right)^{2.15} \left(\frac{\mu_l}{\mu_g}\right)^{5.1}$$

Grönnerud [96]

$$\left(\frac{dp}{dz}\right)_{tp} = \left(\frac{dp}{dz}\right)_{lo} \Phi^2{}_l$$

$$\Phi^2{}_l = 1 + \left(\frac{dp}{dz}\right)_{Fr} \left[\frac{\frac{\rho_l}{\rho_g}}{\left(\frac{\mu_l}{\mu_g}\right)^{0.25}} - 1\right] \text{ where } \left(\frac{dp}{dz}\right)_{Fr} = f_{Fr}\left[x + 4\left(x^{1.8} - x^{10} f_{Fr}{}^{0.5}\right)\right]$$

$$Fr_l = \frac{G^2}{gd\rho^2} \text{ if } Fr_l > 1 \; then \; f_{Fr} = 1$$

$$\text{if } Fr_l < 1 \; then \; f_{Fr} = Fr_l{}^{0.3} + 0.0055\left(\ln\frac{1}{Fr_l}\right)^2$$

Friedel [57]

Normally used for estimation of frictional pressure drop in horizontal and vertical upward flow conditions. This correlation is recommeded for the cases where μ_l/μ_g <1000 and G < 2000 kg/m^{2}s.

$$\left(\frac{dp}{dz}\right)_{tp} = \left(\frac{dp}{dz}\right)_{lo} \Phi^2{}_{lo}$$

$$\left(\frac{dp}{dz}\right)_{lo} = f_{lo}\frac{2G^2}{\rho_l d}$$

$$\Phi^2{}_{lo} = (1-x)^2 + x^2\left(\frac{v_g}{v_l}\right)\left(\frac{f_{go}}{f_{lo}}\right) + 3.24\,x^{0.78}(1-x)^{0.224}\left(\frac{v_g}{v_l}\right)^{0.91}\left(\frac{\mu_g}{\mu_l}\right)^{0.19}\left[1-\left(\frac{\mu_g}{\mu_l}\right)^{0.7}\right]Fr_{tp}{}^{-0.0454}We_{tp}{}^{-0.035}$$

Correlations for vapor quality at dryout incipience

Mori et al. [102]

As per S2 regime, for initiation of dryout

$$x_{di} = 0.58e^{\left[0.52-2.1*10^{-5}We_g{}^{0.96}Fr_g{}^{-0.02}\left(\frac{\rho_g}{\rho_l}\right)^{-0.08}\right]}$$

For dryout completion

$$x_{dc} = 0.61e^{\left[0.57-2.65*10^{-5}We_g{}^{0.94}Fr_g{}^{-0.02}\left(\frac{\rho_g}{\rho_l}\right)^{-0.08}\right]}$$

Wojtan et al. [103]

Revised version of above mentioned correlation from Mori et al. [102]

$$x_{di} = 0.58e^{\left[0.52-0.235*We_g{}^{0.17}Fr_g{}^{0.37}\left(\frac{\rho_g}{\rho_l}\right)^{0.25}*\left(\frac{q''}{q_{critical}}\right)^{0.70}\right]}$$

$$x_{dc} = 0.61e^{\left[0.57-5.8*10^{-3}*We_g{}^{0.38}Fr_g{}^{0.15}\left(\frac{\rho_g}{\rho_l}\right)^{-0.09}*\left(\frac{q''}{q_{critical}}\right)^{0.27}\right]}$$

Where $q_{critical} = 0.131 * \rho_g{}^{0.5} * h_{lg}[g(\rho_l - \rho_g)\sigma]$

Correlations for prediction of Critical Heat Flux

Katto-Ohno [28]

This highly cited correlation was originally developed from an experimental database of single vertical tubes with R12 as the working fluid. While some authors [110] [1] [2] have reported satisfactory predictive value, others have modified this correlation [9] [65] for prediction of their mini/micro channel datasets.

$$\frac{q''_{CHF}}{Gh_{lg}} = f\left[\frac{\rho_l}{\rho_g}, \frac{\sigma\rho_l}{G^2 l}, \frac{l}{d}\right]$$

The wider applicability of this correlation was ensured by its original authors by comparing the predictions for several fluid-channel combinations. The authors observed a linear increase in CHF with increased degree of sub-cooling and they thus revised the original correlation accordingly.

$$q''_{CHF} = q''_{c}\left(1 + K\left(\frac{\Delta h_{sub\ cooling}}{h_{lg}}\right)\right)$$

Zhang et al. [106]

This inlet-condition-dependent (inlet enthalpy, heated length) correlation was developed from a large water database of 3837 data points (2539 saturated) involving both saturated and sub-cooled boiling cases under a wide range of operating conditions (0.1-19 bar, 5.33-134000 kg/m^{2}s, 0.3-6.2 mm). Key parameters were identified using the Artificial Neural Network (ANN) technique. The proposed correlation for prediction of saturated CHF is given as follows:

$$\frac{q''_{CHF}}{Gh_{lg}} = 0.0352\left[We_d + 0.0119\left(\frac{l}{d}\right)^{2.31}\left(\frac{\rho_g}{\rho_l}\right)^{0.361}\right]^{-0.295} \cdot \left(\frac{l}{d}\right)^{-0.311}\left[2.05\left(\frac{\rho_g}{\rho_l}\right)^{0.770} - x_{in}\right]$$

This correlation was developed from experimental datasets under uniform heating conditions, and thus may not give reasonable predictions for non-uniform heating cases.

Wu et al. [105]

This correlation was proposed from a large database (629 data points) collected from the literature involving water and non-aqueous fluids in single and multichannel arrangement. This correlation considers dryout of the thin liquid film on the heating surface as the triggering mechanism for CHF. The authors reported a decrease in Boiling Number with increase in l/d when l/d<50. This correlation is applicable for prediction of saturated CHF when $B_d*Re_l^{0.5}<200$, $x_e>0.05$, G<4000 kg/m^{2}s and l/d<250. It should be mentioned that thermophysical properties are to be calculated at the outlet of the channel. The correlation is quite simple; CHF depends on mass flux, channel geometrical details, heat of vaporization and exit quality, as follows:

$$\frac{q''_{CHF}}{Gh_{lg}} = 0.60\left[\left(\frac{l}{d}\right)^{-1.19} x^{0.817}\right]$$

Wojtan et al. [63]

Developed from a saturated CHF database for R134a and R245fa with uniformly heated vertical, single tubes of 0.5 and 0.8 mm in diameter (heated length was in the range of 20-70 mm). The authors reported an increase in CHF with increasing mass velocity, increasing tube size and reduced heated length. CHF was not affected by variations in the degree of sub-cooling and saturation temperature (G<1000). This correlation is a modified version of the Katto-Ohno correlation [28], with exponents and leading constants modified to fit the experimental data. The authors recommended the use of this correlation only in cases where $\varrho_v/\varrho_l < 0.15$ and for annular flow regimes. While using this correlation, transport properties should be calculated at the inlet conditions. The functional form of this correlation is as follows:

$$\frac{q''_{CHF}}{Gh_{lg}} = 0.437\left[\left(\frac{\rho_g}{\rho_l}\right)^{0.073} We_l^{-0.24}\left(\frac{l}{d}\right)^{-0.72}\right]$$

Ong and Thome [9]

Another modified version of Katto-Ohno's correlation [28] for prediction of saturated CHF in mini/micro-channels was proposed by Ong and Thome. This correlation was developed from the experimental results of three studies (Ong and Thome [9], Wojtan et al. [63] and Park) carried out using R134a, R245fa and R236fa in single and multi micro-channel arrangements. To account for the macro to micro-scale transition two new factors (diameter and viscosity ratio) were introduced.

$$\frac{q''_{CHF}}{Gh_{lg}} = 0.12\left[\left(\frac{\mu_l}{\mu_g}\right)^{0.183}\left(\frac{\rho_g}{\rho_l}\right)^{0.062} We_l^{-0.141}\left(\frac{l}{d}\right)^{-0.70}\left(\frac{d}{d_{th}}\right)^{0.11}\right]$$

Callizo et al. [66]

Another correlation for prediction of saturated CHF in single vertical circular channels was proposed by Callizo et al [66]. This is also a modified form of Katto-Ohno's correlation and was developed from an experimental dataset using R134a, R245fa and R22 in 0.64 mm vertical channel.

$$\frac{q''_{CHF}}{Gh_{lg}} = 0.3216\left[\left(\frac{\rho_g}{\rho_l}\right)^{0.084} We_l^{-0.034}\left(\frac{l}{d}\right)^{-0.942}\right]$$

Mikielewicz et al. [65]

Based on an experimental database for dryout of R134a, R123 and Solkatherm SES36, Mikielewicz et al. [65] proposed another correlation for prediction of saturated CHF in mini/micro-channels. This correlation is also another modified form of Katto-Ohno's correlation [28]. However, care should be exercised when dealing with Weber No, as subscript "d" refers to calculations based on the diameter of the channel, whereas "l" is used when the calculation is based on heated length instead.

$$\frac{q''_{CHF}}{Gh_{lg}} = 0.62\left[\left(\frac{\rho_g}{\rho_l}\right)^{-0.02} We_d^{-0.05}\left(\frac{l}{d}\right)^{-1.17}\right]$$